

JOURNAL OF SCIENCE AND TECHNOLOGY UTHM

ISSN 2229-8460

Volume 4 No.2/December 2012

Editorial Board

iii

Preface

iv

CONTENTS

1. High Pressure Processing of Honey: Preliminary Study of Total Microorganism Inactivation and Identification of Bacteria
M.F. Noor Akhmazillah, M.M. Farid and F.V.M. Silva 1-12
2. Genetically Modified Mosquito: Myth and Reality
Teh Su Yean, Koh Hock Lye and Yeap Kiew Lee 13-22
3. Kenaf Core Particleboard and Its Sound Absorbing Properties
Mohamad Jani Saad and Izran Kamal 23-34
4. Numerical Solution of Mixed Convection Flow about a Sphere in a Porous Medium Saturated by a Nanofluid: Brinkman Model
Leony Tham and Roslinda Nazar 35-46
5. Arsenic(III) Immobilization on Rice Husk
Malay Chaudhuri and Mohammed Ali Mohammed 47-54
6. Numerical Computation of Maximum Shear Stress Intensity for a Nearly Circular Crack Subject to Shear Loading
Koo Lee Feng, Nik Mohd Asri Nik Long, Eshkuvatov Zainidin K and Wong Tze Jin 55-64
7. A Study on Plant Selection for Green Building Design
Izudinshah Bin Abd. Wahab and Lokman Hakim Bin Ismail 65-78
8. A Rank Test on Equality of Population Medians
Pooi Ah Hin 79-86
9. Epoxidation of Palm Kernel Oil Fatty Acids
Michelle Ni Fong Fong and Jumat Salimon 87-98

10. Adjustment of an Intensive Care Unit (ICU) Data in Fuzzy C-Regression Models 99-108
Mohd Saifullah Rusiman, Robiah Adnan, Efendi Nasibov, Kavikumar Jacob
11. Thermal and Solutal Mixed Marangoni Boundary Layers with Suction or Injection Effects 109-118
Noraini Ahmad, Seripah Awang Kechil and Norma Mohd Basir

JOURNAL OF SCIENCE AND TECHNOLOGY

EDITOR-IN- CHIEF

Zaidi Embong

Universiti Tun Hussein Onn Malaysia

EDITORIAL BOARD

Rozaini Roslan, Universiti Tun Hussein Onn Malaysia

Mohd Arif Agam, Universiti Tun Hussein Onn Malaysia

Mohd Ambar Yarmo, Universiti Kebangsaan Malaysia

Azman Jalar, Universiti Kebangsaan Malaysia

Abdul Khamim Ismail, Universiti Teknologi Malaysia

YH Taufiq Yap, Universiti Putra Malaysia

Ali Mamat, Universiti Putra Malaysia

Mohd Shukri Hassan, Jabatan Kimia Malaysia

You Wei Yuan, Hangzhou Dianzi University

Maman A. Djauhari, Institute Technology Bandung

Ismail Khalil Ibrahim, Johannes Kepler University Linz, Austria

FOREWORD

The Journal of Science and Technology is a biannual refereed journal which publishes original research papers in areas of science and technology. Research areas include conventional subjects such as Physics, Mathematics, Biology, Chemistry and Computer Science. Papers relating directly or indirectly to all aspects of these fields are welcome. The journal is intended to provide a forum for expression of new ideas, as well as a place for exposition of these areas of knowledge.

We would like to thank the authors for submitting their papers to this journal. We are grateful to the referees for their work in ensuring the high quality of the submissions. Finally, we would like to thank the UTHM Publisher's staff for their help to make this issue possible.

For article submission, please direct to:

Zaidi Embong
Editor-in-Chief
Journal of Science and Technology
Universiti Tun Hussein Onn Malaysia
86400, Batu Pahat,
Johor,
MALAYSIA

High Pressure Processing of Honey: Preliminary Study of Total Microorganism Inactivation and Identification of Bacteria

M.F. Noor Akhmazillah^{1,2*}, M.M. Farid¹, F.V.M. Silva¹

¹Department of Chemical and Materials Engineering, University of Auckland,
Private Bag 92019
Auckland 1142, New Zealand.

² Department of Chemical and Bioprocess Engineering, Faculty of Civil and
Environment Engineering, Universiti Tun Hussein Onn Malaysia, 86400 Parit Raja,
Batu Pahat, Johor, Malaysia.

*Corresponding email: nmoh311@aucklanduni.ac.nz

Abstract

Due to the demand for better quality and safety food as it provides health benefits, the study of innovative high pressure processing (HPP) is currently one of the most interesting researches in food processing and preservation. As an alternative to classical thermal processing, HPP has potential to produce high quality foods that are microbiologically safe with 'fresh-like' characteristics and improved functionalities. In present work, the use of HPP will be investigated for its ability to inactivate bacteria spores, the heat resistance microbes. Preliminary results show that it is possible to use HPP to inactivate microorganisms present in high sugar content foods, particularly in Manuka honey. Further investigation will be carried out to find an optimal combination of treatment pressure, temperature and time. This project will generate a new approach in honey processing which can guarantee the safety of honey without a compromise on its quality and natural freshness.

Keywords: honey; high pressure processing; microorganism inactivation; bacteria

1. INTRODUCTION

Honey is the world's primary sweetener and nature's original sweetener prepared by honey bees. Honey has been used as a food for at least 6000 years. The popularity of honey is largely due to it being a natural sweetener evolved from the nectar mainly consisting of glucose and fructose. The honey in the nutshell is flower nectar which has been collected, regurgitated and dehydrated by honey bees to enhance its nutritional properties and ready to be consumed by humans. The consumption of honey is on the rise due to the unique combination of components in honey which makes it a prized addition to the diet. According to Food and Agriculture Organization of the United Nations (FAO), total honey production in 1961 was 0.7 million tonnes and it was steadily increased to about 1.5 million tonnes in 2009. The demand for high quality honey is attracting a lot of attention as it provides health benefits and has been shown to possess antimicrobial, antiviral, antiparasitary, anti-inflammatory, antioxidant, antimutagenic and antitumor effects [1]. Diseases prevention through consumption of honey is probably due to the presence of more than 181 substances with a wide range of health promoting phytochemicals, some with antioxidant properties. Honey antioxidant compounds include phenolic acids, flavonoids [2] and amino acids. The importance of these honey bioactive compounds and antioxidants on human health therefore generates a great interest in honey processing research.

Although consumption of honey has remarkably increased in the last years all over the world, the safety of this product is not regularly assessed. One common problem faced by honey producers is its deterioration in quality with storage due to fermentation. Yeasts are spoilage microorganisms of concern in honey and have been reported to grow to very high numbers [3]. *Saccharomyces cerevisiae* was found as the dominant yeast fermenting honey, even at the limited level of water available. It is also known as osmophilic or sugar tolerant yeast because it can withstand the low water content (around 16 - 21 %) and high sugar concentration in honey. Food grade, honey with a very high yeast count (more than 100 000 CFU/g) is not likely to be marketable [3]. With respect to medical health applications, yeast count must be less than 500 CFU/g.

Thus, commercial thermal processing of honey is an important operation which potentially eliminates spoilage microorganisms and decreases the moisture content to a level that retards the microbial growth. Additionally, the use of heat is found to be essential at different stages of honey processing for fast handling, to dissolve large sugar granules and to sustain quality. Conventionally, there are two stages of heating applied in the honey industry which are liquefaction and pasteurization. Liquefaction is operated at approximately 55°C and has a purpose to ensure the honey can stay in liquid form for as long as possible for filtering. Pasteurization is done at 60°C and above to inactivate yeast and other spoilage microorganisms. However, heat treatment above 75°C is not suitable because it

causes degradation of bioactive compounds which could affect the quality of the honey. Phenolic compounds were reported as the main honey bioactive compounds which would be negatively affected by the thermal treatment.

High pressure processing (HPP) is a non-thermal treatment which have an optimal effect on product quality and capable to inactivate microorganisms in various food matrices [4]. Although past research has proven that HPP can inactivate most microorganisms such as *Escherichia coli*, *Salmonella sp.*, *Listeria* and *Vibrio* pathogens without additional heat processing in various food matrices [3], it is not known yet if HPP can inactivate bacterial spores and yeasts especially in high sugar content foods. Hence the effect of HPP on inactivation kinetics of bacterial spores should be carried out. There has been no research on the potential application of HPP to obtain higher quality of honey with ‘fresh-like’ characteristics and improved functionalities.

Besides, a combination of HPP and heat has been used to investigate the efficiency of bacterial spore inactivation [5]. Although HPP is termed a nonthermal process, there is a relationship between pressure and temperature in physical compression due to the adiabatic heating caused by fluid compression at high pressure can cause significant temperature distribution throughout the treated food.

Therefore, it is of paramount importance to establish processing conditions which not only can inactivate the spore forming bacteria and yeasts but also be able to preserve the nutritional quality and bioactive compounds present in honey. This research aims at developing the optimum condition of pressure, temperature and processing time for the inactivation of spore forming bacteria and yeasts to ensure the best honey quality and extended shelf life.

This paper reports pre experimental results of HPP inactivation of total microorganism in Manuka honey at different pressure levels and at different treatment time. The identification of bacterial spore which dominantly found in Manuka honey was also investigated.

2. MATERIALS AND METHODS

2.1 Honey Sample and Packaging

Unprocessed Manuka honey used in this study (with pH of 4.3, 79° Brix and water content of 19 %) was kindly donated by honey producer in New Zealand. Manuka Honey is sourced from New Zealand’s remote and pollution free forests. The bees feed of the Manuka plant (*Leptospermum scoparium*) which has delicate pink or white flowers and is native to New Zealand.

Honey of 2 g, in duplicate, were packed in 5 cm x 5 cm transparent plastic film pouches (Cas-pak plastic vacuum pouch, New Zealand) and thermosealed under vacuum. The plastic film is made of cast polypropylene for excellent transparency and heat sealing qualities which can withstand temperatures up to 125 °C.

2.2 High Pressure Processing Equipment

The HPP unit used in this research was 2L- 700 Laboratory Food Processing System (Avure Technologies, Columbus, Ohio, USA). The equipment consists of a 2-L cylindrical shape pressure treatment chamber, water circulation, a pumping system and the control system operated through a computer with software supplied by the manufacturer. Distilled water was used as the medium in the chamber where the honey samples were placed. The equipment can operate at maximum pressure and temperature of 600 MPa and 90 °C, respectively.

2.3 Thermal Treatment

The water bath used for thermal treatment in this research was Water Bath W28 (Grant Instruments (Cambridge, Ltd, England). The capacity of tank is 28 litres and made from stainless steel with an easy to clean, solvent resistant plastics outer case. The control units, which are mounted on a bridge plate, offer digital temperature setting and display. This provides powerful stirring to ensure good temperature uniformity throughout the bath. Each bath can be fitted with a pump allowing temperature controlled liquid to be circulated through external apparatus. The consistent temperatures control over the range 0 to 99.9 °C. For the treatment, the vacuum-sealed samples were placed into the tank fully submerged in the distilled water. In this experiment, the temperature of 60 °C, 70 °C and 80°C were chosen considering the standard temperatures to which honey is exposed in industrial liquefaction and pasteurization processes which is 45 °C and 80°C, respectively [6].

2.4 Preparation of Agar Plates

A 39 g Difco™ Potato Dextrose Agar (PDA) powder form (Fort Richard, Auckland, New Zealand) was weight using analytical balance (Sartorius Germany CP225 D, Germany) and dissolved in 1L of distilled water and autoclaved at 121 °C for 15 minutes (Tomy Autoclave SS-325, Germany). Thereafter, the hot solution was held at 45 °C in water bath. Under controlled environment, laminar flow hood (Airstream ESCO Class II, Biological Safety Cabinet, ACZ 4E1, Germany), the hot solution was then poured into series of petri dish. Once the agar solidified, the cover was inverted to prevent plate contamination due to condensation build during cooling the plates. The plates were then stored under sterile condition at 4 °C for later use.

2.5 Microbial Enumeration

The microbial enumeration in honey samples was determined as for enumeration of yeasts and moulds. Two grams of each sample was mixed and homogenized with 18 mL of saline water (8.5 g/L) to prepare the initial dilution which is used as the mother dilution. A serial dilution 1/100 to 1/100000 of sample was done. Then, 1 mL of each dilution was inoculated onto PDA agar plates were incubated by spread-plating technique. PDA was used for total microbial counts. The plating was done in duplicate for each series of dilution. The inoculated plates were compute using colony counter (Suntex Colony Counter 570, Taiwan). Only plates presenting 30 – 300 colonies were used for analysis. The colonies were counted as CFU/g.

2.6 Microbial Inactivation in Manuka Honey by HPP and Thermal Treatment

After vacuum-packing the samples, the pouches were subjected to HPP (except for the control samples) within pressure range of 250 MPa to 450 MPa, temperature between 20° C to 60 °C and processing time between 3 min to 40 min. These ranges were chosen based on the previous works carried out with honey as well as other high sugar food such as fruit jam. Two replicates of honey samples were carried out for the pressure, temperature and time as designed by Design Expert 8.0.1. The treatment time only includes the holding time and does not include the come up time and the decompression time. Pressure come up times were approximately 1.5 min to reach the desired pressure and the decompression time was < 20 s. The adiabatic heating was observed during pressurization phase. A slight decrease in the chamber temperature was observed in particular at higher pressure. The temperature of the pressure medium (distilled water) during pressure treatment was measured using a thermocouple. After treatment, the samples were immediately in cooled ice water before the microbial enumeration. For the thermal treatment, the vacuum-sealed samples submerged in the hot distilled water. All the honey samples were taken from the same honey batch.

2.7 Identification of Bacteria in Manuka Honey

The identification for the type of bacteria present in Manuka honey was conducted at School of Biological Sciences (SBS), Thomas Building, and The University of Auckland. The bacteria colonies on the agar plate were viewed under light microscope to get an overview of the shape and size. Then, the samples were identified using PCR technique and DNA sequencing. The sequenced DNA from the colonies tested was run through a program called BLAST found on NCBI. The genus and species of the bacteria was then determined. This experiment was successfully done with Prof Richard Gardner and Whitney from SBS.

3. RESULTS AND DISCUSSION

3.1 Microbial Inactivation in Manuka Honey by HPP and Thermal Treatment

Twenty different experimental conditions (pressure, temperature and time) were tested according to Response Surface Methodology design. The results were analysed using Design Expert 8.0.1 software. Five from 20 runs were found to have incomplete inactivation of microorganism in the samples tested.

Treating samples at 300 MPa showed microbial survivors particularly at lower temperature 30 °C, regardless of treatment time, as tabulated in Table 1. However, the microorganisms were totally inactivated when the temperature increased up to 50 °C. The same pattern was found for treatment at 350 MPa. As comparison with Run 1 (350 MPa, 25 °C, 20 min), increasing temperature up to 40 °C with the same pressure and time (as represented in Run 9 – Run 14) shows total inactivation of the microorganisms present in honey samples. Treatment at 270 MPa and 40 °C for 20 min (Run 6) gave the lowest inactivation of microorganism as compared to other treatments. The result also shows that the pressure of more than 350 MPa and temperature above 40 °C is needed to inactivate microorganism present in Manuka honey.

Table 1: Log of microorganism (CFU/g honey) in unprocessed Manuka honey after HPP treatments at different pressure, temperature and time conditions.

Sample Run	Pressure (MPa)	Temp (°C)	Time (min)	log N± SD (N in CFU/g)
Un processed	Atmospheric pressure (0.101)			6.1 ± 0.1
6	270	40	20	4.0 ± 0.1
2	300	30	10	3.1 ± 0.1
3		30	30	3.1 ± 0.1
16		50	10	not detected
17		50	30	not detected
1	350	25	20	3.6 ± 0.1
7		40	3	3.0 ± 0.1
9		40	20	not detected
10		40	20	not detected
11		40	20	not detected
12		40	20	not detected
13		40	20	not detected
14		40	20	not detected
8		40	37	not detected
20		60	20	not detected
4	400	30	10	not detected
5		30	30	not detected
18		50	10	not detected
19		50	30	not detected
15	450	40	20	not detected

Based on the ANOVA analysis of experimental designed, the value of "Prob > F" is 0.008 (less than 0.05), indicates that the pressure and temperature are significant. However, time was found to be insignificant. The 3D model graph in

Figure 1 showed the relationship between pressure and temperature. Increasing the treatment temperature as well as the treatment pressure will reduce the total microorganisms present in the samples.

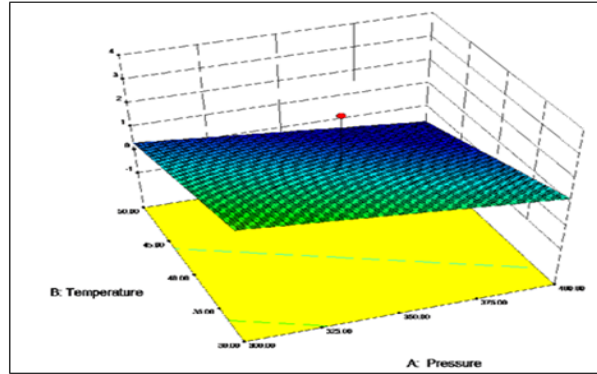


Figure 1: 3-D graph of interaction between treatment temperature and pressure using HPP

Thermal treatment with higher temperature (above 50 °C) was performed. The temperature of 60 °C, 70 °C and 80°C were chosen considering the standard temperatures to which honey is exposed to in industrial liquefaction and pasteurization processes which is 45 °C and 80 °C, respectively [6]. The result obtained shows that as temperature increases, the microorganism levels decrease, even though only a slight decrease in the microorganism numbers was observed particularly at lower temperature, 60 °C. As expected, a higher temperature leads to more microbial inactivation. The log of microorganism survival and their reduction in Manuka honey after being treated at three different temperatures for 30 min were tabulated in Table 2. As shown in the table, the reduction of microorganism counts after treatment at 60 °C, 70 °C and 80 °C were not significant. In addition, the effect of increasing temperatures on the reduction of total microorganism count was also not apparent.

Table 2: Log of microorganism (CFU/g) in Manuka honey after heat-treated with different temperatures for 30 minutes

	log N ± SD (N in CFU/g)	Log reduction N ± SD (N in CFU/g)
Unprocessed	4.0 ± 0.01	
60 °C	3.8 ± 0.01	0.2 ± 0.03
70 °C	3.6 ± 0.02	0.4 ± 0.02
80 °C	3.5 ± 0.05	0.5 ± 0.01

From both HPP and thermal treatment preliminary test, it clearly shows that thermal treatment gave a minor effect on the microbial inactivation as compared with HPP treatment. This has been proven when 60 °C was applied in thermal treatment, the applied heat was not sufficient to inactivate all microorganism (with 3.8 ± 0.01 log CFU/g of microorganism survival), but when 350 MPa was applied in combination with 60 °C, the microorganism in the samples were not detected.

This preliminary result suggests, by using mild heat in combination with high pressure, a higher quality safe and durable honey can be produced. Based on the amount of microorganism surviving after thermal treatment at 80 °C (with 3.5 ± 0.01 log CFU/g), it is necessary to find out what is the species of microorganism present in the samples. The next section was then discuss on the identification of bacterial species.

3.2 Identification of Bacterial Spore in Manuka Honey

The ability of microorganism to survive after heat treatment, even at higher temperature (80 °C for 30 min), leads to the hypothesis that the microorganisms present in Manuka honey were spore forming bacteria. The hypothesis made was based on the characteristics of the bacterial spores which are resistant to high temperature as noted by previous works [3,8]. The bacterial spores are highly resistant to heat compared to vegetative cells due the endospore content.

The identification of microorganism present in Manuka honey started with cultivation of microorganism on Potato Dextrose Agar (PDA) after heat treatment of samples. The plates were then incubated at 25 °C for 5 days. After 5 days incubation, the white and creamy with round shape colonies were observed on the plate agar as shown in Figure 2.

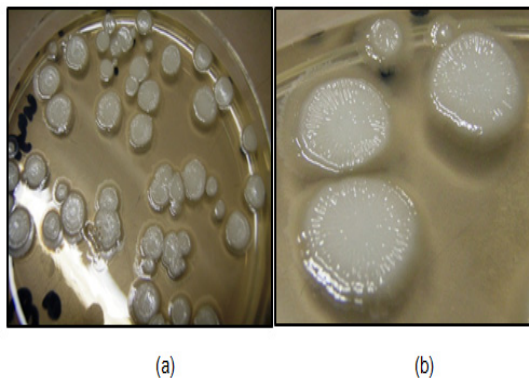


Figure 2: (a) Microorganism colonies found in Manuka honey samples after treated at 80 °C for 30 min and (b) the colonies were well grown on the Potato Dextrose Agar (PDA) after 5 days incubation at 25° C.

The investigation proceeded with a general observation on the shape and size of the bacteria. The colonies were viewed under light microscope by putting drops of distilled water on a glass with needle tip of colony. The glass was then covered on top and under microscope with a drop of emission oil to get a clearer image. The shape and size of colony viewed under light microscope were shown in Figure 3. It was found that the microorganism were in rod-shape, elongated chain with the size of more than 4 μm . [7] revealed the bacteria size was in range from 0.2-2 μm in width or diameter, and up to 1-10 μm in length for the nonspherical species. Thus, this observation gives a clear assumption that the microorganisms were from bacteria due to the size. Regarding to the shape, the observation of rod-shaped with 4- 6 μm long in size, make a closer to the prediction that the bacteria found was in genus *Bacillus*. [7,9] reported the word *bacillus* (plural *bacilli*) is used to describe any rod-shaped bacterium and the size of *bacillus* of about average size 2.0 to 6.0 m long.

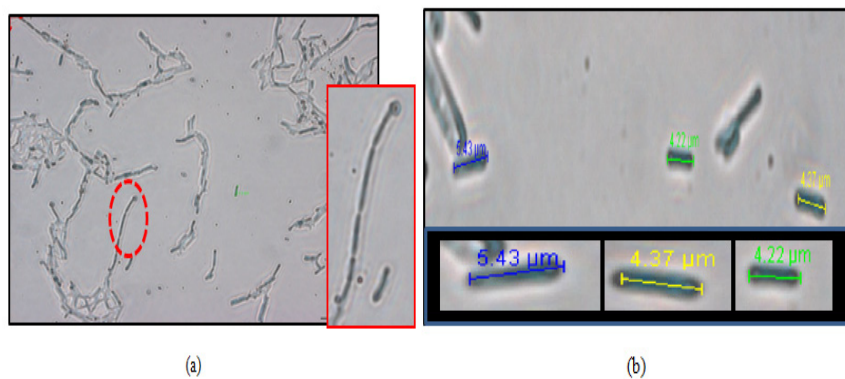


Figure 3: The structure of colony viewed under light microscope (a) shape of the microorganism from the colonies cultivated on the PDA. Small picture shows the clear image of the rod-shaped with elongated chain (b) size of the colonies found were in the range of 4- 6 μm long.

Polymerase Chain Reaction (PCR) technique was then performed together with DNA sequencing in order to get the DNA sequence of targeted bacteria and compare to other known sequences, using BLAST program. This will result in the identification of bacteria genus and species.

A digital of gel electrophoresis for different restrictions digest run on a 1 % w/v agarose agar gel, 3 volt/cm, stained with ethidium bromide was shown in Figure 4. The DNA size marker is a commercial 1 kbp ladder. The position of the wells and direction of DNA migration is noted. In this experiment, yeasts and bacteria markers were used.

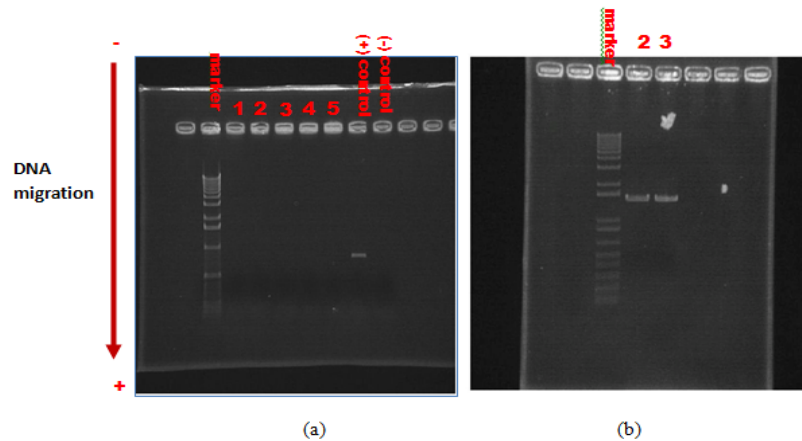


Figure 4: (a) Commercial DNA Yeasts Markers, (b) commercial DNA Bacteria Markers

Figure 4 (a) shows a Commercial DNA Yeasts Markers (1kbplus) in Lane 1, meanwhile Lane 2, 3, 4 and 5 were empty with no bands. Meanwhile, Figure 4 (b) shows another gel electrophoresis using commercial DNA Bacteria Markers (1kbplus) with no positive control this time as it is known they were most probably bacteria. Lane 2 and 3 shows a band showing that the target DNA sequences were compatible with bacteria DNA. From the PCR using 16S primers which amplify the ribosomal DNA from the colonies found on the plates, the sequences have been aligned and were run through a program called BLAST found on NCBI. This gave the result of the colony being a *Bacillus*, most likely the species *cereus*. The same finding was reported in Moroccan honey [10] and Ibadan honey [11]. They found that most of the samples tested were found from genus *Bacillus*. In addition, most of the 94 % spores found in commercial honey samples were from genus *Bacillus* and predominant species was *B. cereus* [12].

4. CONCLUSIONS

It is possible to use HPP to inactivate microorganisms present in high sugar content foods, particularly in Manuka honey. Pressure and temperature are found to be significant parameters that effect the inactivation of microorganism present in honey. The unknown microorganism which was resistant to high temperature (80 °C) in Manuka honey was identified as *Bacillus cereus* using PCR technique. Further works are necessary to find an optimal combination of treatment pressure, temperature and time to ensure the safety of honey without compromising its quality and natural freshness.

Acknowledgement

The financial support from The Ministry of Higher Education of Malaysia and Universiti Tun Hussein Onn Malaysia (UTHM) is gratefully acknowledged. The support of Prof Richard Gardner and Whitney from School Biological Sciences, The University of Auckland is also much appreciated.

REFERENCES

- [1] Alvarez-Suarez, J., et al. (2010) Contribution of honey in nutrition and human health: a review. in *Mediterranean Journal of Nutrition and Metabolism*, Vol. 3. No.1pp. 15-23.
- [2] Socha, R., et al. (2011) , Phenolic profile and antioxidant properties of Polish honeys. *International Journal of Food Science & Technology*. Vol. 46.No.3.pp. 528-534.
- [3] Snowdon, J.A. and D.O. Cliver (1996), Microorganisms in honey. *International Journal of Food Microbiology*, Vol. 31No.1-3.pp. 1-26.
- [4] Butz, P., High Pressure: Minimal Processing. (2010) *Encyclopedia of Agricultural, Food, and Biological Engineering*, New York.
- [5] Norton, T. and Sun D.W (2008), Recent Advances in the Use of High Pressure as an Effective Processing Technique in the Food Industry. *Food and Bioprocess Technology*. Vol.1.No..pp. 2-34.
- [6] Escriche, I., et al., (2009) Influence of simulated industrial thermal treatments on the volatile fractions of different varieties of honey in *Food Chemistry*. Vol. 112No. 2.pp. 329-338.
- [7] Gould, G.W and Hurs., A. *The Bacterial Spore*, (1969), London and New York.
- [8] Nakano, H., et al.,(1992). Detection of *Clostridium botulinum* in natural sweetening. *International Journal of Food Microbiology*. Vol 16. No.2.pp. 117-121.
- [9] Miutrka, B.M. *Methods of Detection and Identification of Bacteria*, (1976),Cleveland, Ohio.

- [10] Naman Malika, Faid Mohamed and El Adlouni Chakib (2005). Microbiological and Physico-Chemical Properties of Moroccan Honey in International Journal of Agriculture & Biology. Vol. 7.pp. 773- 776.
- [11] Adenekan, M.O, Amusa, N.A., Lawal, A.O and Okpeze,V.E. (2010)in Physico-Chemical and Microbiological properties of Honey Samples Obtained from Ibadan. Journal of Microbiology and Antimicrobials.Vol.2 pp. 100-104.
- [12] Kokubo, Y., Jinbo, K., Kaneko, S. and Matsumoto. Prevalence of Spore Forming Bacteria in Commercial Honey. Ann.Rep. Tokyo Metr. Res. Lab. Pub. Health, 1984.(35): 192-196.

Genetically Modified Mosquito: Myth and Reality

Teh Su Yean^{1,*}, Koh Hock Lye² and Yeap Kiew Lee²

¹School of Mathematical Sciences, Universiti Sains Malaysia, 11800 Penang, Malaysia.

²School of Civil Engineering, Universiti Sains Malaysia, Engineering Campus, Seri Ampangan, 14300 Nibong Tebal, Penang, Malaysia.

*Corresponding email: syteh@usm.my

Abstract

Sterile Insect Technique (SIT) has been applied successfully in some agricultural pest control programs in the past, but in many cases, success has not been sustainable in the long run. Various attempts have been made to duplicate this limited success SIT application in agriculture to other areas of applications, particularly in vector control. For example, a recent mosquito control program has been initiated in Malaysia to eliminate dengue-mosquitoes *Aedes aegypti* by releasing large amount of genetically modified GM male mosquitoes into the field to outcompete the wild male mosquitoes. Field experimental data that has been made available in the literature is limited, rendering it difficult to make independent assessment on its short-term efficacy and long-term sustainability of this GM control strategy. This paper presents a preliminary assessment of the effectiveness of GM mosquito in controlling dengue mosquito population by means of model simulations via DEER (Dengue Encephalitis Eradication Routines). Preliminary results indicate negative conclusion regarding the effectiveness of GM mosquitoes in controlling wild *A. aegypti* population over the long-term. Essentially, significant reduction of wild mosquito population is possible only if large over-flooding ratios are applied. Further, repeated releases must be maintained over an infinite time horizon to continue to sustain low population of mosquitoes. Major difficulty remains to be resolved. In particular, in-depth cost-benefit analysis on this control program is essential to ensure long-term institutional and social support.

Keywords: DEER; genetically modified mosquito; simulation

1. INTRODUCTION

Dengue virus is transmitted to human and female mosquitoes through the bites of female *Aedes aegypti* mosquitoes. Dengue has been endemic in Malaysia since 1902. In year 2010, around 43,500 dengue fever cases have been reported with 128 fatalities in Malaysia. Effective prevention strategies could reverse these trends, and vector control aimed at vector reduction and interrupting transmission is seen as a key component of such strategies in the absence of effective vaccine for dengue fever. One such vector control method is the Sterile Insect Technique (SIT). SIT is a species-specific and environmentally nonpolluting method of insect control that relies on the release of large numbers of sterile insects [1,2]. Mating of released sterile males with wild females leads to a decrease in the female's reproductive potential. This eventually would lead to the local elimination or suppression of the pest population if sterile males are released in sufficient numbers over a sufficient period of time. Highly successful, area-wide SIT programs have eliminated or suppressed a range of major veterinary and agricultural pests around the world.

Large rearing facility can produce around 2 billion sterile male Mediterranean fruit flies per week (~20 tons/week). For these agricultural pests, SIT is a proven cost-effective strategy for eradication or suppression of target populations, or to protect areas against invasion or re-invasion. For mosquitoes, the situation is less clear. Field trials in the 1970s and 1980s demonstrated that SIT could also be made to work against mosquitoes, even with the technology then available [3,4]. Recent advances suggest several potential improvements over the methods available in the past. Most current SIT programs use radiation to sterilize the insects. However, it has proven difficult to irradiate mosquitoes to near-complete sterility without significantly weakening them. The field release of a genetically modified (GM) mosquito version of the sterile insect technique (SIT) for *Aedes aegypti* to eliminate the dengue-mosquitoes is recently experimented in Malaysia. The GM mosquitoes being used in these field experiments are *Aedes aegypti* OX513A produced by Oxitec.

The male mosquitoes are genetically modified in such a way that when they breed with wild females, their offspring will die early, leading to reduced wild mosquito population. These field experiments have aroused considerable anxiety among NGOs and concerned scientists, primarily due to the lack of transparency, the absence of meaningful and effective public participation, and the seeming haste in the approval process [5,6,7]. This paper investigates by model simulations the efficacy of controlling natural *Aedes aegypti* mosquito population by the release of GM mosquitoes into the natural habitat.

2. DEER MODEL

The in-house simulation model DEER for mosquitoes is developed based upon adaptation of the concepts contained in the mathematical model (1) – (6) for SIT proposed by Esteva and Yang [8]. The mosquito population is divided into six compartments A , F_s , F_f , F_u , M and M_T (Figure 1). The compartment A consists of immature aquatic form of the mosquito. The adult wing female mosquitoes are divided into three compartments, while the males are divided into two compartments, as required by the concept of SIT. One compartment consists of unmated single females, which is denoted by F_s . Some of these single unmated females remain unmated and therefore remain in F_s , while the remaining singles are mated. The mated females are further divided into two compartments. Those that are fertilized are moved into compartment denoted by F_f , while the unfertilized females are moved to the compartment F_u .

The male mosquitoes are divided into two compartments in order to facilitate modeling the competition between the wild and GM male mosquitoes. Natural male mosquitoes form members of the compartment denoted by M . Finally, the GM male mosquito is grouped into compartment denoted by M_T . This set of compartment notations will be used in this paper. For example, the per capita mortality rates of the immature aquatic form, unmated single females, mated fertilized females, mated unfertilized females, natural male and GM male mosquitoes are denoted by μ_A , μ_s , μ_f , μ_u , μ_M and μ_T , respectively. Other rate constants in this model include the development rate of aquatic forms γ , the mating rate of natural mosquito β , the number of winged GM males released per day α , the oviposition rate of winged fertilized females ϕ , the carrying capacity of aquatic forms C , the proportion of aquatic forms that becomes winged females r , the proportion of winged GM males that are released in adequate places p and the proportion of effective mating rate of winged GM males q . The parameter $\beta_T = pq\beta$ represents the mating rate of winged GM males. The parameter p is related to the proportion of GM males that are released in suitably selected locations and q is related to the proportion of effective mating rate of GM males. The male to female ratio of the adult mosquitoes hatched from eggs is assumed to be 1:1 ($r = 0.5$). The parameter values used in the simulations are summarized in Table 1. Details of the model can be referred to Esteva and Yang [8] and Koh et al. [6].

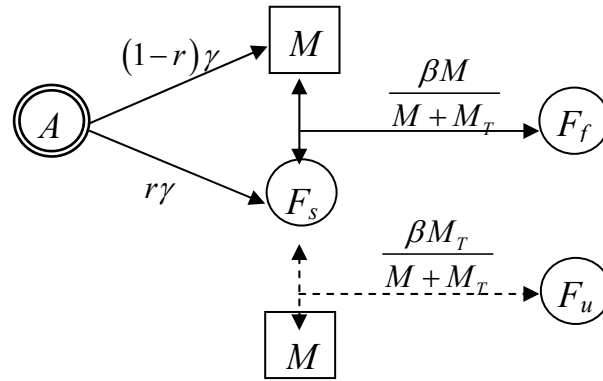


Figure 1: Compartments in DEER model for GM mosquitoes

$$\frac{dA}{dt} = \phi \left(1 - \frac{A}{C} \right) F_f - (\gamma + \mu_A) A \quad (1)$$

$$\frac{dF_s}{dt} = r\gamma A - \frac{\beta M F_s}{M + M_T} - \frac{\beta_T M_T F_s}{M + M_T} - \mu_s F_s \quad (2)$$

$$\frac{dF_f}{dt} = \frac{\beta M F_s}{M + M_T} - \mu_f F_f \quad (3)$$

$$\frac{dF_u}{dt} = \frac{\beta_T M_T F_s}{M + M_T} - \mu_u F_u \quad (4)$$

$$\frac{dM}{dt} = (1-r)\gamma A - \mu_M M \quad (5)$$

$$\frac{dM_T}{dt} = \alpha - \mu_T M_T \quad (6)$$

Table 1: Parameter values used for simulation study [8]

μ_A	μ_s	μ_f	μ_u	μ_M	μ_T
0.05	0.05	0.05	0.05	0.1	0.1
ϕ	γ	r	β	C	pq
5.0	0.075	0.5	1.0	600	0.7

3. RESULTS AND DISCUSSION

3.1 Isolated Release Site

We first consider the case in which the release site is assumed to be completely isolated from its neighbors, with no possibility of wild mosquito recruits coming from neighborhood regions. This scenario is unlikely to prevail. This model scenario represents the most optimal situation for the local success of GM experiments. We consider a one-off release of GM male mosquitoes at simulation time with peak mosquito population. Various one-off release proportions (M_T/F) in increasing order of 1, 10, 100 and 1000 are considered to facilitate the assessment of impact of larger amount of GM release. The proportion M_T/F represents the ratio of the GM male mosquito population to the present total population of female mosquitoes in the simulation site. For example, the proportion $M_T/F = 1$ indicates that the population of GM males released is equal to the present total population of female mosquitoes; while $M_T/F = 10$ indicates that the population of GM males released is ten times the present total population of female mosquitoes. We use the number of aquatic forms scaled to the carrying capacity as a measure of mosquito population.

Figure 2 shows the simulated proportion of aquatic form to its carrying capacity (denoted by A/C). Simulation results indicate that a large one-off release of GM male mosquitoes (of the order of hundreds times the present female mosquito population) will quickly decrease the number of aquatic forms. This is so because most of the aquatic offspring come from female mosquitoes that have mated with GM male mosquitoes, and these will die during the aquatic phase before they can develop into mature form. Hence, the adult form will be decimated. However, without continuous release of GM male mosquitoes after the one-off release, the GM male mosquitoes released into the wild will eventually die. The residual wild mosquito population in the enclosed site will then recover to their normal population levels in the absence of GM males. Of course the time taken to recover to the natural wild population level varies with the one-off release rates. The higher the one-off release rates, the longer will be the time taken to recover to the wild natural state, as higher one-off release rates would decimate the wild population further.

On the other hand, if the GM male mosquitoes are released continuously, the natural mosquitoes will be wiped out eventually as shown in Figure 3 when sufficiently large continuous release rate of GM males is maintained. A continuous release of GM males at a large rate over a long period may not be economically sustainable, however. Cost-benefit analysis must therefore be carefully performed. It should be noted that these simulation results are obtained based upon estimation of the parameter values such as p and q as well as estimated total population of wild mosquitoes at the release site. Under normal field conditions, these parameter values may not be accurately known. Hence controlled field experiments must include these set of parameters to allow reliable assessment of the benefits of GM release.

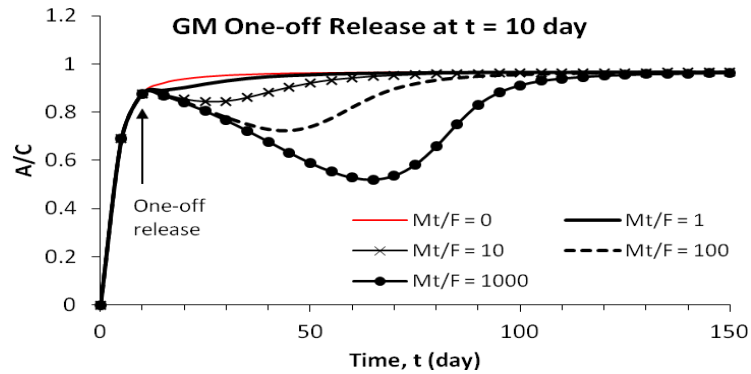


Figure 2: Proportion A/C subject to various one-off release at time $t = 10$ days

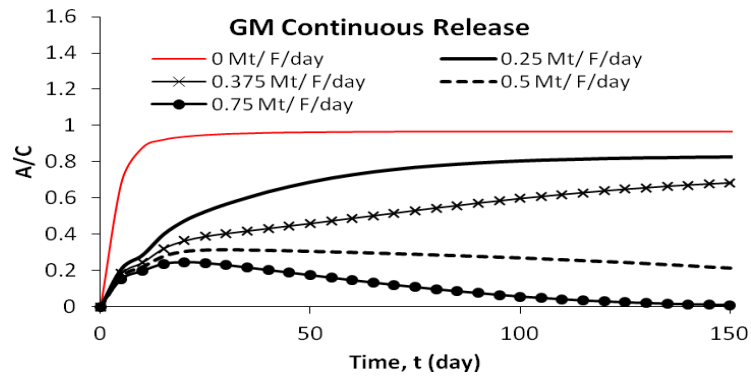


Figure 3: Proportion A/C subject to various continuous release rate

3.2 Natural Release Site

A completely isolated release site is unlikely to prevail as mosquitoes tend to spread over the neighborhoods. Physically connected to neighborhoods, a natural release site is neither completely enclosed nor completely isolated from its neighbors. Hence, spatially-explicit models are needed in order to allow mosquitoes to spread. We enhance the model formulation contained in Equations (1) to (6) into the spatially-explicit framework of DEER to simulate the spatial-temporal distribution of mosquito population subject to GM release [9]. The mosquito population is initiated by a small starting population at location $X = 5$ km in a natural habitat covering a distance of ten kilometers. We assume that the wild mosquito population is zero at the two boundaries, being completely unsuitable for *A. aegypti* mosquitoes (for example, no breeding grounds and blood meals). Given a small starting mosquito population at location $X = 5$ km, the natural mosquito population gradually grows and progressively propagates to the neighborhoods in the natural habitat, in the absence of GM release.

Figure 4 demonstrates the scaled female mosquito population distributed over the distance of 10 km, at five increasing time steps t_1 to t_5 . At each location, the population increases with time, until it reaches the steady state at t_5 . Further, at steady state, the female population gradually decreases near to the computational boundaries, where the conditions are not favorable to mosquitoes. To eradicate the wild mosquito population in this habitat, GM male mosquitoes are released continuously at the location $X = 5$ km at the rate of $0.75 M_T/F/\text{day}$. Figure 5 depicts the spatial distribution of GM male mosquitoes at steady state condition, indicating rapid decrease of GM male population away from the release site.

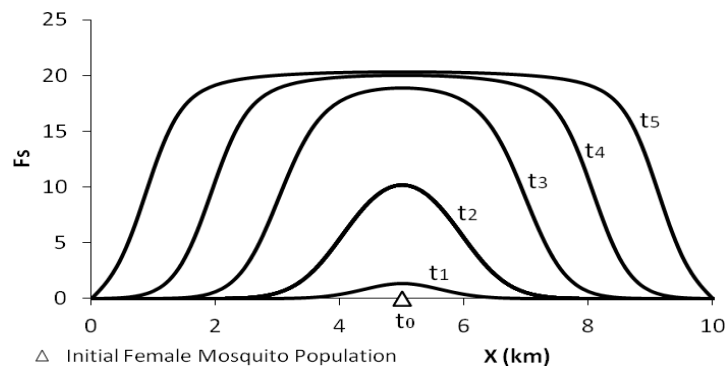


Figure 4: Spatial distribution over time of female mosquitoes in the absence of GM males

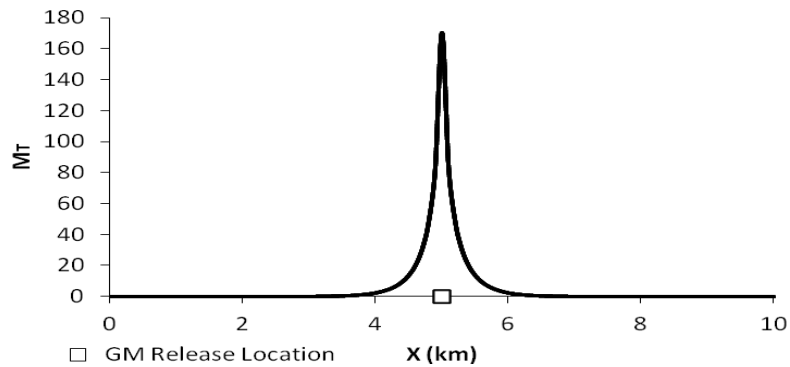


Figure 5: Spatial distribution of GM males with a continuous release ($0.75 M_T/F/\text{day}$) at $X = 5$ km

Figure 6 shows the simulated spatial distribution (over increasing time steps) of females subject to a continuous release of GM males at location $X = 5$ km. Near to the release site, the GM males help to maintain the wild population at low levels as desired. However, wild mosquitoes from adjacent areas gradually invade the GM release site and its neighborhoods. At steady state, female population near to the GM release site has grown significantly. Further, at location barely a few km away from

the release site, the wild populations are hardly affected. The population levels would depend on several key parameters involved in the population dynamics. Yet these key parameters are not accurately known. These simulation results would indicate that the strategy of GM male release to control natural mosquito population is not sustainable in the long run.

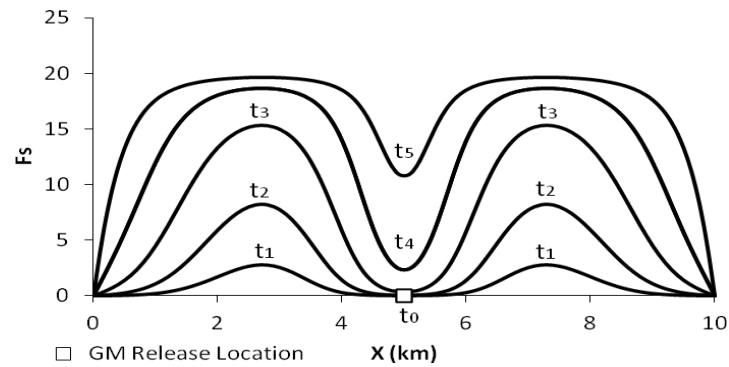


Figure 6: Spatial distribution over time of female mosquitoes subject to continuous release of GM males ($0.75 M_T/F/day$) at $X = 5$ km

4. CONCLUSION

In summary, the proposed GM mosquito release program is not a viable strategy to eradicate natural *A. aegypti* mosquitoes. Significant reduction of wild mosquito population is possible only if large over-flooding ratios are applied. Further, repeated releases must be maintained over an infinite time horizon to continue to sustain low wild mosquito population. Major difficulty remains to be resolved. In particular, in-depth cost-benefit analysis on this control program is essential to ensure long-term institutional support.

Acknowledgement

Financial support provided by Grants 1002/PAWAM/910311, 1001/PAWAM/817024, 1001/PAWAM/817025 and 1001/PMATHS/811093 is gratefully acknowledged.

REFERENCES

- [1] Dyck, V., Hendrichs J. and Robinson, A., eds. (2005). Sterile insect technique: principles and practice in area-wide integrated pest management. Dordrecht, Springer
- [2] Knippling, E. (1955). Possibilities of insect control or eradication through use of sexually sterile males. *Journal of Economic Entomology* 48, 459-462
- [3] Benedict, M.Q. and Robinson, A.S. (2003). The first releases of transgenic mosquitoes: an argument for the sterile insect technique. *Trends in Parasitology* 19, 349-355. PMID:12901936 doi:10.1016/S1471-4922(03)00144-2.
- [4] Klassen W. and Curtis C. (2005). History of the sterile insect technique, In: Dyck V, Hendrichs J, Robinson A, eds. Sterile insect technique: principles and practice in area-wide integrated pest management. Dordrecht, Springer 3-36.
- [5] CAP (2010). Memorandum-Malaysia's GM Aedes mosquito planned release: ethical, legal and human rights concerns. Consumers' Association of Penang, 59 p.
- [6] Koh, H.L., Teh, S.Y., DeAngelis, D.L. and Jiang, J. (2011). Infectious diseases: surveillance, genetic modification and simulation. In: Disaster Management and Human Health Risk Proceedings of the Disaster Management II.
- [7] WHO/TDR (2010). Progress and prospects for the use of genetically-modified mosquitoes to inhibit disease transmission. Report on planning meeting 1: Technical consultation on current status and planning for future development of genetically-modified mosquitoes for malaria and dengue control, 4-6 May 2009, Geneva, Switzerland. WHO/TDR publications10.2471/TDR.10.978-924-1599238. ISBN 978-92-4-159923-8.
- [8] Esteva, L. and Yang, H.M. (2005). Mathematical model to assess the control of *Aedes aegypti* mosquitoes by the sterile insect technique. *Mathematical Biosciences* 198, 132-147.
- [9] Takahashi, L.T., Maidana, N.A., Ferreira Jr., W.C., Pulino, P. and Yang, H.M. (2005). Mathematical models for the *Aedes aegypti* dispersal dynamics: travelling waves by wing and wind. *Bulletin of Mathematical Biology* 67(3), 509–528.

Kenaf Core Particleboard and Its Sound Absorbing Properties

Mohamad Jani Saad^{1,*} and Izran Kamal²

¹Rice and Industrial Crops Research Center, Malaysian Agriculture Research and Development Institute (MARDI) 43400 Serdang, Selangor Darul Ehsan

²Advanced Processing and Design Programme, Forest Research Institute Malaysia (FRIM), 52109 Kepong, Selangor Darul Ehsan

*Corresponding email: jani@mardi.gov.my

Abstract

In this study, kenaf (*Hibiscus cannabinus*) core particleboards as insulation boards were manufactured. The boards were fabricated with three different densities i.e. 350 kg/m³, 450 kg/m³ and 550 kg/m³ at urea formaldehyde resin (UF) loadings of 8%, 10% and 12% (w/w) based on the dry weight of the kenaf core particles. The fabricated boards were evaluated for its noise acoustical coefficients (NAC) by following the ASTM E1050-98 standard requirements. The study revealed that boards with higher kenaf fiber loading and UF loading gave less NAC.

Keywords: *hibiscus cannabinus*; density; urea formaldehyde

1. INTRODUCTION

In recent years, natural fibers are increasingly being used in many products such as biocomposite products, automotive lining components as well as acoustic absorption barriers. In Malaysia, there is plenty of agricultural waste like coconut trunk (*Cocos nucifera*), rice straw and husk (*Oryza sativa*) and oil palm trunk and empty fruit bunch (*Elaeis guineensis*). Researches have revealed that actually these wastes are not really wastes because they can become sources of natural fibers. The natural fibers obtained from the wastes can be modified into useful products with technologies. There are a lot of advantages possessed by natural fibers such as: renewable, non-abrasive, cheaper, abundance and less health and safety concern during handling and processing [1, 2]. The findings have evoked a mindset that everything that we thought wastes are actually useful and should not be thrown away just like that. We just have to find ways to modify them to something more useful.

Researches to find alternative materials to be utilized in the making of acoustical panel especially in the reduction of noise level have been extensively conducted. The common acoustical panels are made from synthetic fibers such as glass fiber and known to be hazardous to our health as well as to the environment. Fabrication of products from the material is also quite expensive and costly. Due to that, more attention has been given to natural fibers as alternative materials in order to produce products with a combination of high acoustic and thermal properties but with less impact to the environment and human health. Natural fibers are chosen to be alternative materials because they have very low toxicity which is good to protect the environment [3].

Previous researches have confirmed that there are some natural fibers which have high potential to be applied as alternative materials of sound absorbing materials. Paddy straw was reported suitable for acoustic panel because of its high elasticity and porosity [4, 5]. A single layer acoustical panel from paddy husk reinforced with sodium silicate showed that the optimum sound absorption coefficient happened at higher silicate content under high range frequencies [6]. Coconut coir has shown good sound absorption under higher frequencies but inferior performance was observed under lower frequencies. An oil palm fibre has showed the high noise absorption due to its higher density [2, 7].

Among the alternative resources, crop like kenaf is more considerable for that purpose because of its fiber properties, especially its bast fibers (outer fibers) which are low cost, low density, good toughness, suitable for recycling, acceptable strength properties and biodegradability [8]. In Malaysia, Kenaf is still new, however, promotions to encourage acceptance upon it among Malaysians, is given fairly great. Kenaf is a warm season annual fiber crop closely related to cotton (*Gossypium hirsutum L., Malvaceae*) and okra (*Abelmoschus esculentus L., Malvaceae*) [9]. Two of the potential advantages that this crop possess are the ability to grow fast as well

as the two types of fibers it has i.e. bast (outer part) and core (inner part) which can be utilized as raw materials for the production of paper products, building materials, absorbents, textiles and livestock feed [10]. Kenaf is able to reach a height of 3 to 5 m within a period of 3 to 5 months, depending on the environment condition of the place it is planted. Kenaf is able to supply between 12 and 25 t/ha of biomass annually, when it is planted under warm and wet conditions [10].

The kenaf core is light and porous, having a bulk density of 0.10-0.20 g/cm³. It can be crushed into light-weight particles. Currently, kenaf core has received less attention compared to bast in paper and bio composite industries, even though numbers of researches have revealed that kenaf core is useful to produce insulation composites [10, 11], medium-density particleboards [12, 13], fire retardant-treated particleboards [12,13,16], polymer composite [21], thermo-acoustic applications and sound barriers (17-18).

Until now, urea formaldehyde resin (UF) remains as one of the most popular resins in composites industry despite the introduction of many advanced resins. The advantages that this conventional resin possesses are low cost, ease of use under a wide variety of curing conditions, low cure temperature, water solubility, and resistance to microorganisms and to abrasion, hardness, and excellent thermal properties (19).

In this study, kenaf core was used because it is low density and has absorbency advantage. The kenaf core was used to produce kenaf core particleboards. The particleboards then were tested for their acoustical property (the sound absorption coefficients) with regards to different resin content to fabricate the particleboards.

2. MATERIALS AND METHODS

2.1 Materials

Four-month old kenaf were harvested at the Kenaf Research Plot of MARDI Serdang, Selangor, Malaysia. Only kenaf stalks of the harvested kenaf were brought to the workshop for further processing. The kenaf core fibers were separated from the bast fibres using a decorticating machine. The separated kenaf core is in chip form. Then the kenaf core chips were flaked to a particle size of between 2-3 mm using Pallmann PHT 120/430 knife ring flaker. The particles were then dried in an oven at a temperature of 70⁰C for two days to achieve 5% moisture content (MC).

Urea formaldehyde (UF) resin at 64% solid content was used as a composites binder. The binder was added with 10% (wt) ammonium chloride solution as a

hardener and 1% (wt) of wax to prevent the produced composites from absorbing moisture excessively from the surrounding.

2.2 Sample Preparation

The kenaf core particles were mixed with the resin using a blender machine. Three percentages of resin loadings were used to mix with the particles separately i.e. 8%, 10% and 12%. Each of the resin loading was based on the oven dry weight of the kenaf core particles. The targeted board densities were 350 kg/m^3 , 450 kg/m^3 and 550 kg/m^3 . The particles and the resin were mixed approximately in the blender for 5 min to ensure that the particles are evenly mixed with the resin.

After the mixing process, the kenaf particles were brought out from the mixer and were scattered in a rectangular-shaped former with a dimension of 340×340 mm, which was first placed on a caul plate covered with a teflon fiber sheet. The furnish (kenaf particles + resin) was pre-pressed in the cold press at a pressure of 35 kg/cm^2 and subsequently pressed in the hot press machine model Taihei to 12 mm thickness at a temperature of 170°C for 6 min. And then, the particleboards were exposed to the surrounding to reduce the temperature of the pressed particleboard and encourage the resin to cure.

Two different diameters in a circle shape were cut from kenaf particleboard and used to cover the full frequency range. Sample with 100 mm diameter was used to measure the frequency range from 125-1600 Hz and 28 mm diameter was used to measure the frequency range of 1200-6000 Hz.



Figure 1: The circle shape of kenaf particleboard for NAC test

2.3 Testing procedures

All samples were kept in a conditioning room which was set at a temperature of $20 \pm 2^\circ\text{C}$ and $65 \pm 5\%$ RH for 3 days prior to the mechanical and acoustic tests. The conditioning was to ensure that the resin in the particleboards have cured uniformly.

To determine the acoustical property of the composites, the sound absorption coefficients were determined by the impedance tube method in accordance with ASTM E1050-98. The test was done by placing a loudspeaker at one end of an impedance tube and the other end of the tube was placed with the testing sample. The loudspeaker generates broadband, stationary random sound waves. The sound waves propagate within the tube strike between the sample and the sound source and they are reflected as standing wave interference pattern on the computer screen. The acoustic absorption coefficient (α) is defined as the ratio of the acoustic energy absorbed by the PB ($I_{\text{incident}} - I_{\text{reflected}}$) to the acoustic energy incident (I_{incident}) on the surface and it depends on the frequency range. The frequency range for testing was 125 – 6000 Hz. The equipment used for the test was as in Figure 1.



Figure 2: The impedance tube gadget for acoustic analysis

3. RESULT AND DISCUSSION

3.1 Effects of Resin Loading

The effects of the resin loading to the noise absorption coefficient (NAC) are stipulated in the Figure 3, 4 and 5. All figures showed the increase of mean NAC values at lower frequency range (125-1000 Hz) and reached the optimum mean NAC value at 3000 Hz and it decreased gradually after 3000 Hz until 6000 Hz. From the study, it was found that UF loading has given no effects to the NAC values as shown in Figure 3, 4 and 5. Board density of 550 kg/m³ at the frequency below 1000 Hz has revealed that the highest mean NAC value (0.054 - 0.15) was recorded from particleboards loaded with 10% UF loading (Figure 3).

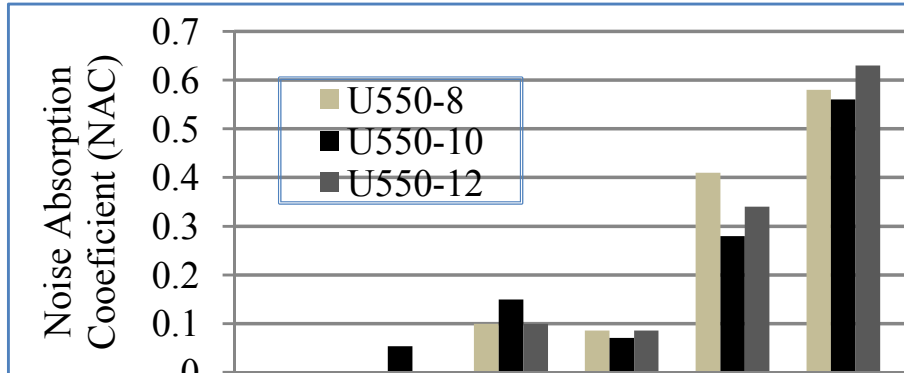


Figure 3: Sound Absorption Coefficient versus Frequency of Kenaf Core Particleboard at a Density of 550 kg/m³ with different UF loading

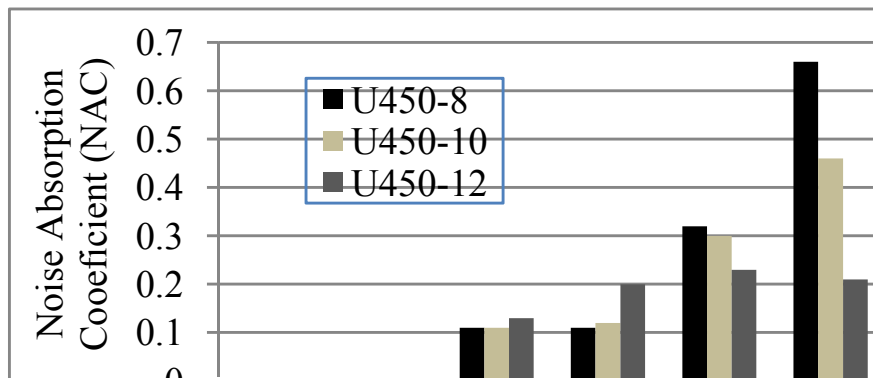


Figure 4: Sound Absorption Coefficient versus Frequency of Kenaf Core Particleboard at Density of 450 kg/m³ and Variable UF loading

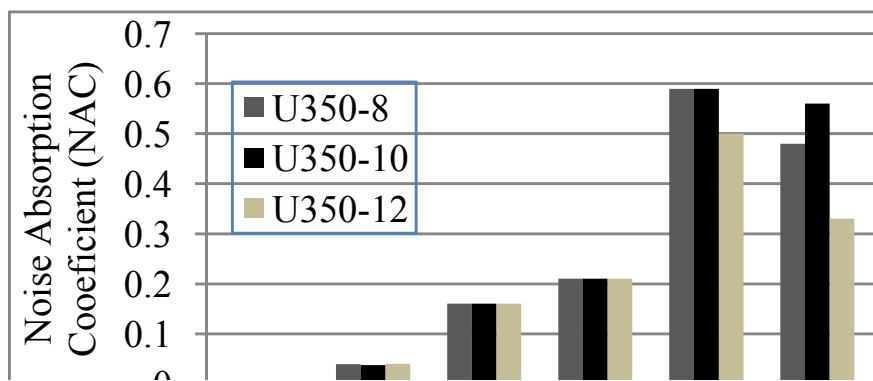


Figure 5: Sound Absorption Coefficient versus Frequency of Kenaf Core Particleboard at Density of 350 kg/m³ with different UF loading

UF loading at 8% showed the best NAC (0.41) compared to the other UF loading at the frequency of 2000 Hz. As for UF loading at 12%, the maximum mean NAC value (0.63) was reached at the frequency of 3000 Hz. Meanwhile, for 4000 Hz frequency, only boards fabricated with 10% UF loading were able to reach the highest mean NAC value (0.23-0.36). There was no mean NAC values recorded for all boards when the frequency was increased from 5000 to 6000 Hz.

Figure 4 demonstrated that the higher UF loading at 12% exhibited the higher NAC (0.1-0.2) in the lower frequency compared to the other UF loadings but then it became constant in the NAC range of 0.2-0.24 in the medium frequency (1000 Hz – 2000 Hz). Meanwhile, UF loading at 8% showed the optimum NAC (0.66) at the 3000 Hz and the mean NAC value remained high (0.29-0.37) at 4000 Hz until 6000 Hz.

There were same values revealed in the low frequency among the three UF loadings as in Figure 5. In the medium and high frequencies which are 2000 Hz until 6000 Hz, UF 10% gave the highest mean NAC value followed by UF 8% and UF 12%.

Kenaf fiber tested with NAC test was found to increase its NAC value from the low frequency (100 Hz – 800 Hz) until it reached the optimum NAC of 0.91 in the frequency range of 1000 Hz – 1600 Hz and later its NAC decreased and maintained around 0.83-0.84 in the range of 2000 Hz – 5000 Hz [3].

3.2 Effects of Kenaf Loading

The effects of kenaf core loading to the NAC value are presented in Figure 6, 7 and 8. Generally, Figure 6 (all boards manufactured with 8% UF loading) have exhibited that boards with the lower kenaf loading are the best noise absorbers. Both low and high frequencies have demonstrated that kenaf boards at 350 kg/m³ density was having the best mean NAC value compared to kenaf boards with densities at 450 kg/m³ or 550 kg/m³. Similar trend was observed in Figure 7 and 8 for boards of 10% and 12% UF loading, respectively.

Porous sound absorbing materials have good acoustic insulating properties over a wide frequency range. The larger the pores, the better the acoustic insulation. Kenaf boards at the densities of 400 kg/m³ and 600 kg/m³ have presented higher sound absorption coefficients than 800 kg/m³ in the 500-8000 Hz frequency range. These might due to the porosity of the lower density boards which was greater than denser boards. It is believed that in the boards with the density of 800 kg/m³, many of the pores (voids) are filled with the kenaf particles, thus have reduced the total pore volume of the board. Even though the mechanical properties of the boards have improved but reduction was observed on the sound absorption coefficient [20].

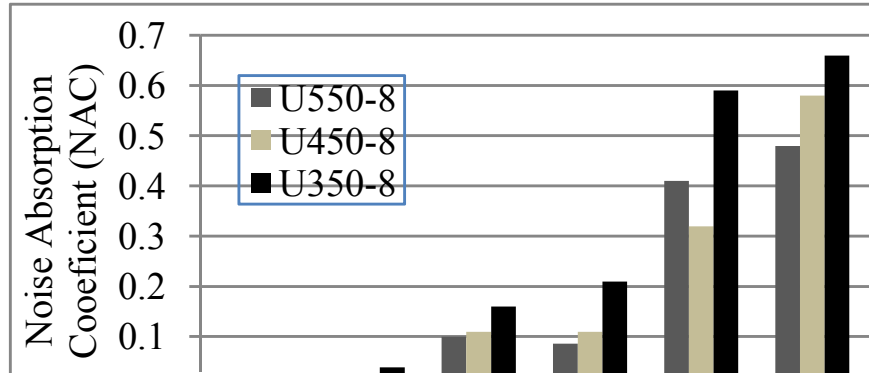


Figure 6: Sound Absorption Coefficient versus Frequency of Kenaf Core Particleboard at UF Loading of 8% and Variable Board Density

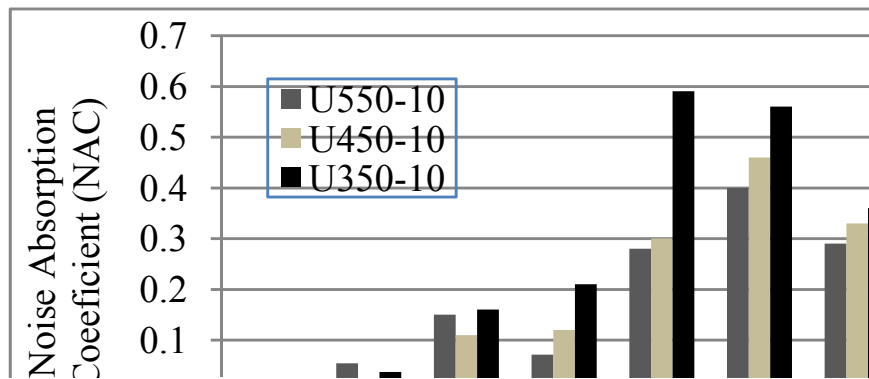


Figure 7: Sound Absorption Coefficient versus Frequency of Kenaf Core Particleboard at UF Loading of 10% and Variable Board Density

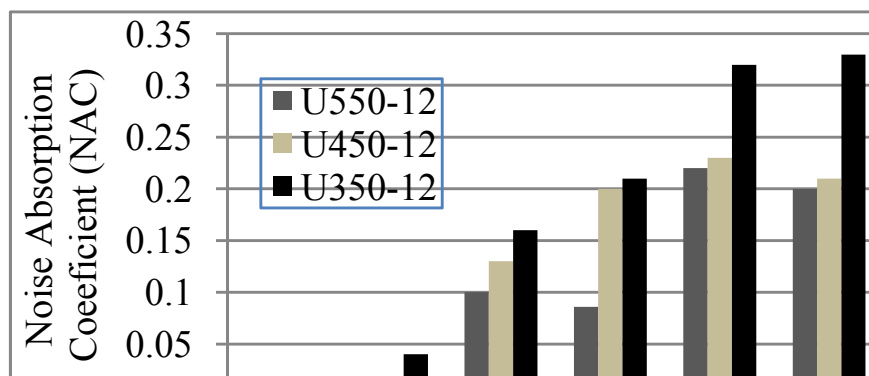


Figure 8: Sound Absorption Coefficient versus Frequency of Kenaf Core Particleboard at UF Loading of 12% and Variable Board Density

Fiberboard, particleboard and plywood have shown a decrease of NAC value as the frequency increased due to their specific characteristic of absorbing sound in the low frequency range but reflecting sound in the middle and high frequency ranges [20].

Commercial insulation materials are made of glass fiber, glass foam and others toxic materials which are noxious to human beings and cause environmental problem. Kenaf core PB can solve this problem. It was not noxious, product that can be renewable and biodegradable.

Sound absorption coefficient of rice straw – wood particle composite boards are higher than other wood – based materials in the 500-8000 Hz frequency range, which is caused by the low specific gravity of composite boards, which are more porous than other wood – based materials [20].

4. CONCLUSIONS

This study shows by using the impedance tube test method to determine noise absorption coefficients of kenaf core particleboards have been successfully carried out. Influence of UF adhesive and the kenaf content were detected on the boards. Results show the NAC of board containing of 8% and 10% are found the best noise absorber rather than 12% UF loading. It was found in the low, medium or even in the high noise frequencies. Board at the 350 kg/m³ density absorbed more noise might be due to its better porosity behavior which able to reduce noise interference

REFERENCES

- [1] Abdul Razak, M.A., Khoo, K.C., and Khozirah, S. 1988. Prospects and Potential Of The Oil Palm Trunk as a Source Of Lignocellulosic Raw Material, *The Malayan Forester*, Vol 51(3):164-175.
- [2] Zulkifli, R., Mohd Nor, M.J., Ismail, A.R., Nuawi, M.Z., Abdullah, S., Mat Tahir, M.F., Ab Rahman, M.N.2009. Comparison properties between coir fibre and oil palm fibre. *European Journal of Scientific Research*. Vol. 33, No 1, pp 144-152.
- [3] D'Alessandro, F. and Pispola G. 2005. *Sound absorption properties of sustainable fibrous materials in an enhanced reverberation room*. Paper presented in The 2005 Congress and Exposition on Noise Control Engineering. Rio de Janeiro, Brazil. 07-10 August.

- [4] Christina E., Mediastika. 2007. *Potential of Paddy Straw as Material Raw of Acoustic Panel*. Architecture Dimension, Vol 35, No 2. Pp 183-189.
- [5] Christina E., Mediastika. 2008. *Paddy Straw as Walling Panel*. Architecture Dimension, Vol 36, No 1. Pp 20-27.
- [6] Fahmi, R. 2006. *Develop single layer acoustic sample made of paddy husk and normal absorption characteristics*. Institut Teknologi Bandung: Undergraduate Theses.
- [7] Zulkifli R., et al. 2009. Effect of perforated size and air gap thickness on acoustic properties of coir fiber sound absorption. *European Journal of Scientific Research*. Vol. 28, No 1, pp 242-252.
- [8] Xue, Y., Du, Y., Elder, S., Devin, S., Horstemeyer, M., and Zhang, J. 2007. *Statistical Tensile Properties of Kenaf Fibres and Its Composites*, 9th International Conference on Wood & Biofiber Plastic Composite, 22 May 2007, Mississippi State University, Available online: <http://www.forestprod.org/woodfiber07xue.pdf>.
- [9] Charles, L.W., Venita, K.B., and Robert, E.B., 2002. *Kenaf harvesting and processing*. ASHS Press, Alexandria, VA.
- [10] Charles, W., and Bledsoe, V.K., 2001. *Kenaf yield components and plant composition*. National symposium on new crops and new uses. Sunnyville ave, USA.
- [11] Sheikkariem, A.R. 2000. *Properties of particle-based panels from kenaf, wood, and sugarcane residues bonded with modified adhesive systems*. M.S. dissertation, P: 10-41. Louisiana State University library, Baton Rouge, LA.
- [12] Charles, W., R. Charles, B. Robert and B. Judy. 1998. Production properties of industrial Grade kenaf particleboard. <http://www.nal.usda.gov/ttic/tektran/data/000009/15/0000091567.html>.
- [13] Grogoriou, A., C. Passialis and E. Voulgaridis. 2000. Experimental particleboard from kenaf plantations grown in Greece. *Holz als Roh-und Werkstoff*, 58: 309-314.
- [14] Izran, K., Zaidon, A., Abdul Rashid, A.M., Abood, F., Mohamad Jani, S., 2009a. Fire Propagation and Strength Performance of Fire Retardant-Treated *Hibiscus cannabinus* Particleboard, *Asian Journal of Applied Sciences* 2:446-455.

- [15] Izran, K. Abdul Rashid, A.M., Mohd Nor, M.Y., Khairul, M., Zaidon, A. and Abood, F. 2009b. Physical and Mechanical Properties of Flame Retardant-Treated *Hibiscus cannabinus* Particleboard, *Journal of Modern Applied Science* 3(8):1-8.
- [16] Izran, K., Zaidon, A., Abdul Rashid, A.M., Abood, F., Mohd. Nor, M.Y., Nor Yuziah, M.Y., MohdZharif, A.T and Khairul, M. 2009c. *Potential of Flame Retardant-Treated Hibiscus cannabinus Particleboard as Furniture Input*, poster presented at Seminar on Wooden Furniture Industry, Forest Research Institute Malaysia.
- [17] Xu, J., Sugawara, R., Widyorini, R., Han, G., Kawai, S. 2009. Manufacture and properties of low density binder less particleboard from kenaf core. *Journal of Wood Science*. Vol 50: 62-67. Tormos, D.R., Romina, Fernandes, A. R., Vicente, S.J. 2007. *Proposal an empirical model for absorbent acoustical materials based in kenaf*. 19th International congress on acoustics. Madrid, Spain.
- [18] Anthony, H.C., 1996 *Urea formaldehyde adhesives resins*. Forest Product Laboratory, USDA Forest Service.
- [19] Yang, H.S., Kim, D.J., and Kim, H.J., 2003. Rice straw – wood particle composite for sound absorbing wooden construction material, *Bioresource Technology*, Vol. 86: 117.

Numerical Solution of Mixed Convection Flow about a Sphere in a Porous Medium Saturated by a Nanofluid: Brinkman Model

Leony Tham¹, Roslinda Nazar^{2,*}

¹ Faculty of Agro Industry and Natural Resources, Universiti Malaysia Kelantan, 16100 Pengkalan Chepa, Kota Bharu, Kelantan, Malaysia

² School of Mathematical Sciences, Faculty of Science & Technology, Universiti Kebangsaan Malaysia, 43600 UKM Bangi, Selangor, Malaysia

*Corresponding e-mail: rmn@ukm.my

Abstract

In the present study, the steady mixed convection boundary layer flow about a solid sphere with a constant surface temperature and embedded in a porous medium saturated by a nanofluid has been investigated via the Brinkman model for both the assisting and opposing flow cases. The resulting system of nonlinear boundary layer equations in the form of partial differential equations is solved numerically using an implicit finite-difference scheme known as the Keller-box method. Numerical results are obtained and discussed for the skin friction coefficient, local Nusselt number, local Sherwood number, velocity profiles, temperature profiles and nanoparticle volume fraction profiles. These results are presented for different values of the governing parameters, namely the mixed convection parameter and the Darcy-Brinkman parameter. It is found that the boundary layer separates from the sphere for some negative values of the mixed convection parameter (opposing flow). Increasing the mixed convection parameter delays the boundary layer separation and the separation can be completely suppressed for sufficiently large values of the mixed convection parameter.

Keywords: numerical solution; mixed convection flow; porous medium; nanofluid; brinkman model

1. INTRODUCTION

The “nanofluid” term was defined as the dilution of nanometer-sized particles (smaller than 100nm) in a fluid such as water, ethylene glycol and oil [1]. According to Khanafer et al., as the diluted nanoparticles size is extremely small, they can easily flow smoothly through the microchannels, and could improve the thermal conductivity and convective heat transfer coefficient compared to the base fluid only, and as such, nanofluids are widely used as coolants, lubricants and heat exchangers [2]. The utility of a particular nanofluid as a heat transfer medium can be established by modelling the convective transport in such nanofluid [3]. Meanwhile, Buongiorno and Hu considered a study on the convective transport in nanofluids and concluded that turbulence is not affected by the presence of the nanoparticles [4]. A comprehensive study on the nanofluids characteristics had also been well documented by Das et al. [5].

Convective heat transfer in porous medium is important in thermal engineering applications, such as geophysical thermal and insulation engineering, chemical catalytic reactors, ceramic processes, fiber and granular insulations and petroleum reservoirs. Many studies have been performed by Nield and Bejan [6] and Ingham and Pop [7], which focused on the free and mixed convection in porous media based on Darcy’s law and Forschheimer’s law, an extended Darcy’s law models. However, as Darcy’s law neglected the viscous force involved in convection heat transfer, and is only valid for slow viscous flow, that is with Reynolds number less than 1 cases, as such, Brinkman [8] introduced another Darcy’s extended law, the Brinkman model, which suggested that the momentum equation for a porous medium flow with a high permeability must be reduced to the viscous flow limit and advocated that classical frictional term to be included in the Darcy’s law. Further, the Brinkman model for the forced convection over an impermeable heated plate embedded in a porous medium was studied by Vafai and Tien [9] and they pointed that the viscous effect on the surface and the bulk viscous forces are equally important. Nazar et al. [10] considered the Brinkman model for the mixed convection boundary layer flow from a horizontal circular cylinder embedded in a fluid-saturated porous medium, and concluded that the results for the Brinkman model differed significantly than the results for Darcy’s law model, and the increased of the Darcy-Brinkman parameter led to the decreased of the surface heat transfer and the skin friction coefficient.

In this paper, the nanofluids equation model proposed by Buongiorno [11] and the transformations proposed by Nazar et al. [10] for the mixed convection boundary layer flow about a solid sphere immersed in a viscous (non-porous) and incompressible fluid are adopted to study the problem of mixed convection boundary layer flow about a solid sphere embedded in a porous medium saturated by a nanofluid using the Brinkman model.

2. ANALYSIS

Consider the steady mixed convection boundary layer flow about an impermeable solid sphere of radius a embedded in a porous medium filled with a nanofluid. It is assumed that the constant surface temperature of the sphere is T_w , while the constant ambient temperature is T_∞ , where $T_w > T_\infty$ for a heated sphere (assisting flow) and $T_w < T_\infty$ for a cooled sphere (opposing flow). It is also assumed that the velocity of the external flow (inviscid flow) or the local free stream velocity is $U_e(x)$, where x is the coordinate measured along the surface of the sphere starting from the lower stagnation point. It is assumed that the nanoparticles are suspended in the nanofluid using either surfactant or surface charge technology. We consider a porous medium whose porosity is denoted by ϕ and permeability by K . Under these assumptions along with the Oberbeck-Boussinesq approximation and the basic equations for the steady flow, we obtain the following boundary layer equations for the problem under consideration in dimensionless[12] form:

$$\frac{\partial(ru)}{\partial x} + \frac{\partial(rv)}{\partial y} = 0, \quad (1)$$

$$\frac{\partial u}{\partial y} = \Gamma \frac{\partial^3 u}{\partial y^3} + \left(\frac{\partial \theta}{\partial y} - Nr \frac{\partial \phi}{\partial y} \right) \lambda \sin x, \quad (2)$$

$$u \frac{\partial \theta}{\partial x} + v \frac{\partial \theta}{\partial y} = \frac{\partial^2 \theta}{\partial y^2} + Nb \frac{\partial \phi}{\partial y} \frac{\partial \theta}{\partial y} + Nt \left(\frac{\partial \theta}{\partial y} \right)^2, \quad (3)$$

$$Le \left(u \frac{\partial \phi}{\partial x} + v \frac{\partial \phi}{\partial y} \right) = \frac{\partial^2 \phi}{\partial y^2} + \frac{Nt}{Nb} \frac{\partial^2 \theta}{\partial y^2}, \quad (4)$$

with the boundary conditions

$$\begin{aligned} v = 0, \quad u = 0, \quad \theta = 1, \quad \phi = 1 \quad \text{at} \quad y = 0, \\ u \rightarrow u_e(x), \quad \theta \rightarrow 0, \quad \phi \rightarrow 0 \quad \text{as} \quad y \rightarrow \infty, \end{aligned} \quad (5)$$

where we assume that $u_e(x) = (3/2)\sin x$. Here θ and ϕ are the dimensionless temperature and nanoparticle volume fraction, respectively, $r(x)$ is the radial distance from the symmetrical axis to the surface of the sphere, Γ is the Darcy-Brinkman parameter, Le is the Lewis number, λ is the mixed convection parameter, Nr is the buoyancy ratio parameter, Nb is the Brownian motion parameter and Nt is the thermophoresis parameter, which are defined as

$$\begin{aligned} \Gamma = \frac{\tilde{\mu}}{\mu_f} Da Pe, \quad Le = \frac{\alpha_m}{\phi D_B}, \quad \lambda = \frac{Ra}{Pe}, \quad Nr = \frac{(\rho_p - \rho_{f\infty})(C_w - C_\infty)}{\rho_{f\infty} \beta (T_w - T_\infty)(1 - C_\infty)}, \\ Nb = \frac{\phi(\rho c)_p D_B (C_w - C_\infty)}{(\rho c)_f \alpha_m}, \quad Nt = \frac{\phi(\rho c)_p D_T (T_w - T_\infty)}{(\rho c)_f \alpha_m T_\infty}, \end{aligned} \quad (6)$$

with $\phi = \mu_f / \tilde{\mu}$, $Da = K/a^2$ and $Ra = (1-C_\infty)gK\beta(T_w-T_\infty)a/(v_f \alpha_m)$ being the porosity, the Darcy and the modified Rayleigh numbers for the porous medium, respectively, and v_f is the kinematic viscosity of the fluid. It is worth mentioning that $\lambda > 0$ is for the assisting flow ($T_w > T_\infty$), $\lambda < 0$ for the opposing flow ($T_w < T_\infty$) and $\lambda = 0$ corresponds to the forced convection flow.

Integrating equation (2) with the boundary conditions (5) at $y \rightarrow \infty$, introducing the stream function ψ , which is defined such that $u = \partial\psi / \partial y$ and $v = -\partial\psi / \partial x$, and introducing the variables $\psi = x r(x)f(x, y)$, $\theta = \theta(x, y)$, $\phi = \phi(x, y)$, we obtain

$$\frac{\partial f}{\partial y} = \Gamma \frac{\partial^3 f}{\partial y^3} + \left[\frac{3}{2} + (\theta - Nr\phi)\lambda \right] \frac{\sin x}{x}, \quad (7)$$

$$\frac{\partial^2 \theta}{\partial y^2} + f \frac{\partial \theta}{\partial y} + Nb \frac{\partial \phi}{\partial y} \frac{\partial \theta}{\partial y} + Nt \left(\frac{\partial \theta}{\partial y} \right)^2 = x \left(\frac{\partial f}{\partial y} \frac{\partial \theta}{\partial x} - \frac{\partial f}{\partial x} \frac{\partial \theta}{\partial y} \right), \quad (8)$$

$$\frac{\partial^2 \phi}{\partial y^2} + Le f \frac{\partial \phi}{\partial y} + \frac{Nt}{Nb} \frac{\partial^2 \theta}{\partial y^2} = Le x \left(\frac{\partial f}{\partial y} \frac{\partial \phi}{\partial x} - \frac{\partial f}{\partial x} \frac{\partial \phi}{\partial y} \right), \quad (9)$$

with the boundary conditions

$$\begin{aligned} f = 0, \quad \partial f / \partial y = 0, \quad \theta = 1, \quad \phi = 1 \quad \text{at} \quad y = 0, \\ \partial f / \partial y \rightarrow (3/2) \sin x / x, \quad \theta \rightarrow 0, \quad \phi \rightarrow 0 \quad \text{as} \quad y \rightarrow \infty. \end{aligned} \quad (10)$$

It is worth mentioning that when Nr , Nb and Nt are all zero, equations (8) and (9) involve just two dependent variables, namely f and θ , and the boundary-value problem for these two variables reduces to the corresponding problem of the mixed convection boundary layer flow about a sphere embedded in a fluid-saturated porous medium using the Darcy-Brinkman model (The boundary value problem for ϕ then becomes ill-posed and is of no physical significance).

Quantities of practical interest are the skin friction coefficient C_f , the local Nusselt number Nu and the local Sherwood number Sh , which are defined as

$$C_f = \frac{\tau_w}{\rho U_\infty^2}, \quad Nu = \frac{a q_w}{k_m (T_w - T_\infty)}, \quad Sh = \frac{a q_m}{D_B (C_w - C_\infty)}, \quad (11)$$

where τ_w , q_w , and q_m are the wall shear stress, the wall heat flux and the mass heat flux from the surface of the sphere, respectively, which are given by

$$\tau_w = \mu_f \left(\frac{\partial \bar{u}}{\partial \bar{y}} \right)_{\bar{y}=0}, \quad q_w = -k_m \left(\frac{\partial T}{\partial \bar{y}} \right)_{\bar{y}=0}, \quad q_m = -D_B \left(\frac{\partial C}{\partial \bar{y}} \right)_{\bar{y}=0}, \quad (12)$$

where k_m is the effective thermal conductivity of the porous medium. Substituting variables of boundary layer approximations and stream functions into (11) and (12), we obtain

$$(\text{Pr } Pe^{1/2})C_f = x \frac{\partial^2 f}{\partial y^2}(x, 0), \quad Pe^{-1/2} Nu = -\frac{\partial \theta}{\partial y}(x, 0), \quad Pe^{-1/2} Sh = -\frac{\partial \phi}{\partial y}(x, 0), \quad (13)$$

where $\text{Pr} = \nu_f / \alpha_m$ is the Prandtl number for the porous medium.

3. RESULTS AND DISCUSSION

Equations (7) to (9) subject to the boundary conditions (10) have been solved numerically for different values of the parameters Γ , Le and λ , and at some streamwise positions x , using an efficient implicit finite-difference scheme known as the Keller-box method along with the Newton's linearization technique as described by Cebeci and Bradshaw [13] for both the assisting ($\lambda > 0$) and opposing ($\lambda < 0$) flow cases. The skin friction coefficient $(\text{Pr } Pe^{1/2})C_f$, the local Nusselt number $Pe^{-1/2}Nu$, the local Sherwood number $Pe^{-1/2}Sh$, the velocity profiles $f'(y)$, the temperature profiles $\theta(y)$, and the nanoparticles volume fraction profiles $\phi(y)$, have been obtained for the following range of parameters: mixed convection parameter, $\lambda = 1$ (assisting flow), Γ Darcy-Brinkman parameter, Lewis number, $Le = 2, 6$ and 10 , Brownian number, $Nb = 0.5$, buoyancy ratio parameter, $Nr = 0.5$, and thermophoresis parameter, $Nt = 0.5$, at different positions x . It seems that the values of the parameters considered usually exist in geophysical and engineering applications [14].

Some values of the skin friction coefficient, $(\text{Pr } Pe^{1/2})C_f$, the local Nusselt number, $Pe^{-1/2}Nu$, the local Sherwood number $Pe^{-1/2}Sh$, are given in Tables 1 to 3 for some values of $Le = 2$, $\Gamma = 0.1$, $Nb = 0.5$, $Nr = 0.5$, $Nt = 0.5$ and various values of λ . These tables show that the boundary layer separates from the sphere for some values of $\lambda < 0$ (opposing flow). Increasing λ delays separation and the separation can be completely suppressed in the range $0 \leq x < 120^\circ$ for sufficiently large values of λ . A value of $\lambda = \lambda_0 (< 0)$ is found below which the boundary layer solution is not possible. The actual value of $\lambda = \lambda_s (< 0)$ which first gives no separation is difficult to determine exactly as it has to be found by successive integration of the equations. However, the numerical solutions indicate that the value of λ_s which first gives no separation lies between -2.99 and -3 .

Our objective is to observe the influence of the parameters Γ and Le on the heat, mass and fluid flow characteristics, and thus we will present the results in figure forms for the above parameters effect. Figures 1 and 2 show the variations of the skin friction coefficient, $(\text{Pr } Pe^{1/2})C_f$ with the parameters Γ and Le , respectively.

The skin friction coefficient increases with the increase in the parameters Le , while decreases with increasing Γ . Figures 3 and 4 show the variations of the local Nusselt number $Pe^{-1/2}Nu$ with the parameters Γ and Le , respectively. The local Nusselt number decreases with the increase of parameters Γ and Le , which corresponds to an increase in the thermal boundary layer thickness. Figures 5 and 6 show the variations of the local Sherwood number $Pe^{-1/2}Sh$ with the parameters Γ and Le , respectively. The pattern of the effects is similar to the case of skin friction coefficient, that is, the local Sherwood number increases with the increase in the parameters Le , while decreases with increase of Γ .

The samples of velocity, temperature and the nanoparticle volume fraction profiles are given in Figures 7 and 8. In Figure 7, it is observed that the thicknesses of the thermal and the mass fraction boundary layers decrease with increasing values of Le . The increasing of Lewis number tends to increase the buoyancy-induced flow along the surface at the expense of the reduced concentration and its boundary layer thickness. From the observation made on Figures 7 and 8, the profiles satisfy the far field boundary conditions (10) asymptotically, which support the numerical results obtained.

Table 1: Values of skin friction coefficient $(Pr Pe^{1/2})C_f$ for $\Gamma = 0.1$, $Le = 2$, $Nb = 0.5$, $Nr = 0.5$, $Nt = 0.5$ and various values of λ .

x	λ										
	- 3.04	- 3.01	- 3.0	- 2.99	- 2.0	-1.0	0	1.0	2.0	5.0	10.0
0°	0.0000	0.0000	0.0000	0.0000	0.0000	0.0000	0.0000	0.0000	0.0000	0.0000	0.0000
10°	0.0023	0.0083	0.0113	0.0143	0.2967	0.5653	0.8233	1.0733	1.3168	2.0184	3.1189
20°	0.0036	0.0154	0.0213	0.0272	0.5830	1.1122	1.6207	2.1136	2.5940	3.9779	6.1497
30°	0.0030	0.0202	0.0288	0.0374	0.8493	1.6236	2.3680	3.0901	3.7941	5.8232	9.0094
40°	0.0001	0.0221	0.0331	0.0441	1.0868	2.0833	3.0426	3.9737	4.8819	7.5016	11.6187
50°		0.0208	0.0338	0.0469	1.2879	2.4773	3.6239	4.7379	5.8253	8.9647	13.9044
60°		0.0167	0.0313	0.0460	1.4463	2.7934	4.0944	5.3598	6.5961	10.1696	15.8006
70°		0.0104	0.0262	0.0419	1.5577	3.0222	4.4397	5.8204	7.1708	11.0797	17.2505
80°		0.0030	0.0194	0.0358	1.6192	3.1571	4.6494	6.1054	7.5314	11.6661	18.2080
90°			0.0123	0.0287	1.6301	3.1945	4.7171	6.2057	7.6657	11.9081	18.6382
100°			0.0058	0.0218	1.5910	3.1341	4.6408	6.1174	7.5681	11.7940	18.5192
110°			0.0007	0.0159	1.5045	2.9784	4.4230	5.8423	7.2395	11.3214	17.8422
120°				0.0108	1.3743	2.7331	4.0701	5.3876	6.6875	10.4978	16.6121

Table 2: Values of local Nusselt number $Pe^{-1/2}Nu$ for $\Gamma = 0.1$, $Le = 2$, $Nb = 0.5$, $Nr = 0.5$, $Nt = 0.5$ and various values of λ .

x	λ										
	- 3.04	- 3.01	- 3.0	- 2.99	- 2.0	-1.0	0	1.0	2.0	5.0	10.0
0°	0.2288	0.2325	0.2343	0.2360	0.3483	0.4160	0.5487	0.5091	0.5450	0.6312	0.7361
10°	0.2276	0.2313	0.2331	0.2349	0.3470	0.4147	0.4774	0.5076	0.5435	0.6295	0.7342
20°	0.2243	0.2280	0.2298	0.2315	0.3435	0.4108	0.4689	0.5032	0.5390	0.6246	0.7289
30°	0.2189	0.2225	0.2243	0.2261	0.3376	0.4044	0.4604	0.4962	0.5316	0.6166	0.7200
40°	0.2115	0.2152	0.2170	0.2187	0.3294	0.3956	0.4500	0.4863	0.5214	0.6054	0.7077
50°		0.2060	0.2078	0.2095	0.3191	0.3843	0.4374	0.4737	0.5082	0.5910	0.6919
60°		0.1952	0.1970	0.1987	0.3065	0.3705	0.4223	0.4582	0.4922	0.5734	0.6725
70°		0.1831	0.1849	0.1865	0.2919	0.3544	0.4047	0.4400	0.4732	0.5526	0.6494
80°		0.1703	0.1719	0.1735	0.2753	0.3359	0.3846	0.4190	0.4512	0.5284	0.6226
90°			0.1588	0.1601	0.2567	0.3150	0.3619	0.3952	0.4263	0.5009	0.5920
100°			0.1465	0.1475	0.2362	0.2918	0.3366	0.3685	0.3982	0.4698	0.5573
110°			0.1364	0.1369	0.2141	0.2664	0.3087	0.3388	0.3670	0.4350	0.5184
120°				0.1292	0.1902	0.2386	0.2780	0.3061	0.3325	0.3963	0.4747

Table 3: Values of local Sherwood number $Pe^{-1/2}Sh$ for $\Gamma = 0.1$, $Le = 2$, $Nb = 0.5$, $Nr = 0.5$, $Nt = 0.5$ and various values of λ .

x	λ										
	- 3.04	- 3.01	- 3.0	- 2.99	- 2.0	-1.0	0	1.0	2.0	5.0	10.0
0°	0.5051	0.5130	0.5168	0.5206	0.7622	0.9069	1.0404	1.1052	1.1819	1.3659	1.5905
10°	0.5024	0.5103	0.5142	0.5180	0.7594	0.9039	1.0101	1.1019	1.1784	1.3621	1.5864
20°	0.4950	0.5030	0.5069	0.5107	0.7516	0.8955	1.0007	1.0926	1.1688	1.3516	1.5748
30°	0.4831	0.4910	0.4949	0.4988	0.7388	0.8817	0.9865	1.0773	1.1529	1.3343	1.5557
40°	0.4668	0.4748	0.4787	0.4825	0.7211	0.8625	0.9665	1.0560	1.1307	1.3101	1.5291
50°		0.4545	0.4584	0.4623	0.6986	0.8380	0.9407	1.0287	1.1024	1.2791	1.4949
60°		0.4308	0.4347	0.4385	0.6714	0.8083	0.9092	0.9954	1.0677	1.2412	1.4531
70°		0.4043	0.4081	0.4118	0.6397	0.7734	0.8720	0.9562	1.0268	1.1963	1.4034
80°		0.3762	0.3797	0.3831	0.6036	0.7334	0.8292	0.9109	0.9795	1.1443	1.3458
90°			0.3510	0.3539	0.5633	0.6884	0.7808	0.8596	0.9258	1.0850	1.2799
100°			0.3244	0.3265	0.5190	0.6384	0.7267	0.8021	0.8655	1.0182	1.2054
110°			0.3029	0.3038	0.4709	0.5834	0.6668	0.7383	0.7985	0.9436	1.1218
120°				0.2879	0.4193	0.5234	0.6011	0.6679	0.7243	0.8604	1.0282

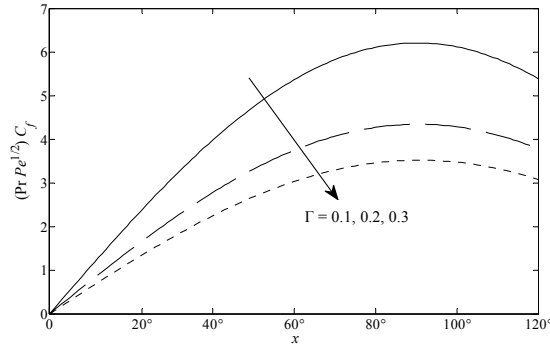


Figure 1: Variation of the skin friction coefficient $(Pr Pe^{1/2})C_f$ with x for $\Gamma = 0.1, 0.2, 0.3$, $Le = 2$, $Nb = 0.5$, $Nr = 0.5$, $Nt = 0.5$ and $\lambda = 1$

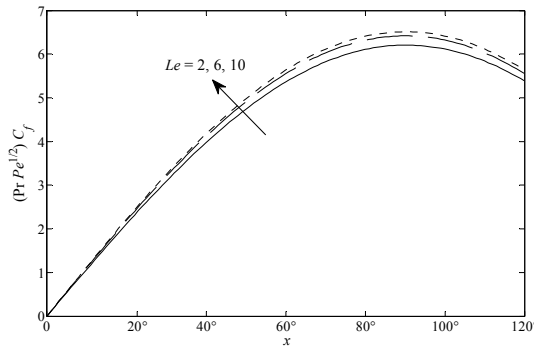


Figure 2: Variation of the skin friction coefficient $(Pr Pe^{1/2})C_f$ with x for $\Gamma = 0.1$, $Le = 2, 6, 10$, $Nb = 0.5$, $Nr = 0.5$, $Nt = 0.5$ and $\lambda = 1$

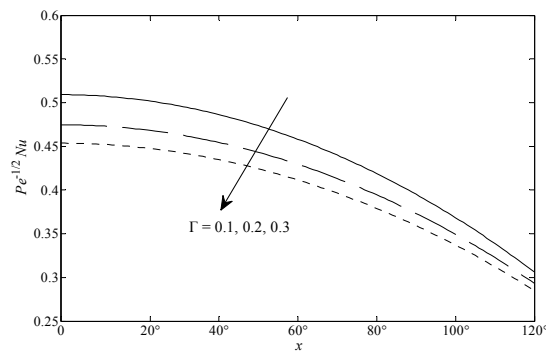


Figure 3: Variation of the local Nusselt number $Pe^{-1/2}Nu$ with x for $\Gamma = 0.1, 0.2, 0.3$, $Le = 2$, $Nb = 0.5$, $Nr = 0.5$, $Nt = 0.5$ and $\lambda = 1$

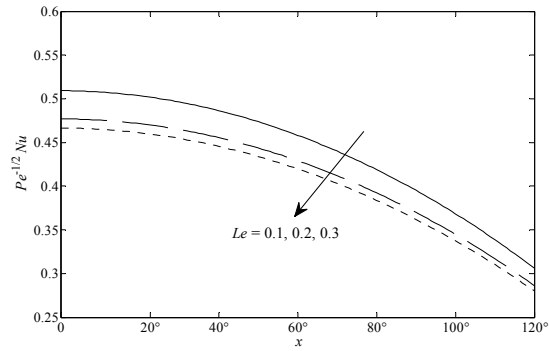


Figure 4: Variation of the local Nusselt number $Pe^{-1/2} Nu$ with x for $\Gamma = 0.1$, $Le = 2, 6, 10$, $Nb = 0.5$, $Nr = 0.5$, $Nt = 0.5$ and $\lambda = 1$

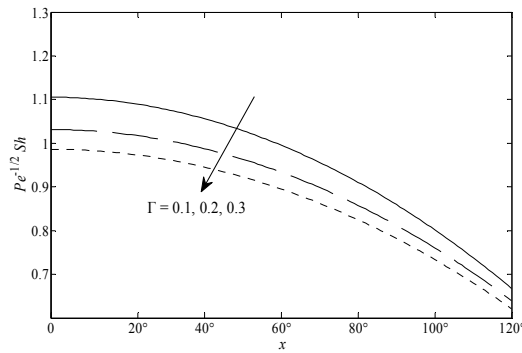


Figure 5: Variation of the local Sherwood number $Pe^{-1/2} Sh$ with x for $\Gamma = 0.1, 0.2, 0.3$, $Le = 2, Nb = 0.5$, $Nr = 0.5$, $Nt = 0.5$ and $\lambda = 1$

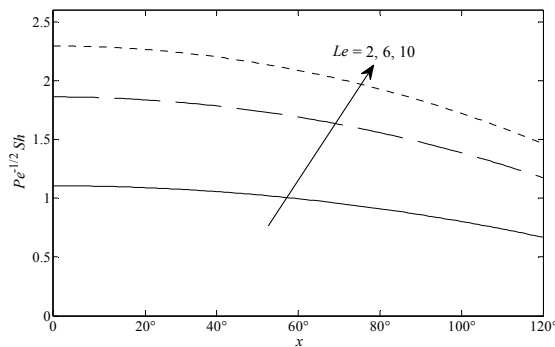


Figure 6: Variation of the local Sherwood number $Pe^{-1/2} Sh$ with x for $\Gamma = 0.1$, $Le = 2, 6, 10$, $Nb = 0.5$, $Nr = 0.5$, $Nt = 0.5$ and $\lambda = 1$

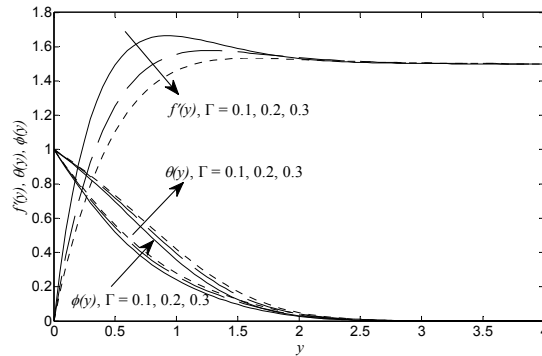


Figure 7: Variation of the velocity profiles $f'(y)$, temperature profiles $\theta(y)$ and the nanoparticles volume fraction profiles $\phi(y)$ at $x=0$ for $\Gamma = 0.1, 0.2, 0.3$, $Le = 2$, $Nb = 0.5$, $Nr = 0.5$, $Nt = 0.5$ and $\lambda = 1$

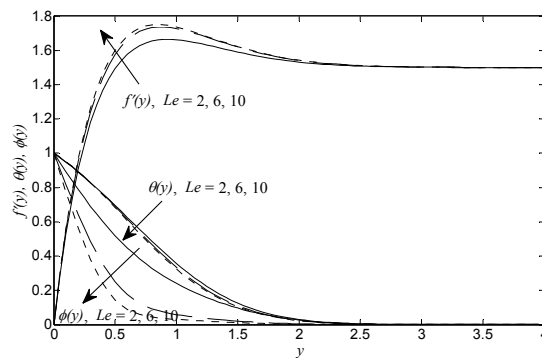


Figure 8: Variation of the velocity profiles $f'(y)$, temperature profiles $\theta(y)$ and the nanoparticles volume fraction profiles $\phi(y)$ at $x=0$ for $\Gamma = 0.1$, $Le = 2, 6, 10$, $Nb = 0.5$, $Nr = 0.5$, $Nt = 0.5$ and $\lambda = 1$

4. CONCLUSIONS

In this paper, we have studied the problem of steady mixed convection boundary layer flow about a solid sphere with a constant surface temperature and embedded in a porous medium saturated by a nanofluid with Buongiorno-Brinkman model. From this study, we could draw the following conclusions for the assisting flow case: the skin friction coefficient, $(Pr Pe^{1/2})C_f$ and the local Sherwood number $Pe^{-1/2}Sh$ increased when the value of the Lewis number Le , Brownian number Nb and thermophoresis parameter Nt increased, while opposite effect observed for Darcy-Brinkman parameter Γ and buoyancy ratio parameter Nr ; the local Nusselt number, $Pe^{-1/2}Nu$ decreased when the value of the Darcy-Brinkman parameter Γ , Lewis number Le , buoyancy ratio parameter Nr , and thermophoresis parameter Nt increased, while opposite effect observed for Brownian number Nb .

Acknowledgment

The authors would like to acknowledge the financial support received in the form of fundamental research grant scheme (FRGS) from the Ministry of Higher Education, Malaysia.

REFERENCES

- [1] Choi, S. (1995). "Enhancing thermal conductivity of fluids with nanoparticles" in: The Proceedings of the 1995 ASME International Mechanical Engineering Congress and Exposition, San Francisco, USA, ASME, FED 231/MD., 99-105.
- [2] Khanafer, K -, Vafai, K. & Lightstone, M. (2003). "Buoyancy-driven heat transfer enhancement in a two dimensional enclosure utilizing nanofluids" in Int. J. Heat Mass Trasfer, Vol. 46 pp. 3639-3653..
- [3] Kumar, S., Prasad, S.K. & Banerjee, J. (2010). "Analysis of flow and thermal field in nanofluid using a single phase thermal dispersion model" in Appl. Math. Modelling, Vol. 34 pp. 573-592. Brinkman, H. C. (1947). "A calculation of the viscous force exerted by a flowing fluid on a dense swarm of particles" in Appl. Sci. Res., Vol. 1 pp. 27-34.
- [4] Buongiorno, J. & Hu, W. (2005). "Nanofluid coolants for advanced nuclear power plants" Paper no. 5705, in: Proceedings of ICAPP '05, Seoul.

- [5] Das, S.K., Choi, S.U.S. Yu, W. & Pradet, T. (2007). *Nanofluids: Science and Technology*. Wiley, New Jersey.
- [6] Nield, D.A. & Bejan, A. (1999). *Convection in Porous Media*, second ed.. Springer, New York.
- [7] Ingham, D.B. & Pop, I. (1998). *Transport Phenomena in Porous Media*. Pergamon, Oxford
- [8] Brinkman, H. C. (1947). "A calculation of the viscous force exerted by a flowing fluid on a dense swarm of particles" in *Appl. Sci. Res.*, Vol. 1 pp. 27–34.
- [9] Vafai, K. & Tien, C.L. (1981). "Boundary and inertia effects on flow and heat transfer in porous media" in *Int. J. Heat Mass Transfer*, Vol. 24 pp. 195-203.
- [10] Nazar, R., Amin, N. & Pop, I. (2002). "On the mixed convection boundary-layer flow about a solid sphere with constant surface temperature" in *Arab. J. Sci. & Eng.*, Vol. 27 pp. 117-135.
- [11] Buongiorno, J. (2006). "Convective transport in nanofluids" in *ASME J. Heat Transfer*, Vol. 128 pp. 240-250.
- [12] Kuznetsov, A.V. & Nield, D.A. (2009). "Thermal instability in a porous medium layer saturated by a nanofluid: Brinkman model" in *Trans. Porous Media*, Vol. 81 pp. 409-422
- [13] Cebeci, T. & Bradshaw, P. (1984) *Physical and Computational Aspects of Convective Heat Transfer*. Springer, New York.
- [14] Nield, D.A. & Kuznetsov, A.V. (2009). "The Cheng–Minkowycz problem for natural convective boundary-layer flow in a porous medium saturated by a nanofluid" in *Int. J. Heat Mass Transfer*, Vol. 52 pp. 5792–5795 at *Mass Transfer*, Vol. 24 pp. 195-203.

Arsenic(III) Immobilization on Rice Husk

Malay Chaudhuri^{1,*}, Mohammed Ali Mohammed²

¹Department of Civil Engineering, Universiti Teknologi PETRONAS, Bandar Seri Iskandar, 31740 Tronoh, Perak Darul Ridzuan, Malaysia

² Department of Civil Engineering, Universiti Teknologi PETRONAS, Bandar Seri Iskandar, 31740 Tronoh, Perak Darul Ridzuan, Malaysia

*Corresponding email: m_chaudhuri@petronas.com.my

Abstract

A number of large aquifers in various parts of the world have been identified with contamination by arsenic. Long-term exposure to arsenic in drinking water causes cancer of the skin, lungs, urinary bladder and kidney, as well as skin pigmentation and hyperkeratosis. Arsenic occurs in groundwater in two valence states, as trivalent arsenite [As(III)] and pentavalent arsenate [As(V)]. As(III) is more toxic and more difficult to remove from water by adsorption on activated alumina. In this study, immobilization (adsorption) of As(III) by quaternized rice husk was examined. Batch adsorption test showed that extent of adsorption was dependent on pH, As (III) concentration, contact time and rice husk dose. Maximum adsorption occurred at pH 7-8, and equilibrium adsorption was attained in 2 h. Equilibrium adsorption data were described by the Langmuir and Freundlich isotherm models. According to the Langmuir isotherm, adsorption capacity of quaternized rice husk is 0.775 mg As(III)/g, which is 4.3x higher than that (0.180 mg As(III)/g) of activated alumina. Quaternized rice husk is a potentially useful adsorbent for removing arsenic from groundwater.

Keywords: arsenic(III); activated alumina; adsorption; immobilization; quaternized rice husk

1. INTRODUCTION

A number of large aquifers in various parts of the world have been identified with arsenic occurring at high concentrations. The most noteworthy occurrences are in parts of West Bengal (India) and Bangladesh, Taiwan, northern China, Hungary, Mexico, Chile, Argentina and many parts of the USA [1]. Arsenic contamination of groundwater in Vietnam and Cambodia [2], Nepal [3] and Pakistan [4] has also been reported. Long-term exposure to arsenic in drinking water causes cancer of the skin, lung, urinary bladder and kidney, as well as skin pigmentation and hyperkeratosis [5].

Arsenic occurs in groundwater in two valence states, as trivalent arsenite [As(III)] and as pentavalent arsenate [As(V)] [6]. As(III) is more toxic and more difficult to remove from water. Adsorption by activated alumina is most commonly used for arsenic removal in small municipal drinking water system and point-of-use treatment. Arsenic adsorption capacity of activated alumina is 11-24 mg As(V)/g [7] and 0.180 mg As(III)/g [8]. Lee et al. [9] examined quaternized rice husk with high abundance of the quaternary ammonium cation for arsenic adsorption and its arsenic adsorption capacity was found to be 19 mg As(V)/g. In the present study, immobilization (adsorption) of As(III) by quaternized rice husk was examined.

2. MATERIALS AND METHODS

2.1 Quaternized Rice Husk

Quaternized rice husk was prepared according to the method reported by Lee et al. [9] and Lazlo [10]. Rice husk was ground to a size of 212-500 μm and treated with 1% sodium carbonate solution for 45 min to remove color, followed by washing with distilled water and drying at 60-70°C. One hundred grams of the rice husk was treated with 125 mL of 5M sodium hydroxide solution for 30 min. Thereafter, 100 mL of 4M N-(3-chloro-2-hydroxypropyl)-trimethylammonium chloride solution was added to the mixture, thoroughly mixed and kept in an oven at 60-70°C for 4 h with intermittent mixing. The mixture was then rinsed with distilled water, suspended in dilute hydrochloric acid at pH 2, rinsed further with distilled water and dried at 60-70°C.

2.2 Adsorption Test

Batch adsorption test was carried out by shaking 100 mL of sodium arsenite (NaAsO_2) solution with 0.75 g of quaternized rice husk in a stoppered glass bottle placed on an orbital shaker at 150 rpm and room temperature (22°C). After a predetermined contact time, the bottle was removed from the shaker and the supernatant was filtered through 0.45 μm membrane filter and analyzed for arsenic

concentration by Method 3111 B of Standard Methods [11]. The effect of pH (5-8), contact time (0-4 h), As(III) concentration (0.25-1.0 mg As(III)/ L), and quaternized rice husk dose (2.5-12.5 g/L) on adsorption were evaluated. Adsorption isotherm was determined by batch equilibrium test at the optimum pH and contact time for adsorption with 100 mL of 0.1-1.0 mg As(III) /L arsenic solution and 0.1 g quaternized rice husk.

3. RESULTS AND DISCUSSION

3.1 Effect of pH on Adsorption

Effect of pH on As(III) adsorption from a 0.25 mg As(III)/L arsenic solution in 24 h is shown in Fig. 1. pH higher than 8 was not considered because it is outside the range of groundwater pH.

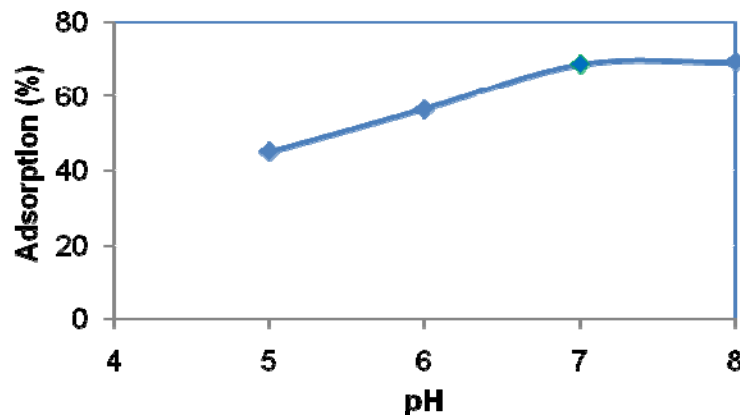


Figure 1: Effect of pH on adsorption.

It is observed that adsorption increased with pH up to pH 7 and maximum adsorption (69%) occurred at pH 7-8, similar to that reported by Singh and Pant [8], Lin and Wu [12] and Xu et al. [13] for adsorption of As(III) by activated alumina and by Deliyanni et al. [14] for adsorption of As(III) by cationic surfactant modified akaganetite. The trend of As(III) adsorption may be explained by considering the fact that even though below pH 8 the predominant As(III) species is non-ionic H_3AsO_3 , concentration of the anionic $H_2AsO_3^-$ species increases with pH from pH 6 [13]. All subsequent adsorption tests were conducted at pH 7.

3.2 Effect of Contact Time and As(III) Concentration on Adsorption

Effect of contact time and As(III) concentration on adsorption are shown in Fig. 2. Extent of adsorption increased with increase in contact time and decrease in As(III) concentration and equilibrium adsorption was attained in 2 h. A contact time of 2 h was used in all subsequent adsorption tests.

3.3 Effect of Quaternized Rice Husk Dose on Adsorption

Effect of quaternized rice husk dose on As(III) adsorption from a 0.25 mg As(III)/L arsenic solution is shown in Fig. 3. Adsorption increased with dose and attained maximum adsorption (73%) at 10 g/l quaternized rice husk dose.

3.4 Adsorption Isotherm

In adsorption in a solid-liquid system, the distribution ratio of the solute between the liquid and the solid phase is a measure of the position of equilibrium. The preferred form of depicting this distribution is to express the quantity q_e as a function of C_e at a fixed temperature, the quantity q_e being the amount of solute adsorbed per unit weight of the solid adsorbent, and C_e the concentration of solute remaining in the solution at equilibrium. An expression of this type is termed an *adsorption isotherm* [15].

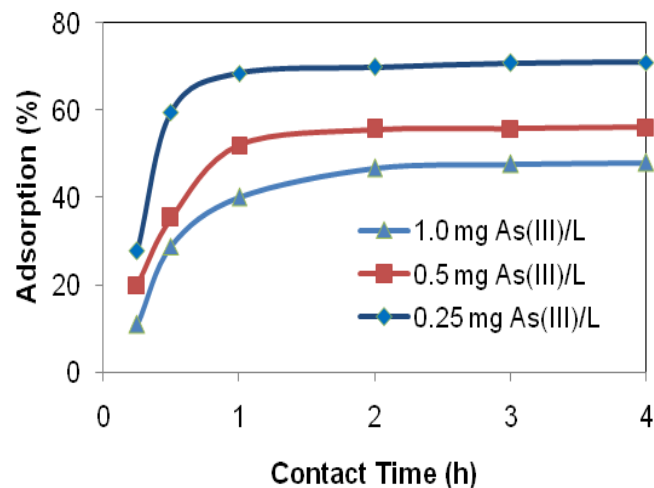


Figure 2: Effect of contact time and As(III) rice husk concentration on adsorption

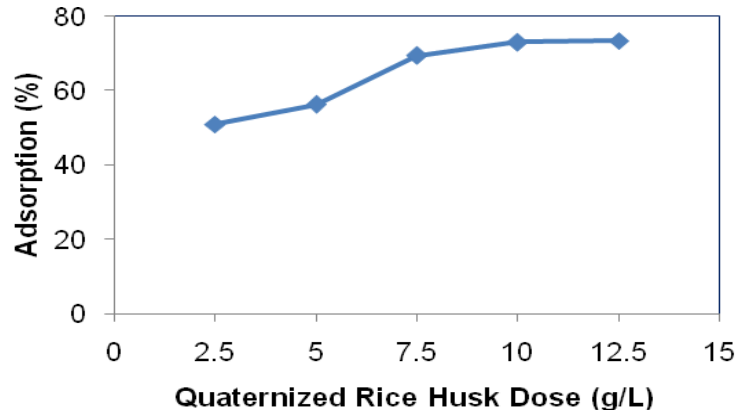


Figure 3: Effect of quaternized dose on adsorption.

The Langmuir adsorption isotherm is

$$q_e = \frac{Q^\circ b C_e}{1 + b C_e} \quad (1)$$

where, Q° is the number of moles of solute adsorbed per unit weight of adsorbent in forming a monolayer on the surface (monolayer limiting adsorption capacity) and b is a constant related to the energy of adsorption.

The Freundlich adsorption isotherm is

$$q_e = K_f C_e^{1/n} \quad (2)$$

where, K_f is the Freundlich constant (adsorption capacity) and $1/n$ represents the adsorption intensity.

Isotherm for As(III) adsorption was determined by batch equilibrium test using optimum contact time and pH (2 h and pH 7) for adsorption. The isotherm was fitted to the linear form of the Langmuir equation [$1/q_e = 1/Q^\circ + (1/bQ^\circ)(1/C_e)$] (Fig. 4) and Freundlich equation [$\log q_e = \log K_f + (1/n)\log C_e$] (Fig. 5). The values of Langmuir constants Q° and b , and Freundlich constants K_f and $1/n$ are shown in Table 1. Adsorption capacity of quaternized rice husk (0.775 mg As(III)/g) is 4.3x higher than that (0.180 mg As(III)/g) [8] of activated alumina.

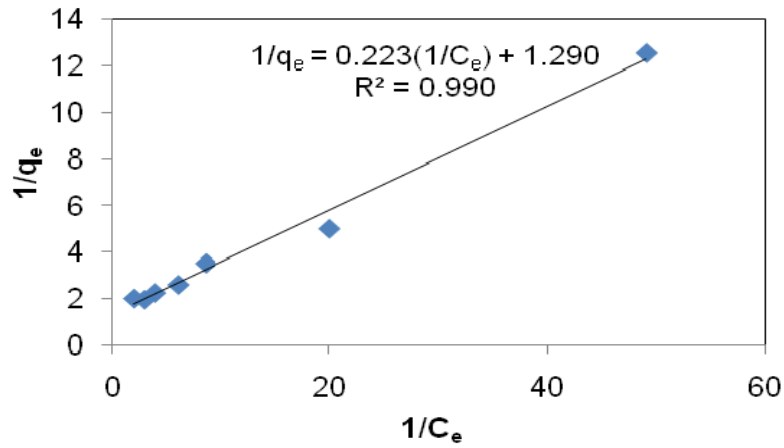


Figure 4: Langmuir adsorption isotherm.

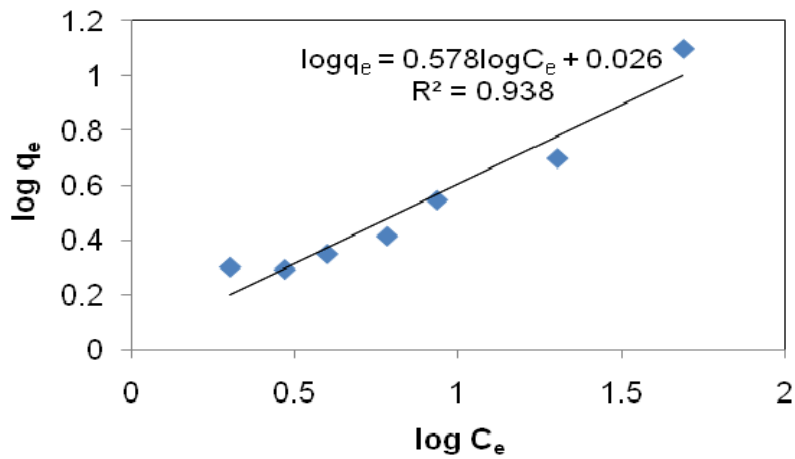


Figure 5: Freundlich adsorption isotherm.

Table 1: Langmuir and Freundlich constants.

Langmuir constant		Freundlich constant	
Q^o	b	K_f	$1/n$
0.775	5.785	1.062	0.578

Arsenic adsorption capacity of quaternized rice husk is 0.775 mg As(III)/g and 19 mg As(V)/g [9] compared to 0.180 mg As(III)/g [8] and 11-24 mg As(V)/g [7] of activated alumina. Thus, quaternized rice husk is a potentially useful adsorbent for removing arsenic (As(III) and As(V)) from groundwater.

4. CONCLUSIONS

Maximum As(III) adsorption by quaternized rice husk occurred at pH 7-8 and equilibrium adsorption was attained in 2 h. The quaternized rice husk showed higher As(III) adsorption capacity compared with activated alumina. The quaternized rice husk is a potentially useful adsorbent for removing arsenic from groundwater.

Acknowledgment

The authors are thankful to the management and authorities of the Universiti Teknologi PETRONAS (UTP) and the Civil Engineering Department, UTP for providing facilities for this research. Research support through grant FRGS/2/2010/TK/UTP/01/6 is gratefully acknowledged.

REFERENCES

- [1] Kinniburgh, D. G.; and Smedley, P.L. (Eds.). (2001). *Arsenic Contamination of Groundwater in Bangladesh*. British Geological Survey Technical Report WC/00/19. British Geological Survey, Keyworth, United Kingdom.
- [2] Berg, M.; Stengel, C.; Pham, T. K.; Pham, H. V.; Sampson, M. L.; Leng, M.; Samreth, S.; and Fredericks, D. (2007). Magnitude of Arsenic Pollution in the Mekong and Red River Deltas – Cambodia and Vietnam. *Science of the Total Environment* 372(2-3): 413–425.
- [3] Tendulkar, N.; Bhattacharya, P.; Neku, A.; and Mukherjee, A. B. (2006). Extent and Severity of Arsenic Poisoning in Nepal. In *Managing Arsenic in the Environment: From Soil to Human Health*. Naidu, R.; Smith, E.; Owens, G.; Nadebaum, P.; and Bhattacharya, P. (eds.). Melbourne: CSIRO Publishing.
- [4] Nickson, R.; McArthur, J.M.; Shrestha, B.; Kyaw-Myint, T.O.; and Lowry, D. (2005). Arsenic and other Drinking Water Quality Issues, Muzafargarh District, Pakistan. *Applied Geochemistry* 20(1): 55–68.
- [5] WHO. (2001). *Arsenic and Arsenic Compounds. Environmental Health Criteria 224*. Geneva: World Health Organization.
- [6] Cullen, W. R.; and Reimer, K. J. (1989). Arsenic Speciation in the Environment. *Chemical Reviews* 89(4): 713–764.

- [7] Ghosh, M. M.; and Yuan, J. R. (1987). Adsorption of Inorganic Arsenic and Organoarsenicals on Hydrous Oxides. *Environmental Progress* 6(3): 150–156.
- [8] Singh, T. S.; and Pant, K. K. (2004). Equilibrium, Kinetics and Thermodynamic Studies for Adsorption of As(III) on Activated Alumina. *Separation and Purification Technology* 36(2): 139–147.
- [9] Lee, C. K.; Low, K. S.; Liew, S. C.; and Choo, C. S. (1999). Removal of Arsenic(V) from Aqueous Solution by Quaternized Rice Husk. *Environmental Technology* 20(9): 971–978.
- [10] Lazlo, J. A. (1996). Preparing an Ion Exchange Resin from Sugarcane Bagasse to Remove Reactive Dye from Wastewater. *Textile Chemists and Colorist* 28(5): 13–17.
- [11] *Standard Methods for the Examination of Water and Wastewater, 21st ed.* (2005). Washington DC: American Public Health Association.
- [12] Lin, T-S.; and Wu, J-K. (2001). Adsorption of Arsenite and Arsenate within Activated Alumina Grains: Equilibrium and Kinetics. *Water Research* 35(8): 2049–2057.
- [13] Xu, H.; Allard, B.; and Grimvall, A. (1991). Effects of Acidification and Natural Organic Materials on the Mobility of Arsenic in the Environment. *Water Air Soil Pollution* 57-58(1): 269–278.
- [14] Deliyanni, E. A.; Oeleka, E. N.; and Matis, K. A. (2007). Effect of Cationic Surfactant on the Adsorption of Arsenites onto Akaganeite Nanocrystals. *Separation Science and Technology* 42(5): 993-1012.
- [15] Weber W.J., Jr. (1972). Adsorption (Chapter 5). In *Physicochemical Processes for Water Quality Control*. Weber, W. J. Jr. (ed.). New York: Wiley–Interscience.

Numerical Computation of Maximum Shear Stress Intensity for a Nearly Circular Crack Subject to Shear Loading

Koo Lee Feng^{1,*}, Nik Mohd Asri Nik Long², Eshkuvatov Zainidin K², Wong Tze Jin¹

¹Department of Basic Science and Engineering, Faculty of Agriculture and Food Sciences, Universiti Putra Malaysia Bintulu Campus, 97008 Bintulu, Sarawak, Malaysia.

²Department of Mathematics and Institute for Mathematical Research, University Putra Malaysia, 43400 Serdang, Selangor, Malaysia.

**Corresponding email: kooleefeng@yahoo.com*

Abstract

Maximum shear stress intensity for nearly circular cracks subjected to equal and opposite shear stresses are considered. A hypersingular integral equation containing the crack opening displacement is formulated. Conformal mapping technique is employed to transform the obtained hypersingular equation into a similar equation over a circular crack. A suitable collocation points are chosen to reduce the hypersingular integral equation into a system of linear equations. Numerical solution of the linear equations and the corresponding maximum shear intensity is obtained and presented graphically. Our results seem to agree with the existing asymptotic solution.

Keywords: maximum shear intensity; nearly circular crack; conformal mapping; shear load

1. INTRODUCTION

The solution of plane cracks of arbitrary shape inside an isotropic elastic medium has become very interesting and important topic in fracture mechanic. Different approaches have been used by researchers in dealing with the plane crack problems. Mastrojannis et al. [1] formulated the plane crack problem to the solution of a system of two dimensional Fredholm integral equations and numerical solution for tensile mode stress intensity factor is obtained. Singh and Danyluk [2] extended Kassir's work [3,4] in finding the stress intensity factor for coplanar rectangular shaped crack subject to normal loading. Ioakimidis [5] derived a hypersingular integral equation for a flat crack subject to tensile pressure. Qin and Tang [6,7] derived a set of hypersingular integral equation for a flat crack subject to arbitrary loads in three dimensional elasticity using Somigliana formula and finite part integral while a complex hypersingular integral equation was suggested by Linkov and Mogilevskaya [8] to solve the elastic plane problem. Martin [9,10] applied the hypersingular integral equation to solve the crack problems subject to normal and shear loading, respectively and Chen et al. [11] used the hypersingular integral equation to solve the penny shaped crack problem. Theotokoglou [12] applied the hypersingular boundary integral equation method to solve the plane crack in infinite three dimensional bodies under shear loading.

Other approaches are perturbation method by Rice and Gao [13,14], variant formula by Borodachev [15,16] and Frechet derivative of some nonlinear operation [15]. In this study, the hypersingular integral equation approach is used to compute the maximum shear stress intensity for a nearly circular crack and we compare our computational result with Gao's [17].

2. PROBLEM FORMULATION

Consider a three dimensional infinite, homogenous, elastic and isotropic solid body containing a flat circular crack, Ω located on the Cartesian coordinate (x, y, z) with origin O and Ω lies in the plane $z = 0$. Let the radius of the crack, Ω be α and $\Omega = \{(r, \theta) : 0 \leq r \leq \alpha, -\pi \leq \theta < \pi\}$. Assume that the stress at infinity and the body force are absent. Now, equal and opposite shear stresses in the X directions, $q(x, y)$ are applied to the crack plane and on the planes, the shear stress component is given by

$$\tau_{xz} = \frac{\mu}{1-\nu} q_x(x, y)$$

where ν is the Poisson's ratio and μ is the shear modulus. Adopted the Somigliana formula [18], followed by integration by part and making use of the relationship of Cauchy principle value and hypersingular equation [20], then, the plane crack problem subject to shear loading is given as [10]

$$\frac{1}{8\pi} H.S. \int_{\Omega} \frac{(2-\nu) + 3\nu e^{j2\Theta}}{R^3} w(x,y) d\Omega = q(x_o, y_o)$$

(1) where Ω denotes the crack domain with boundary $\partial\Omega$, $w(x,y)$ is the unknown crack opening displacement, the over bar denote complex conjugation with respect to j -complex, with $j = \sqrt{-1}$, R is defined as

$$R^2 = (x - x_o)^2 + (y - y_o)^2$$

and the angle Θ is

$$x - x_o = R \cos \Theta \text{ and } y - y_o = R \sin \Theta$$

Equation (1) is solved subjected to $w(x,y) = 0$ on $\partial\Omega$. The notation of $H.S$ in front of the integral sign on the left hand side of equation (1) should be interpreted as Hadamard finite part integral [21].

3. NEARLY CIRCULAR CRACK

Assume that Ω is an arbitrary shaped crack with smooth boundary with respect to the origin O , such that Ω is written as

$$\Omega = \{(r, \theta) : 0 \leq r < \rho(\theta) < -\pi\}$$

where the boundary of Ω , $\partial\Omega$ is given by $r = \rho(\theta)$. Next, let the polar coordinate defined as $\zeta = s e^{i\varphi}$ where $|\zeta| < 1$, hence, the unit disc D is given by

$$D = \{(s, \varphi) : 0 \leq s < 1, -\pi \leq \varphi < \pi\}$$

Employed the properties of Rieman mapping theorem, Ω is mapped onto the unit disc, D using $z = af(\zeta)$ where

$$f(\zeta) = \zeta + c\zeta^2 \tag{3}$$

The domain is circular if $c = 0$ and as $2|c| \rightarrow 1$, a cusp developed.

Substitution equation (3) into (2) gives [16]:

$$\begin{aligned} & \frac{2-\nu+3\nu e^{2j\theta}}{8\pi} H.S \int_D \frac{W(\xi, \eta)}{S^3} d\xi d\eta + \frac{2-\nu}{8\pi} C.P \int_D W(\xi, \eta) K^{(1)}(\zeta, \zeta_o) d\xi d\eta \\ & + \frac{3\nu}{8} \int_D W(\xi, \eta) K^{(2)}(\zeta, \zeta_o) d\xi d\eta = Q(\xi_o, \eta_o) \end{aligned} \tag{4}$$

where $S = |\zeta - \zeta_o|$, $K^{(1)}(\zeta, \zeta_o)$ and $K^{(2)}(\zeta, \zeta_o)$ are Cauchy-type and weakly singular kernel [18]

$$K^{(1)}(\zeta, \zeta_o) = \frac{|f'(\zeta)|^{\frac{3}{2}} |f'(\zeta_o)|^{\frac{3}{2}}}{|f(\zeta) - f(\zeta_o)|^3} e^{j(\delta - \delta_o)} - \frac{1}{|\zeta - \zeta_o|^3}$$

$$K^{(2)}(\zeta, \zeta_o) = \frac{|f'(\zeta)|^{\frac{3}{2}} |f'(\zeta_o)|^{\frac{3}{2}}}{|f(\zeta) - f(\zeta_o)|^3} e^{j(2\theta - \delta - \delta_o)} - \frac{1}{|\zeta - \zeta_o|^3} e^{2j\phi}$$

ϕ and δ are defined as $\zeta - \zeta_o = Se^{i\phi}$ and $f'(\zeta) = |f'(\zeta)|e^{i\delta}$, respectively. The notation C. P. is denoted as Cauchy Principle value integral. The hypersingular integral equation over a circular disc D is to be solved subject to $W = 0$ on $s = 1$.

Now, write W as

$$W(\xi, \eta) = \sum_{n,k} W_k^n Y_k^n(s, \varphi) \tag{5}$$

where

$$Y_k^n(s, \varphi) = s^{|n|} C_{2k+1}^{|n|+\frac{1}{2}}(\sqrt{1-s^2}) e^{jn\varphi} \tag{6}$$

and

$$\sum_{n,k} = \sum_{n=-N_1}^{N_1} \sum_{k=0}^{N_2}$$

Introduce

$$L_h^m(s, \varphi) = s^{|m|} C_{2h+1}^{|m|+\frac{1}{2}}(\sqrt{1-s^2}) \cos(m\varphi) \tag{7}$$

such that the relationship of these two function is

$$\int_{\Omega} \frac{Y_k^n(\zeta) L_h^m(\zeta) s ds d\varphi}{\sqrt{1-s^2}} = B_k^n \delta_{hk} \delta_{nm} \tag{8}$$

where δ_{ij} is the Kroneker delta and

$$B_k^n = \frac{\sigma_n}{2} h_{2k+1}^{n+\frac{1}{2}},$$

$$h_{2k+1}^{n+\frac{1}{2}} = \frac{\pi}{2^{2n}} \frac{\Gamma(2k+2n+2)}{(2k+n+\frac{3}{2})(2k+1)! \left[\Gamma(n+\frac{1}{2}) \right]^2}$$

$$\sigma_n = \begin{cases} 2\pi & n=0 \\ \pi & n \neq 0 \end{cases}$$

Both functions $L_h^m(s, \varphi)$ and $Y_k^m(s, \varphi)$ have square-root zeros at $s = 1$.

Define

$$W_k^n = -\overline{W}_k^n G_{2k+1}^{|n|+\frac{1}{2}} \sqrt{\frac{E_k^n}{B_k^n}}$$

Substitute equation (5) into (4) and multiply with equation (6) and perform integration over D using the relationship of (8) leads to

$$\sum_{n,k} \overline{W}_k^n \left(-\frac{2-v+3ve^{2k\Theta}}{2} \delta_{hk} \delta_{|n||m|} + S_{hk}^{mm} \right) = Q_k^n; \tag{9}$$

$$-N_1 \leq m \leq N_1; 0 \leq k \leq N_2$$

where

$$S_{hk}^{mm} = \frac{2-v}{8\pi \sqrt{E_k^m B_k^m} \sqrt{E_h^n B_h^n}} T_{hk}^{mm},$$

$$T_{hk}^{mm} = \int_D L_h^m(\zeta) \int_D Y_k^n(\zeta) H(\zeta, \zeta_o) d\zeta d\zeta_o,$$

$$Q_k^n = \frac{1}{\sqrt{E_k^n B_k^n}} \int_D Y_k^n(\zeta_o) Q(\zeta_o) d\zeta_o$$

and

$$H(\zeta, \zeta_o) = (2-v)K^{(1)}(\zeta, \zeta_o) + 3vk^{(2)}(\zeta, \zeta_o).$$

In (9), we have used the following notation :

$$\zeta_o = \zeta_o(s_o, \varphi_o), Q(\zeta_o) = Q(s_o \cos \varphi_o, s_o \sin(\varphi_o)) \text{ and } d\zeta_o = s_o ds d\varphi$$

Equation (9) is a system of linear equations and is to be solved for the coefficients, \overline{W}_k^n , which will be used later in finding the maximum shear stress intensity. The integration in (9) are all regular, solving them should give no much difficulties. Here, we have used the Gaussian quadrature and trapezoidal formulas for the radial and angular direction, with the appropriate choice of collocation points (s, φ) and (s_o, φ_o) , respectively.

4. MAXIMUM SHEAR STRESS INTENSITY FACTOR

The maximum shear stress intensity factor is defined as [17]

$$K(\varphi) = \sqrt{[K_2(\varphi)]^2 + [K_3(\varphi)]^2} \quad (10)$$

where $K_2(\varphi)$ and $K_3(\varphi)$ are shear and tearing modes stress intensity factor, respectively. The stress intensity factor is defines as

$$K_j(\varphi) = T_j \left\{ |f'(e^{i\varphi})|^{-1} \sum_{n,k} \frac{\overline{W}_k^n}{\sqrt{E_k B_k^n}} Y_k^n(\varphi) \right\}; j = 2,3 \quad (11)$$

where T_j is constant,

$$Y_k^n(\varphi) = D_{2k+1}^{|n|+\frac{1}{2}}(0) \cos(n\varphi) \text{ and } C_{2k+1}^{|n|+\frac{1}{2}}(\sqrt{1-s^2}) = \sqrt{1-s^2} D_{2k+1}^{|n|+\frac{1}{2}}(\sqrt{1-s^2})$$

5. NUMERICAL RESULT

Numerical calculation have been carried out and shows that our numerical scheme converges rapidly with only a small value of N .

Table 1: Numerical convergence maximum stress intensity factor $f(\zeta) = \zeta + 0.1\zeta^2$

N	$K(0.00)$	$K_2(\frac{\pi}{4})$	$K(\frac{\pi}{2})$	$K(\frac{3\pi}{4})$	$K(\pi)$
0	1.1397E-06	9.7723E-07	8.1972E-07	1.0053E-06	1.1862E-06
1	0.0000E+0000	0.0000E+0000	1.4571E-06	0.0000E+0000	0.0000E+0000
2	3.0662E-07	5.0149E-26	1.8584E-06	4.6429E-25	3.1914E-07
3	1.2477	1.0551	0.8555	1.0137	1.1790
4	1.2477	1.0551	0.8555	1.0137	1.1790
5		1.0551	0.8555	1.0137	
6			0.8555		

Figure 1, 2 and 3 shows that the variations of $K(\varphi)$ against φ for $c = 0.001$, $c = 0.01$ and $c = 0.1$, respectively. It can be seen that the maximum shear stress intensity has local extremal value when the crack front is at $\cos(\varphi) = \pm 1$ or $\sin(\varphi) = \pm 1$.

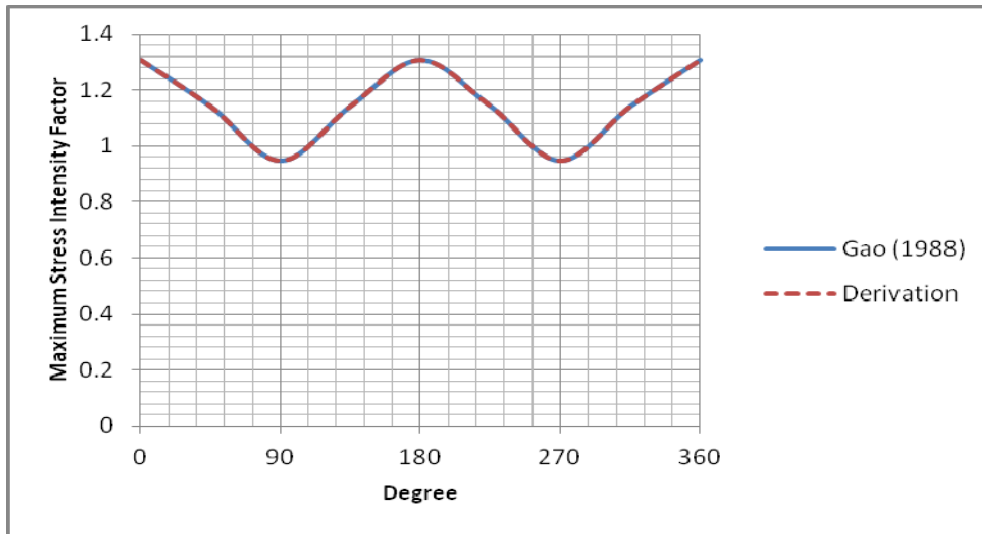


Figure 1: The maximum shear stress intensity for $f(\zeta) = \zeta + 0.001\zeta^2$.

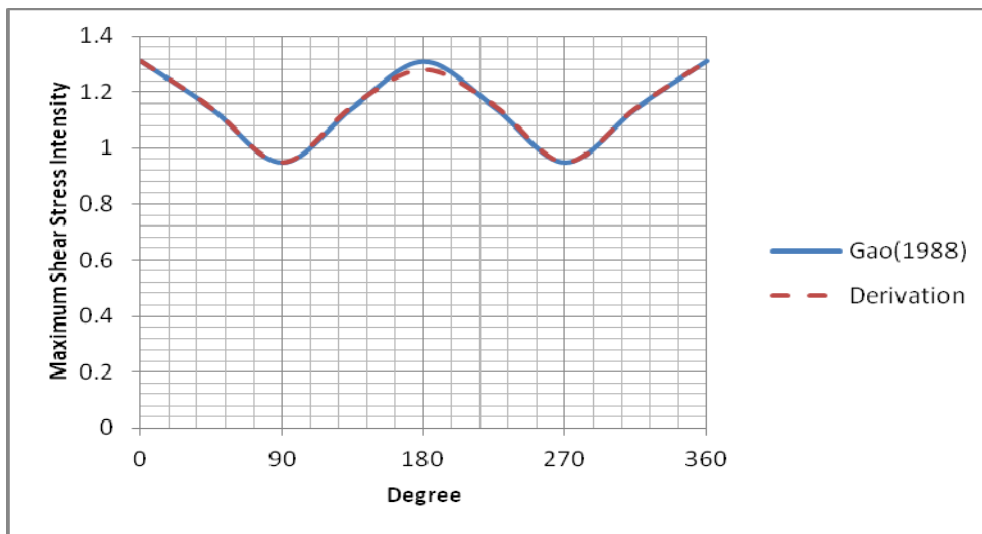


Figure 2: The maximum shear stress intensity for $f(\zeta) = \zeta + 0.01\zeta^2$.

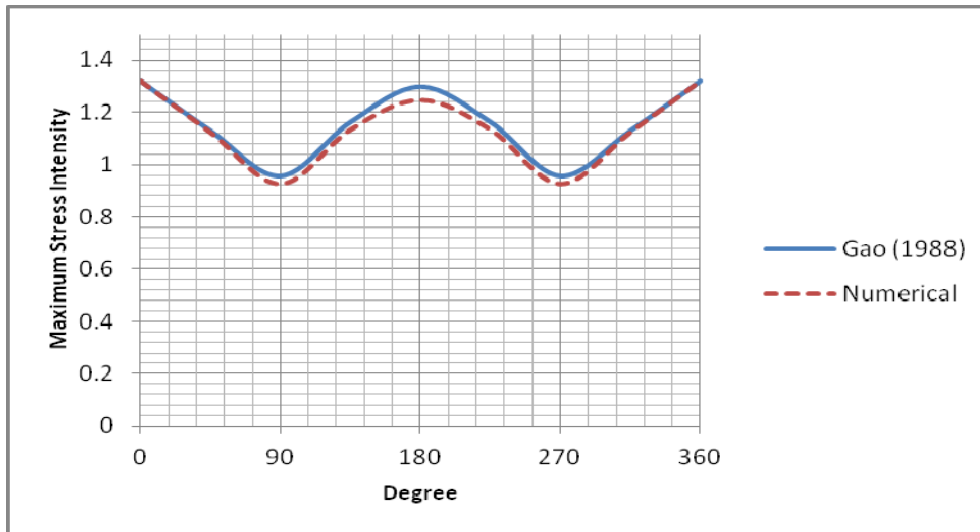


Figure 3: The maximum shear stress intensity for $f(\zeta) = \zeta + 0.1\zeta^2$.

6. CONCLUSION

In this study, a hypersingular integral equation for crack problem subject to shear loading is formulated. Then, a nearly circular crack is mapped conformally onto a unit circle where the equation is transformed into a similar hypersingular integral equation over a circular crack, which enable us make use of the formula obtained by Krenk [22]. By choosing the appropriate collocation points, this equation is reduced into a system of linear equations and solved for the unknown coefficients, which are later used in finding the maximum shear stress intensity. The maximum shear stress intensity for the mentioned crack subject to shear load presented graphically. Our result seems to agree with the previous work by Gao [17].

Acknowledgments

This project is supported by Ministry of Higher Education Malaysia for the Fundamental Research Grant Scheme, project No:01-04-10-897FR and NSF scholarship.

REFERENCES

- [1] Mastrojannis, E.; Keer, L. M. & Mura, T. (1979), 'Stress intensity factor for a plane crack under normal pressure', *International Journal of Fracture* 15(3), 247-258.
- [2] Singh, B. M. & Danyluk, H. T. (1985), 'Stress intensity factors for two rectangular cracks in three-dimensions', *Engineering Fracture Mechanics* 22(3), 475-483.
- [3] Kassir, M. K. (1982), 'A three dimensional rectangular crack subjected to shear loading', *International Journal of Solids and Structures* 18, 1075-1082.
- [4] Kassir, M. K. (1981), 'Stress-intensity factor for a three dimensional rectangular crack', *Journal of Applied Mechanics, Transactions ASME* 48(2), 309-312.
- [5] Ioakimidis, I. N. (1982), 'Application of finite-part integrals to the singular integral equations of crack problems in plane and three-dimensional elasticity', *Acta Mechanica* 45(1-2), 31-47.
- [6] Qin, T. Y. & Tang, R. J. (1993), 'Finite part integral and boundary element method to solve embedded planar crack problem', *International Journal of Fracture* 60(4), 373-381.
- [7] Qin, T. Y. & Tang, R. J. (1992), 'Finite-part integral and boundary element method to solve flat crack problems', *Applied Mathematics and Mechanics* 13(12), 1089-1095
- [8] Linkov, A. M. & Mogilevskaya, S. G. (1994), 'Complex hypersingular integrals and integral equations in plane elasticity', *Acta Mechanica* 105(1-4), 189-205.
- [9] Martin, P. A. (1996), 'Mapping flat cracks onto penny-shaped cracks, with application to somewhat circular tensile cracks.', *Quarterly of Applied Mathematics* 54, 663-675.
- [10] Martin, P. A. (1995), 'Mapping flat cracks onto penny-shaped cracks: shear loadings', *Journal of the Mechanics and Physics of Solids* 43(2), 275-294.
- [11] Chen, Y. Z.; Lin, X. Y. & Peng, Z. Q. (1998), 'Some particular solutions for penny-shaped crack problem by using hypersingular integral equation or differential-integral equation', *Archive of Applied Mechanics* 68(3-4), 271-280.

- [12] Theotokoglou, E. E. (2004), 'Boundary integral equation method to solve embedded planar crack problems under shear loading', *Computational Mechanics* 33(5), 327-333.
- [13] Gao, H. & Rice, J. R. (1987), 'Somewhat circular tensile crack', *International Journal of Fracture* 33, 155-174.
- [14] Gao, H. & Rice, J. R. (1986), 'Shear stress intensity factors for a planar crack with slightly curved front', *Journal of Applied Mechanics* 53, 774-778.
- [15] Borodachev, N. M. (1993), 'Solution of integral equation for almost circular cracks', *Strength of Materials* 25(4), 275-280.
- [16] Borodachev, N. M. (1989), 'Method of solving problems of a plane crack which is nearly circular', *International Applied Mechanics* 25(7), 718-723.
- [17] Gao, H. (1988), 'Nearly circular shear mode cracks.', *International Journal of Solids and Structures* 24, 177-193.
- [18] Nik Long, N. M. A.; Koo, L. F. & Eshkuvatov, Z. K. (2011), 'Computation of Energy Release Rates For A Nearly Circular Crack', *Mathematical Problem In Engineering*, 2011, 17pages.
- [19] Guidera, J. T. & Lardner, R. W. (1975), 'Penny-shaped cracks', *Journal of Elasticity* 5(1), 59-73.
- [20] Ioakimidis, N. I. (1990), 'Two-dimensional principal value hypersingular integrals for crack problems in three-dimensional elasticity', *Acta Mechanica* 82(1-2), 129-134.
- [21] Hadamard, J. (2003), Lectures on Cauchy's problem: In *linear partial differential equations*, *Dover Publications*
- [22] Krenk, S. (1979), 'A circular crack under asymmetric loads and some related integral equations', *Journal of Applied Mechanics, Transactions ASME* 46, 821-826.

A Study on Plant Selection for Green Building Design

Izudinshah Bin Abd. Wahab^{*,1} and Lokman Hakim Bin Ismail¹

¹Faculty of Civil and Environmental Engineering,
University Tun Hussein Onn Malaysia,
86400, Parit Raja, Batu Pahat, Johor

**Corresponding email: izudin@uthm.edu.my*

Abstract

Previous researches show that incorporating natural elements in design has proven a significant result in balancing building indoor environment. Using plant as part of the design has been widely accepted to contribute good thermal impact as shown in bioclimatic design, green roofing system and living wall elements. As there are so many species of plants for selection, this research was carried out to analyze types of indoor plants that have the potential to contribute thermal comfort to their surrounding. Based on the fact that plant leaves are the part where transpiration and guttation take place, plants are categorized into seven types based on their leaves architecture. They were then tested on their impact on surrounding temperature and humidity. Result shows that Linear, Lanceolate and Oblong shaped leaves categories are good in lowering the relative humidity while the categories that are good in lowering the temperature are Linear, Lanceolate, Cordate and Oblong shaped leaves categories. The study was carried out through series of relative humidity and air temperature monitoring of several room casings that consist with the plants. Both relative humidity and air temperature of the rooms with plants were recorded lower compared with the one without plant. Different categories of plants do give good result in relative humidity and air temperature. Thus, with a good combination of plant installation inside or onto building, it may contribute towards providing a good thermal comfort to the occupants.

Keywords: thermal comfort; air temperature; relative humidity

1. INTRODUCTION

Building is a major shading medium to human. Prevention of excessive increase in building internal temperature is very important to produce a comfortable indoor environment. With the growing concern about the climate change, there has been an increasing interest in using plant as part of sustainable strategy for building environment [1]. Previously, plant may be limited for the used of landscape element. In spite of beautifying the space, they also help to clean the air by filtering out toxins, pollutants and the carbon dioxide that we exhaled - replacing them with life sustaining oxygen [2]. Due to the potential, it is now used as part of the building itself as what we can see in Bioclimatic Designs, green roofing system and living wall elements [3]. This paper aims to show variety of plants' potential in giving impact to their surrounding environment. This may contribute to the process of plant selection in those building design approaches.

In the 1980s, NASA scientists had carried out studies on methods to reduce indoor air pollution. Their research found that houseplants, when grown in a closed, controlled environment, were able to extract volatile organic chemicals from the air. The scientists also found that there are varieties of plant efficiency in filtering out toxins than others when compared between few plant species. Philodendron species, spider plants and pothos were found to be the most efficient in the removal of formaldehyde. Thus, indoor plants are the most efficient and cost effective means of removing air pollution [2]. It is recommends that two plants per 100 square feet or two plants per a small office may keep the air pure and healthy [4,5]. Based on another study, one six-inch houseplant per 100 square feet of living area will do a good job of filtering out pollutants. Also, the more vigorous the plant, the more air it can filter [6]. Besides keeping the surrounding pure and healthy, plants may also helps in providing a good thermal for its surrounding. A well landscaped building surrounding shows a significant potential in keeping the indoor building air cool and less humid [7].

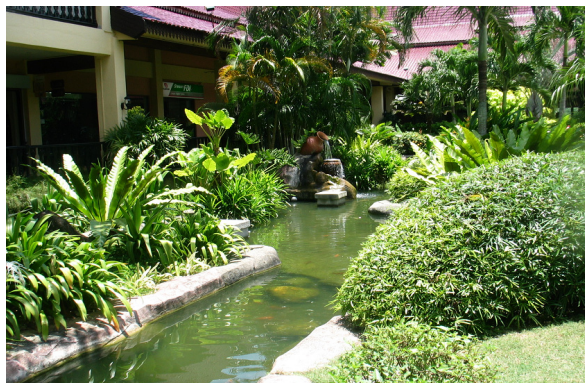


Figure 1: Incorporation of building and plant

The idea of common plants solving Indoor Air Quality problems is attractive. The findings of the two-year study by NASA indicate that plants provide a natural, cost-effective way to clean indoor air and combat "sick building syndrome" [3]. However, due to the different types of field study between architectural engineering and botany, the concept idea was just promoting the usage of plant in building. Further study on the plants potential in the aspect is still an issue. While there are so many species that able to stand the situation of being indoor plants, the selection has to function well in providing good thermal surrounding.

This research was focused on comparing the effect of type of plant towards their thermal surrounding. Considering the fundamental of plant botany, where transmission of air and water happened most at the leaves, this research classified plants based on the leaves architecture.

This research was done to meet the objective of comparing the plant potential to provide good thermal comfort in building space. Thus, the most potential type of plant may be identified due to the aspect. In term of thermal comfort, this research only focused on the effect towards air temperature and surrounding relative humidity (RH). Other variables of thermal comfort like air movement and human comfort variables may not be relevant.

2. METHODOLOGY

Photosynthesis is a major process of plant. It is a process of converting light energy to chemical energy and storing it in the bonds of sugar. The process takes place in the chloroplasts, specifically using chlorophyll, the green pigment involved in photosynthesis. The process primarily takes place in plant leaves.

One of the important components of leaf is stoma. Botanically, stoma is a pore, found in the leaf and stem epidermis that is used for gas exchange. Air containing carbon dioxide and oxygen enters the plant through these openings where it is used in photosynthesis and respiration. At the same time water vapor also released into the atmosphere through these pores in a process called transpiration. This process helps plant to maintain its desirable temperature.

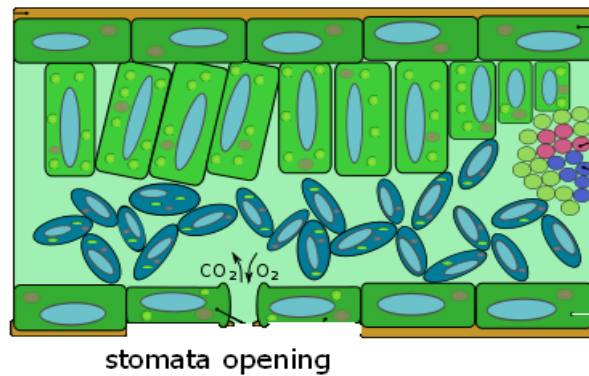






Figure 2: Cross section of leaf showing stomata opening underneath

Thus, when the processes take place, a slight effect on the plant surrounding is predicted. Hence, a number of plants may contribute to significant changes of the surrounding especially when dealing with indoor environment [9]. As most of the processes are mainly related to the leaves, hypothetically, different leaves' architecture may give different effect to the surrounding. As for this research, indoor plants are categorised into seven categories as follows;-

	<p>LINEAR Narrow with approximately parallel sides; a number times longer than wide.</p>
	<p>ELLIPTICAL Shaped like a football; broad at the center and sloping to a point at both ends.</p>
	<p>CORDATE Heart Shaped</p>
	<p>OBLONG Longer than broad, with side nearly parallel.</p>



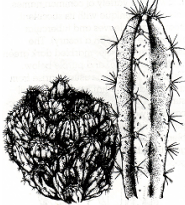
	<p>LANCEOLATE Lance-shaped. Widest about one-third the distance from the base with narrowed ends, several times longer than broad.</p>
	<p>SPATULATE Broadly rounded at tips but tapering to narrow base; narrower than obovate.</p>
	<p>CACTI</p>

Table 1: Type of plant based on leaves shape

8 room models were built using a brickwall with a see through perspex on top of it that act as the roof. Each of the room volume is at 0.729cub. meters. (0.9L x 0.9W x 0.9H). The indoor based of the space were laid with concrete as the flooring. Seven number of plants were then selected to represent each of the leaves category and placed inside the room models. This left a room empty that act as a reference indoor condition for such area. The plants choosed for the test were *Chlorophytum comosum* (spider plant) from Linear category, *Dracaena fragrans 'massangeana'* from Oblong category, *Aglaonema modestum* (Chinese evergreen) from Lanceolate category, *Philodendron domesticum* (Elephant ear philodendron) from Cordate category, *Ficus elastica* (Decora) from Elliptical category, *Peperomia obtusifolia* (Baby rubber plant) from Spatulate category and Melon Cactus (Column Cactus) from Cactus category.

Two sets of data were recorded. The first set consists of the air temperature and relative humidity data comparison between the room with and without the plant. Each plant was compared in the manner to see how significant the presentation of the plant may affect its thernal surrounding. The data were recorded using Hygro Thermo Anemometer for 10 days between 12pm to 2pm everyday.

Then, each of all seven plants were put in a room where the second set of data were taken. The air temperature and relative humidity for every each room were taken for every hour between 8.00am to 3.00pm for three continous days. The mean for the data were plotted in graph to be compared and analyzed.

3. RESULT AND DISCUSSION

3.1 Relative Humidity Comparison

The relative humidity comparison between the room with plant and the room without plant is shown in Table 3.1 to Table 3.7 for each type of plant.

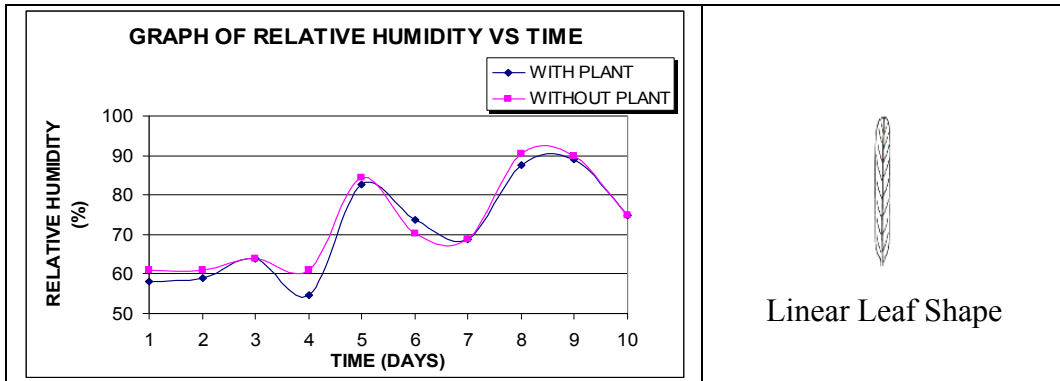


Figure 3.1: Relative Humidity of Linear Leaf Shape Plant Surrounding

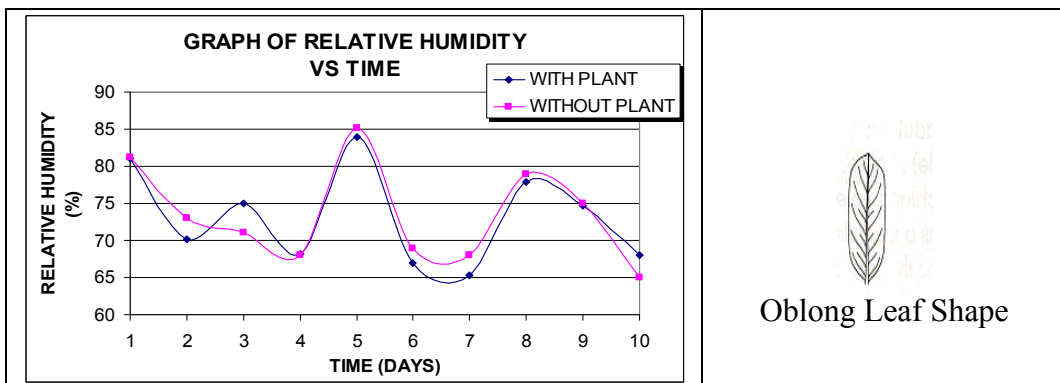


Figure 3.2: Relative Humidity of Oblong Leaf Shape Plant Surrounding

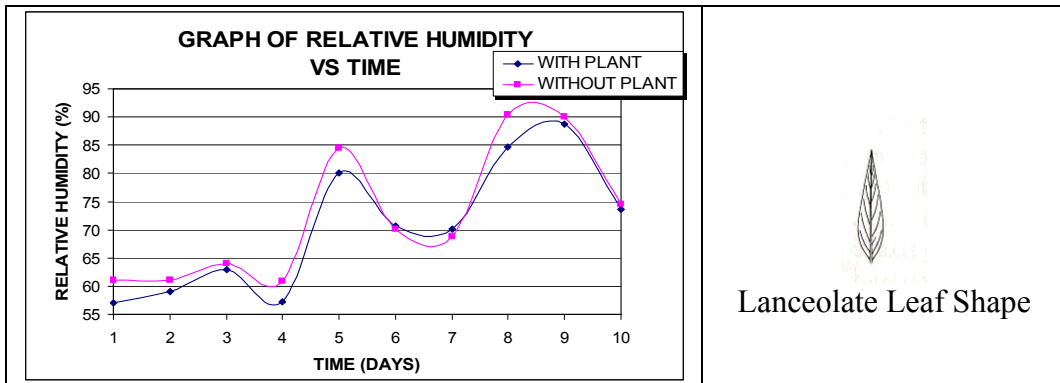


Figure 3.3: Relative Humidity of Lanceolate Leaf Shape Plant Surrounding.

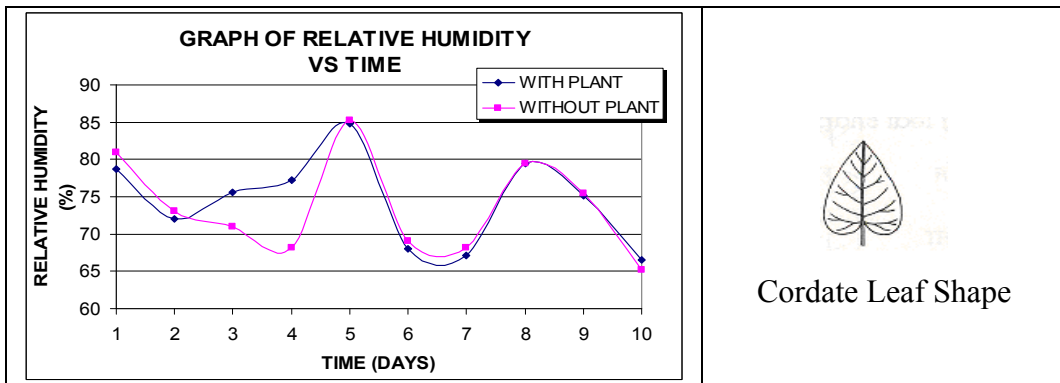


Figure 3.4: Relative Humidity of Cordate Leaf Shape Plant Surrounding.

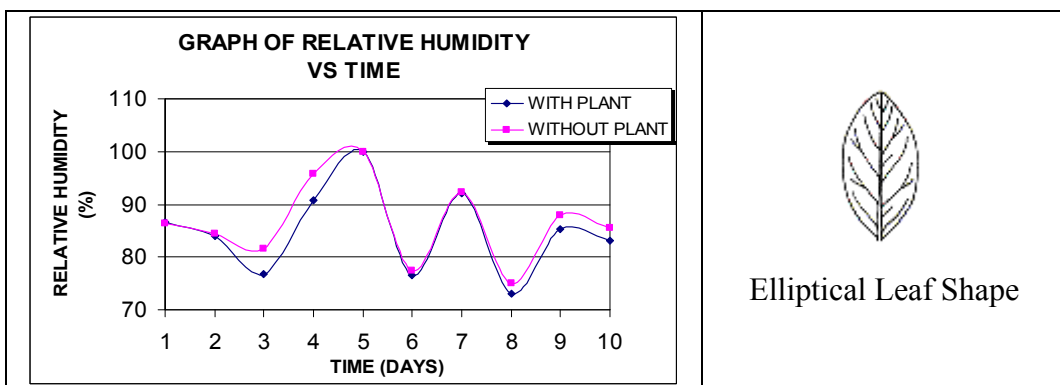


Figure 3.5: Relative Humidity of Elliptical Leaf Shape Plant Surrounding.

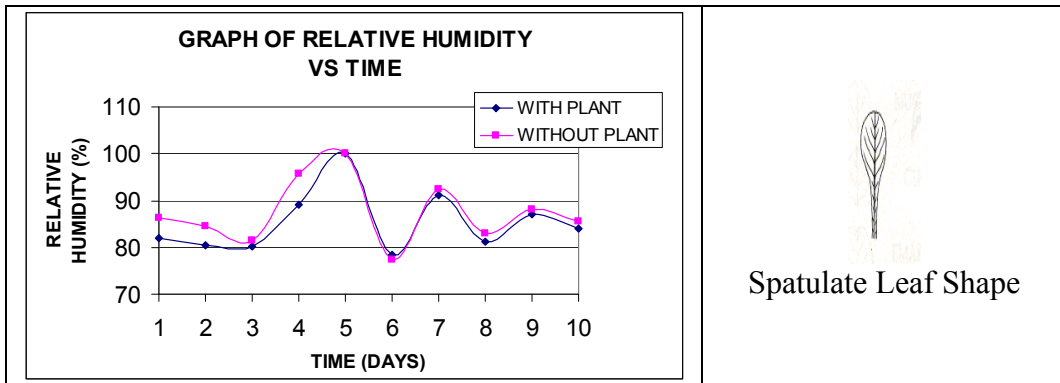


Figure 3.6: Relative Humidity of Spatulate Leaf Shape Plant Surrounding.

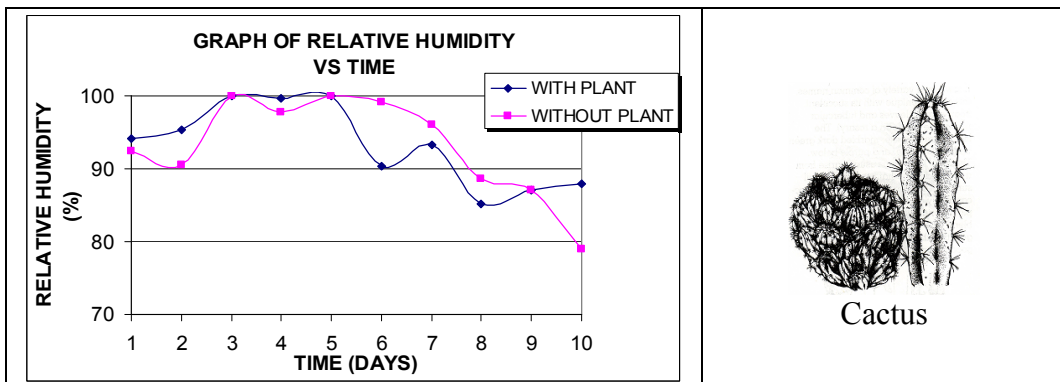


Figure 3.7: Relative Humidity of Cactus Leaf Shape Plant Surrounding.

Based on the figures above, most cases indicate lower relative humidity for rooms with plants compared to the rooms without plant although the graph shows irregular movement. Linear, Lanceolate, Elliptical and Spatulate shaped leaves plant show a constant reduction of air humidity as shown in Figure 3.1, 3.3, 3.5 and 3.6. However, figure 3.7 shows that relative humidity of the room with Cactus indicate a slightly higher relative humidity than an empty room in 4 out of 10 days.

Basically the difference of relative humidity percent between rooms with plant and rooms without plant is about 0.1% to 7% in range.

3.2 Air Temperature Comparison

The air temperature comparison between the room with plant and the room without plant is shown in Figure 3.8 to Table 3.14 for each type of plant.

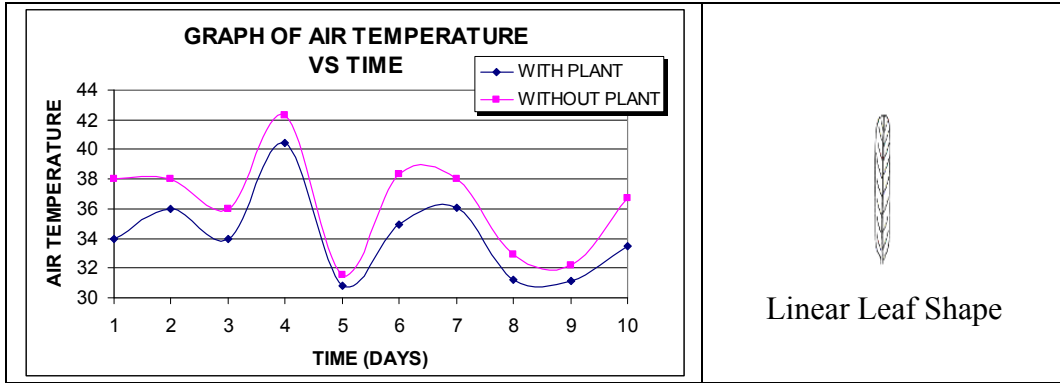


Figure 3.8: Air Temperature of Linear Leaf Shape Plant Surrounding.

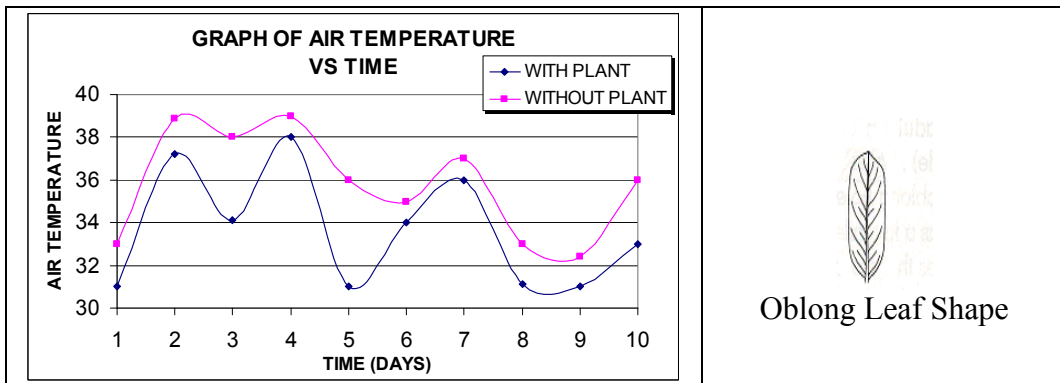


Figure 3.9: Air Temperature of Oblong Leaf Shape Plant Surrounding.

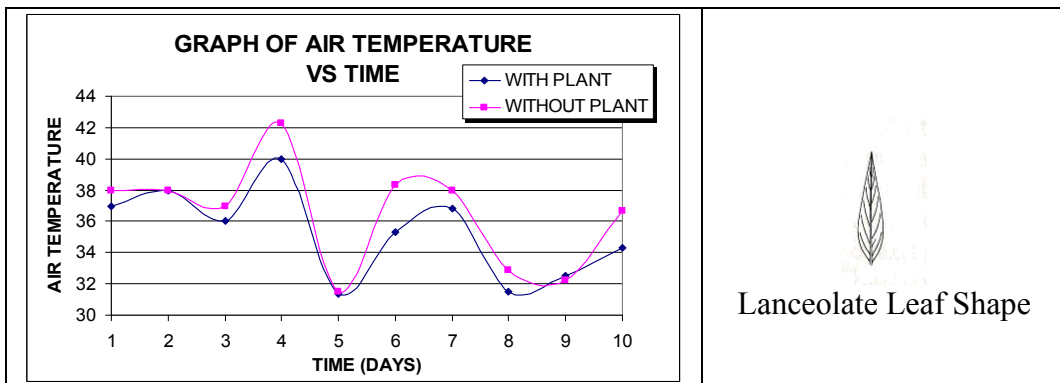


Figure 3.10: Air Temperature of Lanceolate Leaf Shape Plant Surrounding.

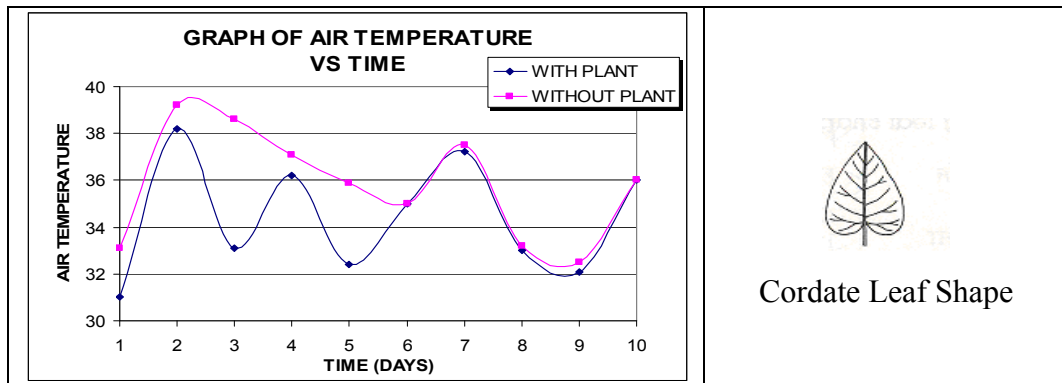


Figure 3.11: Air Temperature of Cordate Leaf Shape Plant Surrounding.

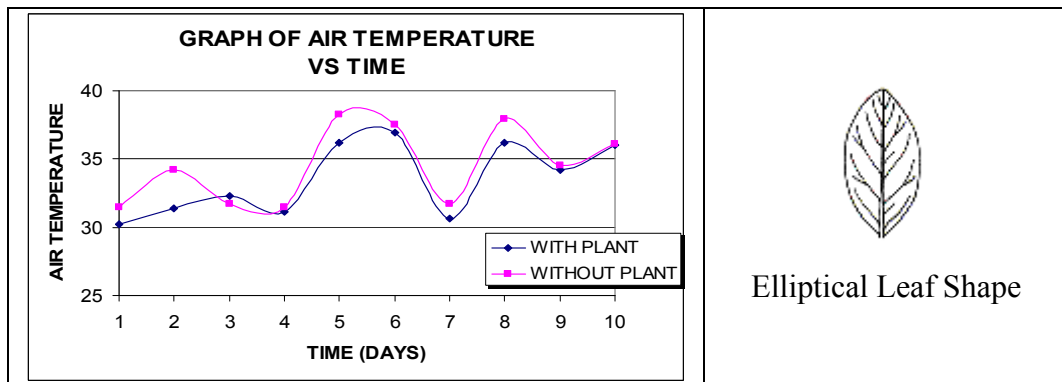


Figure 3.12: Air Temperature of Elliptical Leaf Shape Plant Surrounding.

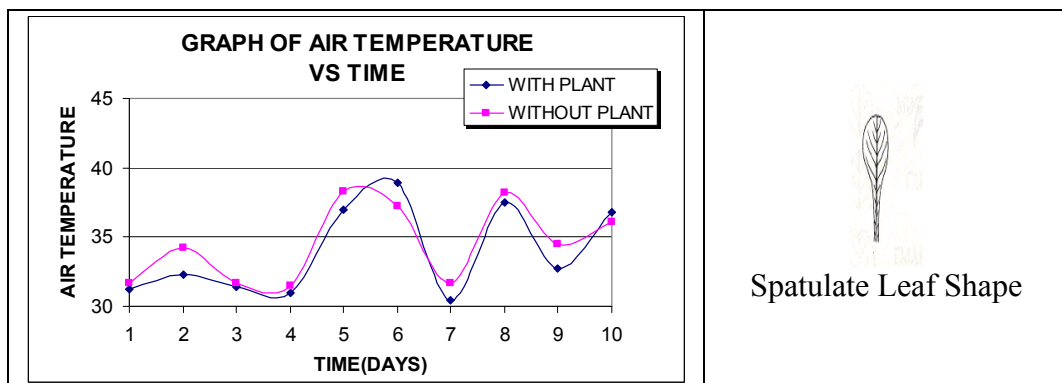


Figure 3.13: Air Temperature of Spatulate Leaf Shape Plant Surrounding.

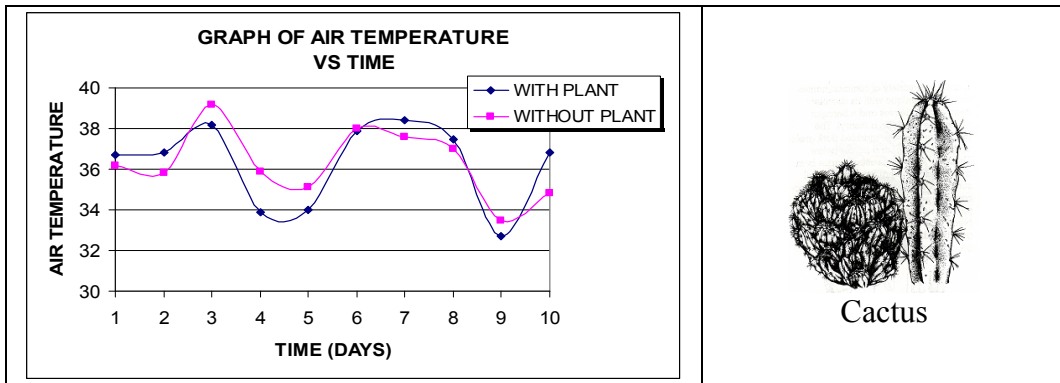


Figure 3.14: Air Temperature of Cactus Leaf Shape Plant Surrounding.

Based on the figure 3.8 to figure 3.14 show that the temperature for rooms with plants is recorded to be lower than rooms without plants besides its irregular pattern.

As the rooms were completely built with concrete blocks as the wall without any windows and come along with a see through perpex roofing, there were signs of green house effect happened in few cases. Figure 3.10 shows a maximum of air temperature level was recorded at 42.3°C for room without plant.. Anyway, as comparison on that particular day, the room with Lanceolate shaped leaves plant only recorded an air temperature at 40.0°C.

Figure 3.9 and figure 3.11 show an obvious air temperature reduction when empty rooms were compared to the rooms with plants with Oblong and Cordate shaped leaves. While again Linear, Lanceolate and Elleptical shaped leaves plants indicate a consistence reduction of air temperature as shown in figure 3.8, 3.10 and 3.12.

From all the graph analysis we can see that the differences of air temperature between rooms with plant and rooms without plan is about 0.1% to 5% in range.

3.3 Comparison Analysis Between Type of Plants

The rooms with plants indicate differences in the percentage of reduction and increment of relative humidity and air temperature when compared with empty rooms. Due to the result, another set of data were taken to compare the performance of relative humidity and air temperature of the plants surrounding simultaneously.

This data were taken for three continous days for all 7 rooms with each type of the 7 plants. Relative humidity and air temperature were taken at every hour from 8.00am to 3.00pm. The grapg shown below are the average of the data taken for three days at that particular hour.

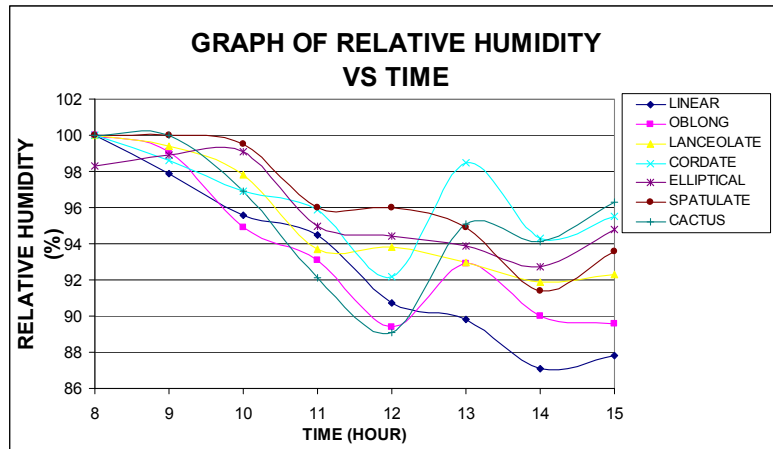


Figure 3.15: Analysis of Average Relative Humidity Comparison for Each Plant Category.

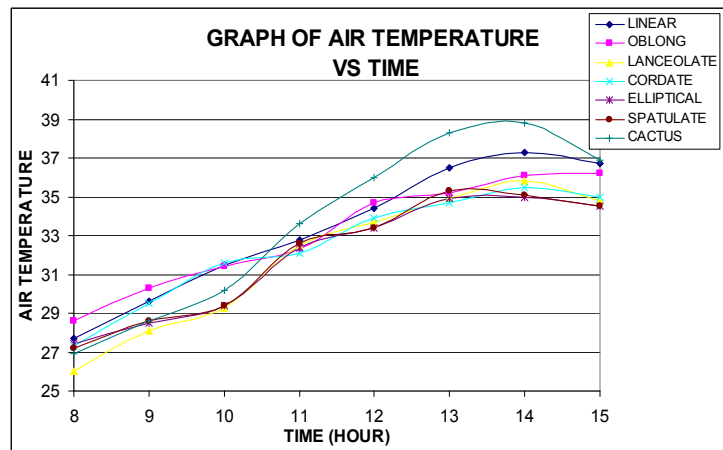


Figure 3.16: Analysis of Average Air Temperature Comparison for Each Plant Category.

Figure 3.15 shows an overall reduction of relative humidity from 8.00am to 3.00pm for all rooms. However rooms with Oblong, Cordate and Cactus shaped leaves plant indicate relative humidity increment at 1.00pm. Room with Linear shaped leaves plant shows a constant and significant reduction of air temperature compared to the rest with the minimum was 87.1% at 2pm.

Figure 3.16 shows an overall increment of air temperature from 8.00am to 3.00pm. As comparison, rooms with Lanceolate and Spatulate shaped leaves plant shows a consistency lower air temperature around 1°C to 2°C compared with other rooms. Room with Linear shaped leaves plant was also recorded with low air temperature during early hours but started to increase at noon.

3.4 Discussion

There are many reasons and factors that affect the increase and decrease of the relative humidity and air temperature. Surrounding weather is the biggest factor. The changes in weather may affect the data collection activity.

From the comparison among the 7 categories, small leaves plants like under category Lanceolate, Spatulate and Linear show a significant effect in lowering both the surrounding relative humidity and air temperature. Sizes of these leaves are small compared to other plants. Anyway, small areas do not guarantee that they cannot release oxygen in high quantity as they are depending on the amount of stomas action. These plants are actually capable in absorbing many types of pollutant like Formaldehyde at the rate of 560 microgram per hour, Xylene at rate 268 microgram per hour and Carbon monoxide gas at 96% [10]. The process may also rely on the quantity of stomas of the plant. Thus, with that significant quantity, it may also contribute in high respiration process in lowering the surrounding air humidity and air temperature.

On the other hand, wide leaves plants like Cordate and Elliptical categories show a significant effect in lowering the air temperature of its surrounding, but not its relative humidity, especially the Cordate type. Despite of having wide leaves that we thought will come with a high quantity of stomas, the Cordate type seems to be not efficient in lowering the humidity. This may be caused by the plant metabolism level which may not absorb the surrounding water rapidly compared to other plant. However, it shows potential in lowering the air temperature despite of inconsistency reduction of the temperature through out the day.

4. CONCLUSIONS

Overall, the result taken was influenced by the physical character of the plant where the shape of leaf has a very significant role in influencing the relative humidity and air temperature result. As the plants came under different species to represent the leaves potential, physically the plants themselves came in various sizes and architectural character. Some comes with bushy leaves while some may come with small quantity of leaves. This may also affect the result of the study. Besides that, the processes are also affected by the stomas number at other part of the plants such as the stems and branches. From the data analysis, the plants that are good in lowering the relative humidity may from Linear, Lanceolate and Oblong shaped leaves categories. While the plants that are good in lowering the air temperature may be from Linear, Lanceolate, Cordate and Oblong categories. Anyway the percentage of reduction in relative humidity and air temperature in this study may not be the same in a bigger and actual scale of room as the rooms used in the study are only with the size of 0.9m x 0.9m x 0.9m.

REFERENCES

- [1] Lokman Hakim, Magda Sibley and Izudinshah, (2011). Bioclimatic Technology in High Rise Office Building Design: A Comparison Study for Indoor Environmental Condition. *Journal of Science and Technology, Vol. 3, No. 2.* UTHM Publication, Malaysia.
- [2] Wolverton, B.C., Anne Johnson and Keith B. (1989). Interior Landscape Plants for Indoor Air Pollution Abatement-Final Report. *National Aeronautics and Space Administration (NASA)*, Stennis Space Centre, USA.
- [3] Yeang, K., (1997). The Skyscraper, Bioclimatically Considered: A Design Primer. Academy Editions, London.
- [4] Wolverton, B.C. and John, D.(1993). Plants and Soil Microorganisms:Removal of Formaldehyde, Xylene,and Ammonia from the Indoor Enviroment. *The Mississippi Academy of Science.* Vol 38, No.2., USA.
- [5] Wolverton, B.C. and John, D. (1996). Interior Plants: The Influence on Airborne Microbes inside Energy Efficient Building. *The Mississippi Academy of Science.* Vol 41, No.2., USA.
- [6] Bill, H. and Sealey, A.(1992). Healthy Building. *1st ed.* Longman Group UK Limited, England. pp 21-22.
- [7] Abakr, Yousif A. (2005). Building performance assessment of an eco-house in Malaysia: A comparative analysis. *Proceeding 2005 World Sustainable Building Conference*, Tokyo, Japan.
- [8] Ismail, M.R. and Barber, J.M., (2001). A field study to determine inside design conditions for Malaysian air conditioning systems. *Architectural Science Review*, Volume 44, pp 83 - 99.
- [9] Briggs, G. and Calvin,C. L.(1987). Indoor Plants. *1st ed.* :John Wiley & Sons, Inc., Canada. pp 377-504.
- [10] Givoni, B., (1994). Passive and Low Energy Cooling of Building, John Wiley & Son. Inc., New York.

A Rank Test on Equality of Population Medians

Pooi Ah Hin*

Sunway University Business School,
Sunway University,
46150 Petaling Jaya, Malaysia

*Corresponding email: ahhinp@sunway.edu.my

Abstract

The Kruskal-Wallis test is a non-parametric test for the equality of K population medians. The test statistic involved is a measure of the overall closeness of the K average ranks in the individual samples to the average rank in the combined sample. The resulting acceptance region of the test however may not be the smallest region with the required acceptance probability under the null hypothesis. Presently an alternative acceptance region is constructed such that it has the smallest size, apart from having the required acceptance probability. Compared to the Kruskal-Wallis test, the alternative test is found to have larger average power computed from the powers along the evenly chosen directions of deviation of the medians.

Keywords : non-parametric test ; population medians ; average power

1. INTRODUCTION

Let $X_{11}, \dots, X_{n_1}, \dots, X_{1K}, \dots, X_{n_K}$ be K independent random samples from continuous distributions with cumulative distribution functions $F(x - \theta_1), \dots, F(x - \theta_K)$, respectively where θ_j denotes a location parameter for the j -th population, frequently interpreted as the median or the treatment effect. We consider here the problem of testing the null hypothesis $H_0 : \theta_1 = \dots = \theta_K$; that is, the hypothesis that there are no differences among the K population medians. The alternative hypothesis is $H_1 : \theta_j \neq \theta_k$ for at least one $j \neq k$.

Let $N = \sum_{j=1}^K n_j$ be the total number of observations in the combined sample.

We first rank all N observations jointly, from least to greatest. Let r_{ij} denote the rank of X_{ij} that is $r_{ij} = \text{Rank}(X_{ij})$ in the combined sample. For $j = 1, 2, \dots, K$, we set

$$R_j = \sum_{i=1}^{n_j} r_{ij}, \quad \bar{R}_j = \frac{R_j}{n_j}, \quad \bar{R}_{..} = \frac{N+1}{2}$$

where R_j is the sum of the ranks for the j -th treatment, \bar{R}_j the average rank for the j -th treatment, and $\bar{R}_{..}$ the average rank in the joint ranking. A way to measure the overall closeness of the \bar{R}_j to $\bar{R}_{..}$ is a weighted sum of the squared

differences $\left(\bar{R}_j - \frac{N+1}{2}\right)^2$, for example, the Kruskal-Wallis statistic:

$$T = \frac{12}{N(N+1)} \sum_{j=1}^K n_j \left(\bar{R}_j - \frac{N+1}{2}\right)^2 \quad (1)$$

Since T is zero when the \bar{R}_j are all equal and is large when there are substantial differences among the \bar{R}_j , the hypothesis is rejected for large values of T . For $K = 2$, the Kruskal-Wallis test reduces to the two-sided Wilcoxon test [1]. By squaring out $\left(\bar{R}_j - \frac{N+1}{2}\right)^2$ and replacing \bar{R}_j by R_j . The statistic T can be rewritten as:

$$T = \left(\frac{12}{N(N+1)} \sum_{j=1}^K \frac{R_j^2}{n_j} \right) - 3(N+1)$$

The null distribution of T can be obtained by using the fact that under H_0 , all $N! / \prod_{j=1}^K n_j!$ assignments of n_1 ranks to the treatment 1 observations, n_2 ranks to the treatment 2 observations, ..., n_K ranks to the treatment K observations, are equally likely. However, this method is computational difficult even K is small [2] provided the upper 10% point of the exact probability distribution of the Kruskal-Wallis test statistic for $K = 3$ samples with $\max(n_1, n_2, n_3) \leq 6$, also $n_1 = n_2 = n_3 = 7$ and 8; $K = 4$ samples with $(n_1, n_2, n_3, n_4) \leq 4$; and $K = 5$ samples with $(n_1, n_2, n_3, n_4, n_5) \leq 3$.

Many approximate distributions of the statistic T under the null hypothesis were proposed because of the computational difficulty for computing the exact null distribution of the T statistic. Kruskal [3] showed that under the null hypothesis, the statistic T has a limiting chi-square distribution with $K - 1$ degrees of freedom if $\min(n_1, \dots, n_K) \rightarrow \infty$, with $n_j / N \rightarrow \lambda_j, 0 < \lambda_j < 1$, for $j = 1, 2, \dots, K$. For finite samples, the approximation based on this asymptotic result is in general conservative; that is, it indicates upper-tail probabilities which are larger than the true ones. An alternative simple approximation is given by Wallace [4]; the B_2 -III approximation. This approximation is generally closer than the preceding one, but it tends to be anticonservative unless the sample sizes are quite disparate, in which case it becomes conservative also. There are several other approximations [5,6].

The acceptance region of the Kruskal Wallis test may not be the smallest region with the probability $1 - \alpha$ under H_0 . Thus if we can find an alternative test of which the acceptance region is smallest and yet having the required probability $1 - \alpha$ under H_0 , then it is likely that the alternative test may be able to achieve larger power under the alternative hypothesis.

In Section 2, we find an approximate multivariate quadratic-normal distribution for $\mathbf{R} = (R_1, R_2, \dots, R_K)$ and use the underlying random variables which have independent standard normal distributions to form the smallest acceptance region with the required acceptance probability.

In Section 3, we compare the powers of the Kruskal Wallis test and the alternative test under different types of distribution of the X_{ij} . It is found that the alternative test has larger average power computed from the powers along the evenly chosen directions of deviation of the medians.

2. AN ALTERNATIVE TEST FOR THE EQUALITY OF POPULATION MEDIANS

We note the Kruskal-Wallis test statistic T is a function of the random variables, R_1, R_2, \dots, R_K which are correlated and non-normally distributed. Therefore the acceptance region given by the values of (R_1, R_2, \dots, R_K) of which T is not larger than a constant T_α may not be the smallest region with the required acceptance probability.

Presently we find an approximate multivariate non-normal distribution for \mathbf{R} in terms of a set of uncorrelated random variables z_1, z_2, \dots, z_{K-1} having the standard normal distributions, and propose an alternative test of which the acceptance region is given by $z_1^2 + z_2^2 + \dots + z_{K-1}^2 \leq \chi_{K-1, \alpha}^2$ where $\chi_{K-1, \alpha}^2$ is the $100(1 - \alpha)\%$ point of the chi-square distribution with $K-1$ degrees of freedom. The bell shape of the normal distributions implies that the acceptance region will be the smallest region with the required probability $1 - \alpha$.

We may use the following procedure to find an approximate multivariate non-normal distribution for \mathbf{R} :

- i. Generate M values of \mathbf{R} using a chosen common continuous distribution for the X_{ij} . As the null distribution of \mathbf{R} does not depend on the common distribution of the X_{ij} , we may choose the common continuous distribution to be the standard normal distribution.
- ii. Compute the sample moments

$$M_{jk}^{(k_1)(k_2)} = \frac{1}{M} \sum_{m=1}^M \bar{R}_{mj}^{k_1} \bar{R}_{mk}^{k_2} \quad j, k = 1, 2, \dots, K; \quad k_1 \geq 0, \quad k_2 \geq 0, \quad 0 \leq k_1 + k_2 \leq 2$$
 where $(R_{m1}, R_{m2}, \dots, R_{mK})$ is the m -th generated value of \mathbf{R} , $\bar{R}_{mj} = R_{mj} - \bar{R}_j$ and $\bar{R}_j = \frac{1}{M} \sum_{m=1}^M R_{mj}$.
- iii. Use the results obtained in Step (ii) to compute the sample variance-covariance matrix of \mathbf{R} .
- iv. Find the K eigenvectors of the sample variance-covariance matrix obtained in Step (iii), and use the $K-1$ eigenvectors with non-negligible eigenvalues to form the matrix \mathbf{B} .
- v. Compute $(S_{m1}, S_{m2}, \dots, S_{m(K-1)})^T = \mathbf{B}^T (R_{m1}, R_{m2}, \dots, R_{mK})^T$.
- vi. Compute $M_j^{(k)} = \frac{1}{M} \sum_{m=1}^M S_{mj}^k$, $k = 2, 3, 4; \quad j = 1, 2, \dots, K-1$
- vii. Find $\tilde{\lambda}^{(j)} = (\lambda_1^{(j)}, \lambda_2^{(j)}, \lambda_3^{(j)})$ such that $E(\varepsilon_j^k) = M_j^{(k)}$, $k = 2, 3, 4$ where

$$\varepsilon_j = \begin{cases} \lambda_1^{(j)} z_j + \lambda_2^{(j)} \left(z_j^2 - \frac{1 - \lambda_3^{(j)}}{2} \right), & \text{for } z_j \geq 0 \\ \lambda_1^{(j)} z_j + \lambda_2^{(j)} \left(\lambda_3^{(j)} z_j^2 - \frac{1 - \lambda_3^{(j)}}{2} \right), & \text{for } z_j < 0 \end{cases} \quad (2)$$

The random variable ε_j in Step (vii) is said to have a quadratic-normal distribution with parameters 0 and $\lambda^{(j)}$ [7] while the vector $\mathbf{R} = (R_1, R_2, \dots, R_K)$ is said to have a $(K-1)$ -dimensional multivariate quadratic-normal distribution with estimated parameters $(\bar{R}_1, \bar{R}_2, \dots, \bar{R}_K)$, \mathbf{B} , and $\lambda^{(i)}$, $i = 1, 2, \dots, K-1$ [8].

3. POWERS OF THE ALTERNATIVE TEST

In this section, we use simulation to estimate the powers of the alternative test under the following three possible distributions of the X_{ij}

- i. $X_{ij} \sim N(\theta_j, 1)$
- ii. $X_{ij} \sim$ Uniform distribution over $[\theta_j, \theta_j + 1]$
- iii. $X_{ij} = \theta_j + X_j^{(1)} + X_j^{(2)}$

where $X_j^{(1)} \sim$ Uniform distribution over $[-0.5, 0.5]$ and $X_j^{(2)} \sim N(0, 1)$

For a given value of $(\theta_1, \theta_2, \dots, \theta_K)$ we may estimate the powers under a given type of distribution of the X_{ij} by first generating M^* values of $\mathbf{X} = (X_{11}, \dots, X_{n_1 1}, \dots, X_{1K}, \dots, X_{n_K K})$. For a generated value of \mathbf{X} , we find the corresponding values of $\mathbf{R}, \mathbf{S}^T = \mathbf{B}^T \mathbf{R}^T$ and $\lambda^{(j)}, j = 1, 2, \dots, K-1$.

By solving Equations (2) with ε_j replaced by the computed S_j , we get the value of $z_j, j = 1, 2, \dots, K-1$. If $\sum_{j=1}^{K-1} z_j^2 > \chi_{K-1, \alpha}^2$, then we get a rejection result. The proportion of the M^* generated values of \mathbf{X} which lead to rejection results is then an estimate of the power of the test evaluated at $(\theta_1, \theta_2, \dots, \theta_K)$.

To compare the power functions of the tests, we choose a number of values of the radial distance ρ in the K dimensional polar coordinates system, and for each chosen value of the radial distance, we choose evenly M_β values of the vector $(\beta_1, \beta_2, \dots, \beta_{K-1})$ of the polar angles. From the value of $(\rho, \beta_1, \beta_2, \dots, \beta_{K-1})$, we determine the value of $(\theta_1, \theta_2, \dots, \theta_K)$ and estimate the corresponding powers of the tests. For each value of ρ , we then find the average of the powers over the M_β evenly

chosen values of the vector of the polar angles. Some results for average powers for the case when $K=3$ are shown in Tables 3.1 and 3.2.

Table 3.1: Average Powers of the Tests ($K=3, n_1=n_2=n_3=3, \alpha=0.05, M=50,000, M^*=10,000, M_\beta=81$)

P	Kruskal-Wallis Tests			Alternative Test		
	Normal	Uniform	Mixed	Normal	Uniform	Mixed
0	0.050285	0.049817	0.049995	0.050119	0.049857	0.049998
0.5	0.072399	0.281719	0.070769	0.073219	0.284216	0.07126
1	0.143315	0.60751	0.136123	0.145281	0.61794	0.138358
1.5	0.254288	0.739375	0.239963	0.25541	0.766064	0.241651
2	0.373773	0.81271	0.354752	0.375146	0.844965	0.356468
2.5	0.477936	0.858073	0.459284	0.482183	0.89261	0.46207
3	0.559098	0.886293	0.542122	0.566735	0.918815	0.54781
3.5	0.620504	0.904128	0.604965	0.632441	0.933756	0.615675
4	0.667812	0.915767	0.654838	0.68412	0.942733	0.669419
4.5	0.705969	0.926141	0.692505	0.726409	0.949969	0.711978
5	0.736262	0.934433	0.725464	0.76017	0.955236	0.747995

Table 3.2: Average Powers of the Tests ($K=3, n_1=2, n_2=5, n_3=8, \alpha=0.05, M=50,000, M^*=10,000, M_\beta=81$)

P	Kruskal-Wallis Tests			Alternative Test		
	Normal	Uniform	Mixed	Normal	Uniform	Mixed
0	0.048917	0.049041	0.048989	0.048607	0.048479	0.048575
0.5	0.090201	0.453569	0.08736	0.088452	0.469756	0.085716
1	0.224562	0.69524	0.210353	0.222264	0.746101	0.207654
1.5	0.399486	0.791251	0.380105	0.406342	0.848244	0.385317
2	0.534953	0.847688	0.518285	0.559169	0.904767	0.539495
2.5	0.615925	0.882475	0.603649	0.652763	0.937301	0.639084
3	0.666621	0.905001	0.656399	0.711836	0.95556	0.699816
3.5	0.704638	0.921752	0.695489	0.75374	0.965957	0.743068
4	0.736279	0.933859	0.726521	0.788341	0.971599	0.778041
4.5	0.76293	0.943414	0.754138	0.816983	0.976267	0.806938
5	0.786169	0.951927	0.777465	0.841758	0.980242	0.832007

Tables 3.1 and 3.2 show that for sufficiently large value of ρ , the average power of the alternative test is always larger than that of the Kruskal-Wallis test, and as the sample sizes become disparate and the distributions of the X_{ij} deviate from normality, the difference between the average powers of the two tests becomes more obvious.

4. CONCLUSION

For the values of K and the n_j chosen so far, it is possible to approximate the null distribution of the vector formed by the sums of the ranks within sample. When the values of K and the n_j are such that the multivariate quadratic-normal distribution is not suitable, we may use other multivariate non-normal distributions formed by replacing the quadratic functions in Equation (2) by other nonlinear functions and apply the method given in Section 2. It is likely that for other values of K , the situation with disparate sample sizes and non-normal distributions of the X_{ij} will continue to be one in which the alternative test will perform better.

REFERENCES

- [1] Lehmann, E.L. (1998). *Nonparametrics: Statistical Methods Based on Ranks*. Upper Saddle River, NJ: Prentice Hall.
- [2] Iman, R.L., Quade, D. and Alexander, D.A. (1975). Exact Probability Levels for the Kruskal–Wallis Test. *Selected Tables in Mathematical Statistics*. 3:329–384.
- [3] Kruskal, W.H. (1952). A Nonparametric Test for the Several Samples Problem. *The Annals of Mathematical Statistics*. 23: 525-540.
- [4] Wallace, D.L. (1959). Simplified Beta-Approximation to the Kruskal-Wallis H Test. *Journal of the American Statistical Association*. 54: 225-230.
- [5] Kruskal, W. H., Wallis, W. A.(1952) Use of ranks in one-criterion variance analysis. *J. Amer. Statist. Assoc.* 47: 583–621.
- [6] Iman, R.L. and Davenport, J.M. (1976). New Approximations to the Exact Distribution of the Kruskal–Wallis Statistic. *Comm. Statist. Theory Methods*. A5(14):1335–1348.
- [7] Pooi, A.H. (2003). Effects of Non-Normality on confidence intervals in linear models. Technical Report No. 6/2003, Institute of Mathematical Sciences, University of Malaya.
- [8] Fam Pei Shan and Pooi Ah Hin (2004). An approximation of multivariate non-normal distribution, Proceedings of the ‘Malaysian Science and Technology Congress 2004’, Oct 2004, Palace of the Golden Horses, Selangor, Malaysia: 5 – 7.

Epoxidation of Palm Kernel Oil Fatty Acids

Michelle Ni Fong Fong¹, Jumat Salimon^{*,1}

¹School of Chemistry & Food Technology, Faculty of Science and Technology
Universiti Kebangsaan Malaysia, 43600 Bangi, Selangor, Malaysia.

**Corresponding email: jumat@ukm.my*

Abstract

Epoxidation of palm kernel oil fatty acids using formic acid and hydrogen peroxide was carried out effectively using a homogeneous reaction. It was found that epoxidation reaction occurred optimally at a temperature of 40°C and reaction time of 120 minits. The oxirane conversion was the highest at 1.46mol and 0.85mol of hydrogen peroxide and formic acid respectively. It was found that a maximum of 99% relative conversion of ethylenic oxirane was obtained, similar to the conversion of iodine value. The formation of epoxide adduct of palm kernel oil fatty acids (FAPKO) was confirmed by ¹H NMR and ¹³C NMR spectral analysis showed the disappearance of double bonds and replaced by epoxy group in the EFAPKO.

Keywords: palm kernel oil; epoxidation, hydrogen peroxide; formic acid

1. INTRODUCTION

Vegetable oils in general have excellent properties such as high viscosity index, high lubricity, high flash point, low evaporative loss, high bio-degradability and low toxicity with regard to their use as base oils for lubricants. On the negative side they are known to possess low thermal, oxidative and hydrolytic stabilities and poor low-temperature characteristics [1,2,3]. The properties of vegetable oils are determined by their fatty acid composition. A high content of linoleic/linolenic acid decreases thermal oxidative stability. Whereas, a higher proportion of long chain saturated fatty acid leads to inferior cold flow behavior. Palm kernel oil belongs to unique group of vegetable oils called lauric oils; similar to coconut oil. The most abundant fatty acid in this group is lauric acid [4].

Fats and oils are renewable resources that can chemically or enzymatically treated to produce materials that can often act as a replacement for materials derived from petroleum. One of the important reactions that can be used to improve these fats and oils' performance is epoxidation. Epoxidation processes are becoming popular due to its role as a starting material to many other reactions. An epoxide is cyclic ether with three ring atoms. This ring approximately defines an equilateral triangle, which makes it highly strained. The strained ring makes epoxides more reactive than other ethers. Fatty epoxides are used directly as plasticizers that are compatible with polyvinyl chloride (PVC) and as stabilizers for PVC resins to improve flexibility, elasticity, and toughness and to impart stability of polymer towards heat and UV radiation. The high reactivity of oxirane ring enables epoxides to act as raw material for a variety of chemicals, such as alcohols, glycols, alkanolamines, carbonyl compounds, olefinic compounds and polymers like polyesters, polyurethanes, and epoxy resin [5,6,7,8].

In recent years, epoxidation process had been carried out using vegetable oils such as soybean oil, canola oil, jatropha oil, castor oil and cottonseed oil. Carbon double bonds of unsaturated fatty acids were epoxidized via acid catalysis producing epoxy functional groups. Parameter used to optimized the epoxidation of vegetable oil were reaction temperature, the concentration of oxygen donor such as hydrogen peroxide, concentration of oxygen carrier and also as catalyst such as formic acid and acetic acid as reported by Dinda et al. [5], Goud et al. [8] and Mungroo et al. [9]. From the oxirane content values, the relative fractional conversion to oxirane reported by Goud et.al [9] was calculated from the following expression:

$$\text{Relative conversion to oxirane (RCO)} = \frac{OOc}{OOt}$$

Where,

OOc = experimental oxygen oxirane

OOt = theoretical maximum oxirane oxygen from the expression:

$$OOt = \left(\frac{IVo/2Ai}{100 + (IVo/2Ai)Ao} \right) Ao \times 100$$

Where,

Ai (126.9) and Ao (16.0) are the atomic weights of iodine and oxygen respectively and IVo is the initial iodine value of sample.

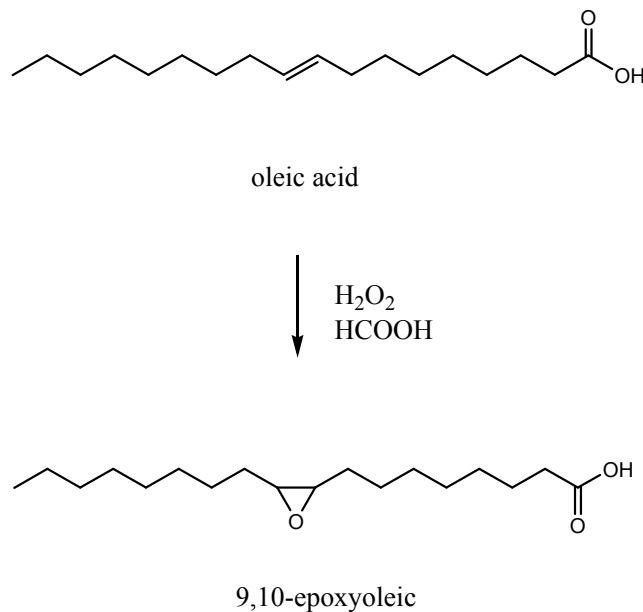


Figure 1: A schematic diagram of epoxidation reaction

In this paper, the main purpose was to develop value-added products from locally available renewable resources in Malaysia. Palm kernel oil is the oil produced from the kernel of an oil palm seeds, *Elaeis guineensis*. Palm kernel oil has been evaluated for its lubricating properties by Musa [4]. Palm kernel oil were compared with heavy duty oil (SAE 40) and light duty oil (SAE 30). The result showed that palm kernel oil's flash/fire point, pour point, specific density and viscosity met the required SAE specifications. Thus, palm kernel oil was a promising base oil for production of value-added lubricating products. Therefore, epoxidation of double bond in palm kernel fatty acid with hydrogen peroxide and performic acid generated *in-situ* was monitored and optimized to produced value-added palm kernel fatty acid epoxides. A further objective of this work was to open the oxirane ring in FAPKO with its major saturated acids to produce improved value biolubricant base stock.

2. MATERIALS AND METHODS

2.1 Materials

RBD palm kernel oil which was used as raw material for free fatty acid production was purchased from Jomalina Sdn Bhd. Aqueous hydrogen peroxide 30%, formic acid 98%, hexane 99% and ethanol were all chemicals from System[®].

2.2 Preparation of FAPKO

Free fatty acid was produced manually in batches by hydrolysis process before epoxidation of the double bonds takes place. 50g of RBD palm kernel oil was filled in a two-necked round bottom flask and was added with ethanolic potassium hydroxide. The solution was mixed together before underwent hydrolysis process at 60°C for 2 hours. Samples were extracted using hexane and wash with water before drying using anhydrous sodium sulphate. Final product was dried using vacuum rotary evaporator.

2.3 Epoxidation of FAPKO

The reaction was studied in a mechanically stirred three-necked round bottom flask (500ml) attached with thermometer on a hot plate. A reflux condenser completed the set-up. Performic acid used in the experiment was prepared in-situ. About 0.85 mol of formic acid per moles of double bonds in FAPKO were added into the reactor and heated to reaction temperature, under vigorous agitation (1200rpm). Then, about 1.46 mol of H₂O₂ solution were added, drop by drop and the reaction mixture was held at constant temperature and under stirring for several hours. After reaction completed, the mixture was washed with a solution of sodium bicarbonate (5 wt%), next with water until complete elimination of acidity in organic phase and finally with sodium chloride (5 wt%). The final product was cooled to solidified organic phase and dried in a refrigerator for 24 hours. Epoxides in FAPKO (EFAPKO) was dried using Whatman no.4.

2.4 Analysis and Data Processing

The stocks of FAPKO were analyzed to check its acidity value that was used in identifying the percentage of free fatty acid present in the sample. Method used was referred from AOCS methods. Iodine value and saponification value were evaluated using PORIM recommended practices. Sample also analyzed by GC, using Agilent Tech 6809 N unit furnished with column BPX-70. The characterization results are shown in Table 1. The evaluation of epoxidation reactions was followed by measuring the oxirane oxygen (%OOc) according to AOCS recommended practices and iodine value (IV). Epoxides formed in FAPKO are analyzed by ¹H-NMR and

^{12}C -NMR spectra on a JEOL JNM-ECP 400 spectrometer using chloroform as solvent in all experiments.

3. RESULTS AND DISCUSSION

Synthesis: Following the formula above, the maximum percentage of theoretical oxirane is 1.16%. The effects of the following reaction parameter were considered: the moles of hydrogen peroxide and formic acid with respect to the moles of oleic acid in FAPKO, reaction time and temperature. Table 1 showed the characteristic of FAPKO.

Table 1: Some of FAPKO physical chemical properties

Acidity ^a	99.92% (max)
Iodine Value ^a	18.7 mgI ₂ /g (average)
C8:0 (capric) ^b	2.79%
C10:0(caprylic) ^b	3.04%
C12:0(lauric) ^b	47.34%
C14:0(miristic) ^b	17.10%
C16:0(palmitic) ^b	8.96%
C18:0(stearic) ^b	2.38%
C18:1(oleic) ^b	16.43%
C18:2(linoleic) ^b	1.97%

^a Following AOCS method & PORIM Recommended Test Method

^b By GC analysis

Epoxide produced in this study was in liquid form in room temperature, deviates from expected solid form that were produced by other vegetable oils with higher unsaturation value. This is due to the abundance of saturated fatty acids such as lauric acid presence in the epoxide mixture. Though palm kernel oil is a drying oil, the abundance of medium chain fatty acids has lower tendency to undergo uniform staking process forming macro crystalline structure than long chain fatty acids of other non-drying product such as soybean oil and cottonseed oil in room temperature [10]. However, in low temperature the epoxide of FAPKO (EFAPKO) will still solidify into solids. The abundance of lauric acids will be used as reactants for ring opening and capping in base oils in further experiments.

Effect of Hydrogen Peroxide to Ethylenic Unsaturation: Figure 2 shows the effects of moles of hydrogen peroxide. As the moles of hydrogen peroxide increase, the oxirane conversion rate increase followed by decreasing of iodine value. The maximum relative conversion obtained is at 1.46 mol of hydrogen peroxide (75%). For higher concentration of hydrogen peroxide at the same conditions; temperature and reaction time, the reaction rate becomes constant. An increase in hydrogen peroxide concentration will increase the oxirane conversion rate. However, the stability of oxirane ring produced in a very high concentration of H_2O_2 is very poor, thus increasing the production of diol and α -glycol as side products [5,9].

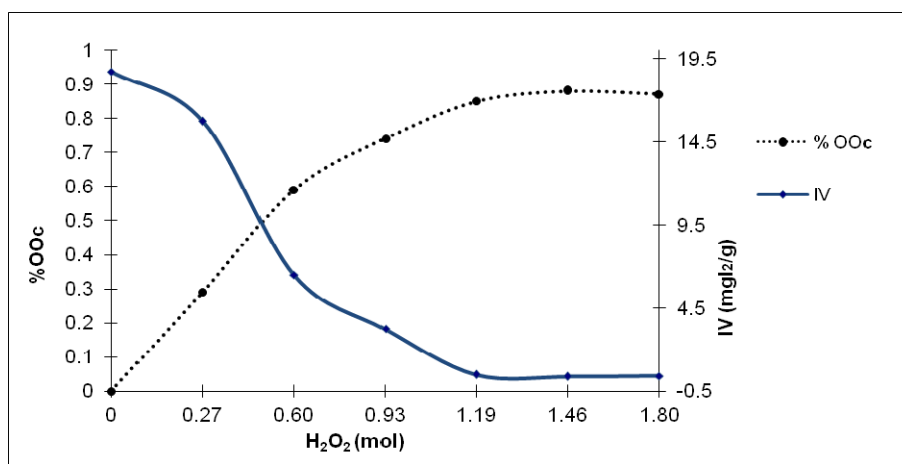


Figure 2: Graph of moles of hydrogen peroxide with oxirane conversion rate and iodine value

Effect of Formic Acid to Ethylenic Unsaturation: Figure 3 expressed the effect of moles of formic acid towards the yield of epoxide. As the concentration of formic acid increase to 0.87mol, the oxirane conversion rate increase to its highest (72%). However, when the formic acid concentration is further increased, %OOC and the iodine value decrease significantly. This showed that the oxirane ring has been degraded from high concentration of formic acid. Formic acid is a good oxygen carrier and indeed crucial for producing enough epoxides in the aqueous phase. Unfortunately, it also is the main culprit that is responsible for the hidrolisis of oxirane rings [11]. The amount of formic acid used per mole of unsaturation recommended by Niederhauser & Koroly 1949 is 1 mole and less. This ratio used not only for economical reasons but also to reduce by-products such as dihydroxy and dihydroxyformoxy derivatives that can reduce the oxirane production [11].

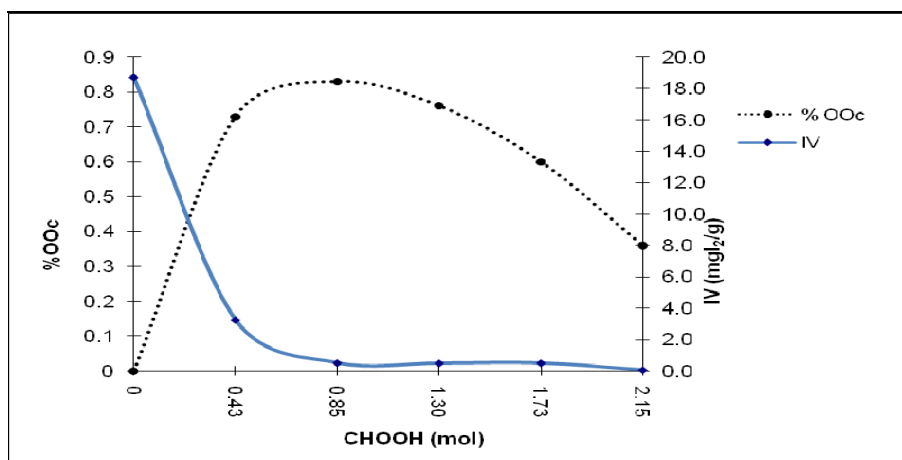


Figure 3: Graph of moles of formic acid with oxirane conversion rate and iodine value

Effect of Time and Temperature: Figure 4 expressed the effect of reaction time toward the yield of epoxides. The maximum %OOC value and percentage conversion of oxirane (99%) obtained within 120 minutes of reaction time. Nonetheless, the almost similarity of %OOC at other reaction time shows that effect of reaction time towards epoxidation of FAPKO is not very obvious. Moreover, oxirane rings produced in the reaction were not considered stable in the presence of acidity. Figure 5 shows the effect of temperature towards the epoxidation reaction. The optimum temperature for epoxidation process that produces maximum %OOC is at 40°C with relative conversion reaching 87%. At lower temperature, FAPKO tends to solidify and lower the chance of interfacial interactions of the reactants. Thus, the epoxide yield decreased. At higher temperature, the yield of epoxide not only decreased, there were evidents of oxirane decomposition shown by the iodine value. This phenomenon was similar in [5,9,11].

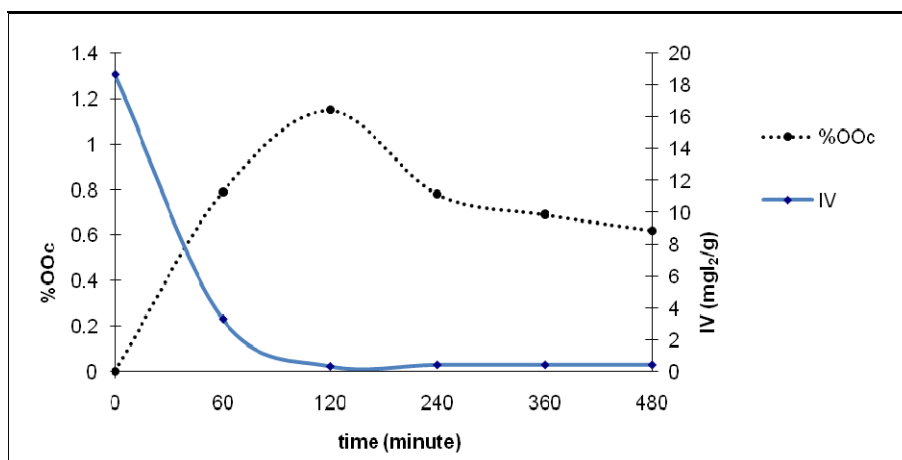


Figure 4: Graph of reaction time with the yield of epoxides

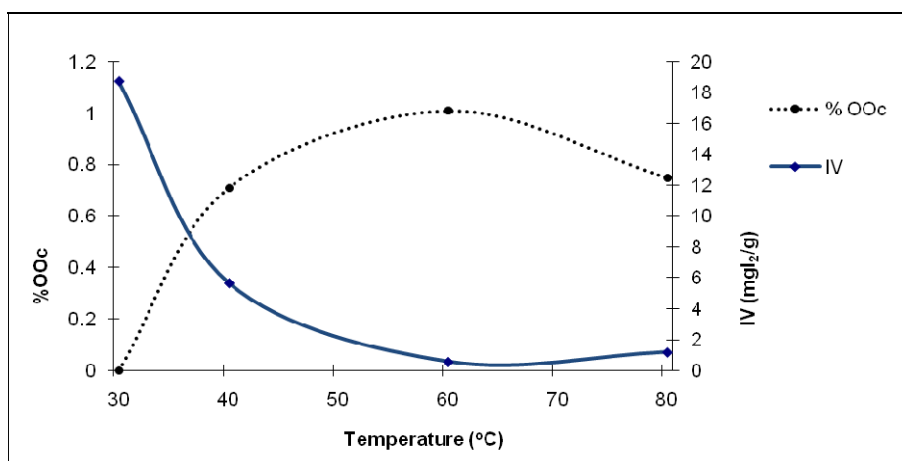


Figure 5: Graph of temperature with the epoxidation reaction

NMR Spectral Analysis: The formation of the epoxide adduct in FAPKO was confirmed by the difference of PKO, FAPKO and EFAPKO chemical shifts in ^1H NMR and ^{13}C NMR spectrum as shown in Table 1 and 2. ^1H NMR for EFAPKO showed the presence of epoxy group in the region of 2.7 ppm and disappearance of double bonds at the region of 1.6-5.2 ppm. However, both ^1H NMR of FAPKO and EFAPKO showed the presence of carboxylic group in the 11-12 ppm region. This showed that there were an abundance of saturated fatty acids in the epoxidized FAPKO. These saturated fatty acids would be use to produced branching molecule in the furthered ring opening reaction. ^{13}C NMR of FAPKO the disappearance of the double bond peaks 120-140 ppm and replaced by chemical shifts at 56-59 ppm region in EFAPKO. Thus, it is found that from NMR spectrum the double bonds in FAPKO have completely undergone epoxidation process to form EFAPKO.

Table 1: The difference of PKO, FAPKO and EFAPKO chemical shifts in ^1H NMR spectrum

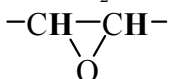
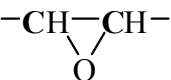
Types of proton	Reference, δ (ppm)	PKO, δ (ppm)	FAPKO, δ (ppm)	EFAPKO, δ (ppm)
α -CH ₂ -COOR	2.1-2.5	2.1-2.2	2.2-2.3	2.0-2.1
R-COO-CH-	3.5-4.8	3.9-4.1	-	-
R-COOH	11.0-12.0	-	11.6	11.0
C=C-H	4.5-6.5	5.1-5.2	5.2	-
C=C-C-H	1.6-2.6	1.4	1.6-1.8	-
R-CH ₃	0.7-1.3	0.7-1.1	0.8	0.7-1.2
R-CH ₂ -R	1.2-1.4	1.1	1.2	1.3
	2.5-3.5	-	-	2.7

Table 2: The difference of PKO, FAPKO and EFAPKO chemical shifts in ^{13}C NMR spectrum

Types of carbon	Reference, δ (ppm)	PKO, δ (ppm)	FAPKO, δ (ppm)	EFAPKO, δ (ppm)
R ₂ -CH ₂ -	15-55	22-31	22-32	28-33
R-CH ₃	8-30	13	14	17
	40-80	-	-	56-59
C=C	100-150	129	128-129	-
R-COOR	155-185	172	-	-
R-COOH	155-185	-	180	179

Reference: Pavia et al. 2001

4. CONCLUSIONS

The epoxidation of palm kernel fatty acids using hydrogen peroxide and performic acid generated *in-situ* was carried out and produced about 80% of epoxidized FAPKO yield. Although the maximum yield of oxirane ring produced from FAPKO were considered very low (1.15%) compare to other industrial vegetable oil due to its saturated nature, but the amount of oxirane conversions are optimum (99%) in the oil itself. From the relative conversion data obtained, it can be concluded that it is possible to develop value-added products, such as epoxide from palm kernel fatty acids.

Acknowledgments

The authors would like to thank the School of Chemical Sciences and Food Technology, Faculty of Science and Technology and Universiti Kebangsaan Malaysia for the financial support via research grant (UKM-GUP-NBT-08-27-113 and UKM-OUP-NBT-29-150/2011).

REFERENCES

- [1] Hwang, H.S. & Erhan, S.Z. 2005. Synthetic lubricant base stocks from Epoxidized soybean oil and Guerbert alcohols. *Industrial Crops and Products* 23: 311-317.
- [2] Lathi, S.P. & Mattiason, B. 2006. Green approach for the preparation of biodegradable lubricant base stock from epoxidized vegetable oil. *Journal of Applied Catalysis B: Environmental* 69: 207-212.
- [3] Sharma, B.K., Adhvaryu, A., Liu, Z. & Erhan Z.S. 2006. Chemical Modification of Vegetable Oils for Lubricant Applications. *JAOCs* 83: 129-136.
- [4] Musa, J.J. 2009. Evaluation of the lubricating properties of palm kernel oil. *Leonardo Electronic Journal of Practice and Technologies* 14: 107-114.
- [5] Dinda, S. Patwardhan, A.V., Goud, V.V. & Pradhan, N.C. 2008. Epoxidation of cottonseed oil by aqueous hydrogen peroxide catalyzed by liquid inorganic acids. *Bioresource Technology* 99: 3737-3744
- [6] Gerbase, A.E., Gregório J.R., Martinelli, M., Brasil M.C. & Mendes, N.F. 2002. Epoxidation of soybean oil by methyltrioxorhenium- $\text{CH}_2\text{Cl}_2/\text{H}_2\text{O}_2$ catalytic biphasic system. *JAOCs* 79: 179-181.
- [7] Goud, V.V., Patwardhan, A.V. & Pradhan, N.C. 2005. Studies on the epoxidation of mahua oil (*Madhumica indica*) by hydrogen peroxide. *Bioresource Technology* 97: 1365-1371.
- [8] Goud, V.V., Pradhan, N.C. & Patwardhan, A.V. 2006. Epoxidation of Karanja. (*Pongamia glabra*) oil by H_2O_2 . *JAOCs* 7 (83): 635-640.
- [9] Gryglewicz, S., Piechocki, W. & Gryglewicz, G. 2003. Preparation of Polyol Esters Based on Vegetable and Animal Fats. *Bioresource Technology* 87: 35-39.

- [10] Kleinová, A., Fodran, P., Brnčalová, L. & Cvengroš, J. 2008. Substituted Esters of Stearic Acid as Potential Lubricants. *Biomass and Bioenergy* 32: 366-371.
- [11] Campanella, A., Fontanini C. & Baltanás M.A. 2008. High Yield Epoxidation Of Fatty Acid Methyl Esters With Performic Acid Generated *In-Situ*. *Chemical Engineering Journal*.

Adjustment of an Intensive Care Unit (ICU) Data in Fuzzy C-Regression Models

Mohd Saifullah Rusiman^{1,*}, Robiah Adnan², Efendi Nasibov³, Kavikumar Jacob¹

¹Faculty of Science, Technology and Human Development, Universiti Tun Hussein Onn Malaysia, 86400 Parit Raja, Batu Pahat, Johor, Malaysia

²Faculty of Science, Universiti Teknologi Malaysia Skudai, 81310 Skudai, Johor Bahru, Johor, Malaysia

³Faculty of Science and Arts, Dokuz Eylul University, Tinaztepe Campus, 35160 Buca, Izmir, Turkey

**Corresponding email: saifulah@uthm.edu.my*

Abstract

This research is an attempt to present a proper methodology in data modification by using analytical hierarchy process (AHP) technique and fuzzy c-mean (FCM) model. The continuous data were built from binary data using analytical hierarchy process (AHP). Whereas, the binary data were created from continuous data using fuzzy c-means (FCM) model. The models used in this research are fuzzy c-regression models (FCRM). A case study in scale of health at an intensive care unit (ICU) ward using the AHP, FCM model and FCRM models was carried out. There are six independent variables involved in this study. There are four cases considered as a result of using AHP technique and FCM model toward independent data. After comparing the four cases, it was found that case 4 appeared to be the best model, having the lowest mean square error (MSE). The original data have the MSE value of 97.33, while the data of case 4 have MSE by 83.48. This means that the AHP technique can lower the MSE, while the FCM model cannot lower the MSE in modelling scale of health in the ICU. In other words, it can be claimed that the AHP technique can increase the accuracy of modelling prediction.

Keywords: analytical hierarchy process (AHP); fuzzy c-means (FCM) model; fuzzy c-regression models (FCRM); mean square error (MSE)

1. INTRODUCTION

Regression model has become one of the standard tools in data analysis since the mathematical equation from its analysis could explain the relationship between the dependent and independent variables. It is available in computer packages, easy to interpret and has been widely used in applied sciences, economic, engineering, computer, social sciences and other field. Fuzzy modelling has become popular for the past few years because it describes complex systems better. The fuzzy c-mean (FCM) model proposed by Bezdek [1] in 1981 develops hyper-spherical-shaped clusters. In contrast, the fuzzy c-regression models (FCRM) proposed by Hathaway and Bezdek [2] in 1993, develop hyper-plane-shaped clusters. Analytical hierarchy process (AHP) has been proposed by Thomas L. Saaty [3] in 1977 in handling factor weights due to a lack of historic information. It has been widely used in decision making, since it includes the natural feelings of human beings. Many researchers employ AHP technique in handling data mining problem [4,5].

The intensive care unit (ICU) plays an important role in the medical care sector not only for the critically ill, who makes up 5% of inpatients, but also in terms of generating a major contribution of health care funds. The United States health care industry makes up 15-20% total hospital cost. In 1968, the first ICU in Malaysia was established. Intensive care has then developed rapidly and it is now available in all tertiary care hospitals and selected secondary care hospitals. The National Audit on Adult Intensive Care Units in Malaysia in 2002 is modeled on the UK experience in 1994 and coordinated by a national committee comprising of senior intensive care specialists in the Ministry of Health. This audit unit develops a national database to assess fundamental aspects of intensive care functions within a hospital. The clinical indicators developed by ACHS (The Australian Council on Healthcare Standard) are useful tools for clinicians to flag potential problems and areas for improvement [6].

Currently, there was common method used in ICU involves logistic regression such as Colpan et al. [7]. Only Pilz and Engelmann [8] did a basic fuzzy rule to determine the medical decision in ICU. This work inspires us to do work in fuzzy model into ICU area that could give a challenge to this study. The first research on mortality rates in Malaysian ICU has been done at a general hospital in Ipoh, involving only a logit model [6]. The second research is continued by Rusiman et al. [9] on the analysis of logit, probit and linear probability models. As a comparison among the three models, logit model has been appeared to be the best model.

The objective of this research is to explore data modification using AHP technique and FCM model in scale of health at the ICU. The other objective is to make a comparison among the beginning data (without any method), AHP technique, FCM model or any combination of methods which are applied to data in order to find the best model. So, we can make recommendation based on this data mining method in predicting scale of health in the general hospital.

2. MATERIAL

In this study, the data were obtained from the intensive care unit (ICU) of a general hospital in Johor . The data obtained were classified as a cluster sampling. It involves 1311 patients in the ICU within the interval of January, 2001 to August, 2002. The dependent variable is scales of health or score of SAPS II discharge from hospital (s2sdisc). There are six independent variables considered in this study which are sex, race, organ failure (orgfail), comorbid diseases (comorbid), mechanical ventilator (mecvent) and score of SAPS II admit (s2sadm). The s2sdisc and s2sadm scores are 15 accumulated values for heart rate, blood pressure, age, body temperature, oxygen pressure, urine result, urea serum level, white blood count, potassium serum level, sodium serum level, bicarbonate serum level, bilirubin level, glasgow coma score, chronic illness and type of admittance as proposed by Le Gall et al. [10].

3. METHODOLOGY

3.1 AHP technique

The AHP technique is a complete decision making process that permits more complete consideration of multi-factors/criteria. The AHP procedure involves three steps as;

Step 1: Establish the decision hierarchy

In this step the decision maker must identify the overall decision, the factors that must be weighted or used to make the decision and the alternative choices from which a decision it to be made. Once these are identified they are placed in a decision hierarchy.

Step 2: Compute the weighted of alternatives

In this step the decision maker or expertise must compare each alternative with all other alternatives for one factor at one time. The rating measure scale used to rate the alternatives on a range from 1 to 9 as it relates to each of the factors. The weighted or probabilities obtained from a paired comparison matrix, summing to 1.

Step 3. Compute the weighted of factors

In this step the decision maker uses the previously determined comparison ratings to compute a set of priorities for the individual factors. This involves several small computation sub-steps where the probabilities or weighted obtained from a paired comparison matrix with the total of one [5].

3.2 FCM model

In FCM clustering, based on the Dunn [11] and Bezdek [1] algorithm, we have to minimise the criterion J in (1),

$$J = \sum_{j=1}^c \sum_{i=1}^N u_{ij}^w d_{ij}^2, w > 1 \tag{1}$$

where u_{ij} is the membership values, d_{ij}^2 is $\left\| x_i - \frac{\sum_{i=1}^N u_{ij}^w x_i}{\sum_{i=1}^N u_{ij}^w} \right\|^2$ or the Euclidean distances, N is the number of objects, c is the number of clusters and w is the weight or fuzzifier. In order to minimize (1), we have to;

- i. Fix the value of c . Initialise membership values \mathbf{U} or u_{ij} at random. Choose the termination tolerance $\delta > 0$.
- ii. Update Euclidean distances, d_{ij} for given \mathbf{U} by computing the weighted averages for each group.
- iii. Update membership values in (2),

$$u_{ij} = \frac{1}{\sum_{k=1}^c \left(\frac{d_{ij}}{d_{ik}} \right)^{\frac{2}{w-1}}}, \quad \text{for } w > 1$$

$$u_{ij} = \begin{cases} 1 & \text{if } d_{ij} = \min(d_{ik}) \\ 0 & \text{otherwise} \end{cases} \quad \text{for } w = 1 \tag{2}$$

- iv. Calculate the criterion J in (1) and check for convergence. If $|J_{old} - J_{new}| < \delta$ stop the iteration, else go to step (ii).

3.3 FCRM models

There are no conditions needed in FCRM models. Based on the algorithm in Hathaway & Bezdek [2], Abonyi & Feil [12] and Kung & Su [13], we have to,

- i. Fix the number of cluster c , $c \geq 2$. Choose the termination tolerance $\delta > 0$. Fix the weight, w , $w > 1$ (a common choice in practice is to set $w = 2$) and initialise the initial value for membership function matrix, $\mathbf{U}^{(0)}$ satisfying (4).
- ii. Estimate $\theta_1, \dots, \theta_c$ simultaneously by modifying the FCM algorithm. If the regression functions $f_i(x; \theta_i)$ are linear in the parameters θ_i , the parameters can be obtained as a solution of the weighted least squares,

$$\theta_i = [\mathbf{X}_b^T \mathbf{W}_i \mathbf{X}_b]^{-1} \mathbf{X}_b^T \mathbf{W}_i \mathbf{Y} \quad (3)$$

where $\mathbf{X}_b = [\mathbf{X}, 1]$.

iii. Calculate the objective function:

$$E_w[\mathbf{U}, \{\theta_i\}] = \sum_{i=1}^c \sum_{j=1}^d u_{ij}^w E_{ij}[\theta_i] \quad (4)$$

where

- a. u_{ij} is membership degree ($i = 1, \dots, c ; j = 1, \dots, N$).
- b. $E_{ij}[\theta_i]$ is the measure of error with $E_{ij}[\theta_i] = \|Y_j - f_i(X_j; \theta_i)\|^2$. The most commonly used is the squared vector Euclidean norm for $Y_j - f_i(X_j; \theta_i)$.

iv. Do iterations in order to minimize the objective function in (4). Repeat for $l = 1, 2, \dots, \infty$ until $\|\mathbf{U}^{(l)} - \mathbf{U}^{(l-1)}\| < \delta$. Next, follow the steps below:

Step 1 : Calculate model parameters $\theta_i^{(l)}$ to globally minimize (4).

Step 2 : Update \mathbf{U} with $E_{ij} = E_{ij}[\theta_i^{(l-1)}]$, to satisfy:

$$u_{ij}^{(l)} = \begin{cases} \frac{1}{\sum_{k=1}^c \left(\frac{E_{ij}}{E_{kj}}\right)^{\frac{2}{w-1}}}, & \text{for } I_j = \phi \\ 0, & \text{for } I_j \neq \phi \text{ and } i \notin I_j \end{cases} \quad (5)$$

where $I_j = \{i \mid 1 \leq i \leq c \text{ and } E_{ij} = 0\}$

until $\|\mathbf{U}^{(l)} - \mathbf{U}^{(l-1)}\| < \delta$.

The mean square error (MSE) is used as follow,

$$MSE = \frac{1}{N} \sum (Y_i - \hat{Y}_i)^2 \quad (6)$$

where Y_i denotes the real data, \hat{Y}_i represents the predicted value of Y_i and N is number of data.

4. DATA ANALYSIS

4.1 AHP technique

The AHP technique is applied to organ failures variable (orgfail). This independent variable only has two binary data, that is, patients who have or do not have organ failures. This technique will fuzzify the binary data of organ failures to be a continuous data within the interval $[0, 1]$. Organ failures are divided into 6 types which are: (*M*) Respiratory failure, (*N*) Cardiovascular failure, (*O*) Neurological failure, (*P*) Renal failure, (*Q*) Hepatic failure and (*R*) Haematological failure. Referring to the expert physicians in the general hospital, they stated that *N* and *P* have a twice higher probability that contribute

to high mortality if compared to the M and R . In fact, the M and R have a twice higher probability if compared to the O and Q . However, N and P have the same weightage. The same weightage are also given to the M and R . O and Q also receive the same weightage. The paired comparison matrix and probabilities (weighted) are shown in Table 1.

Table 1: The paired-comparison matrix and weighted for organ failures

	N	P	M	R	O	Q	Total	Weighted
N	1	1	2	2	4	4	14	0.2857
P	1	1	2	2	4	4	14	0.2857
M	$\frac{1}{2}$	$\frac{1}{2}$	1	1	2	2	7	0.1429
R	$\frac{1}{2}$	$\frac{1}{2}$	1	1	2	2	7	0.1429
O	$\frac{1}{4}$	$\frac{1}{4}$	$\frac{1}{2}$	$\frac{1}{2}$	1	1	3.5	0.0714
Q	$\frac{1}{4}$	$\frac{1}{4}$	$\frac{1}{2}$	$\frac{1}{2}$	1	1	3.5	0.0714

4.2 FCM model

In order to get categorical data of s2sadm with ‘1’ and ‘2’ coded, we have to cluster s2sadm data based on FCM clustering algorithm. The data for cluster 1 with 860 data ranges from 0 to 43 whereas the data for cluster 2 with 443 data ranges from 44 to 126. This is the same as the cluster given by the doctors who indicated that the s2s score over 43 is classified as a bad condition. The membership function graph for variable s2sadm is shown in Figure 1.

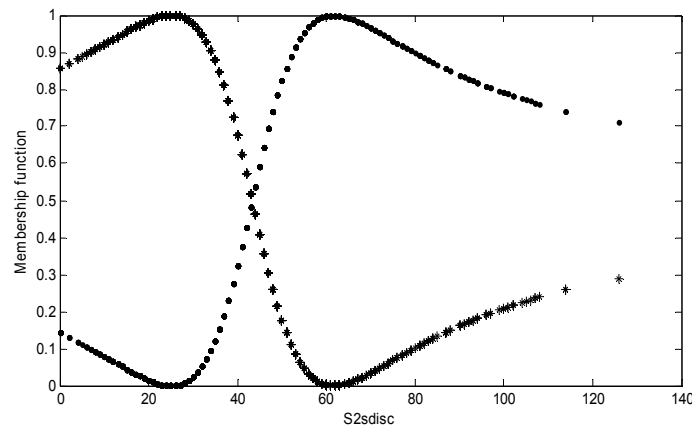


Figure 1: Plot for s2sadm membership function (FCM Clustering)

4.3 FCRM models

In this study, there are four cases considered as in Table 2 as a result of using AHP and FCM model toward independent data. The four cases involves six variables with different combination of variable types in each case were considered in order to find the best model using FCRM models. The variables involved are sex (x_1 is binary), race (x_2 is category), orgfail (x_3 is binary or continuous), comorbid (x_4 is binary), mecvent (x_5 is binary) and s2sadm (x_6 is binary or continuous). Case 3 is the beginning data without any modification being carried out.

Table 2: Different case of multivariate data (Y vs $x_1, x_2, x_3, x_4, x_5, x_6$)

Case	1	2	3	4
x_1	B	B	B	B
x_2	Ca	Ca	Ca	Ca
x_3	B	Co	B	Co
x_4	B	B	B	B
x_5	B	B	B	B
x_6	B	B	Co	Co
MSE for MLR(SV)	632.14 (VA)	526.40 (VA)	498.29 (VB)	463.10 (VA)
MSE for FCRM(AV)	116.05	114.71	98.28	84.01
MSE for FCRM(SV)	121.92(VA)	97.29(VA)	97.33(VB)	83.48(VA)

Note:

B:Binary, Ca:Category, Co:Continuous, AV:All variables SV:Significant variables(VA, VB)

VA: 4 Variables chosen - x_1, x_3, x_4 & x_6 , VB: 5 Variables chosen - x_1, x_3, x_4, x_5 & x_6

There are four cases considered as a result of combination cases with/without using AHP technique and/or FCM model toward independent data. Table 3 shows that case 4 is the best case with the lowest MSE, that is, when x_1 is binary, x_2 is category, x_3 is continuous, x_4 is binary, x_5 is binary and x_6 is continuous. The MSE value for FCRM models for case 4 is 84.01 (all variables) and 83.48 (significant variables - x_1, x_3, x_4, x_6). The MSE value for significant variables shows better result. The MSE value for case 3 (original data) is 97.33, while the MSE value for case 4 is 83.48. The MSE values for the other cases are 97.29 and 121.92. In conclusion, case 4 is the best case in which data modification involves only the

orgfail variable. These chosen models (y vs x_1, x_3, x_4, x_6) are represented in (7) with two clusters.

Cluster 1

$$R^1 : \text{IF } x_1 \text{ is } A_1^1 \text{ and } x_3 \text{ is } A_3^1 \text{ and } x_4 \text{ is } A_4^1 \text{ and } x_6 \text{ is } A_6^1 \\ \text{THEN } y^1 = 2.4644 x_1 + 12.8113 x_3 + 4.6925 x_4 + 0.1721 x_6 + 61.2967$$

Cluster 2

$$R^2 : \text{IF } x_1 \text{ is } A_1^2 \text{ and } x_3 \text{ is } A_3^2 \text{ and } x_4 \text{ is } A_4^2 \text{ and } x_6 \text{ is } A_6^2 \\ \text{THEN } y^2 = 1.2257 x_1 - 1.8245 x_3 + 4.0093 x_4 + 0.4788 x_6 - 4.8764 \quad (7)$$

5. CONCLUSIONS

In this research, data modifications were done to the case study in ICU where the binary data (s2sadm variable) were built from continuous data using FCM model, whereas the continuous data (orgfail variable) were created from binary data using AHP technique. There are four cases considered as a result of combination cases with/without using AHP technique and/or FCM model toward independent data. After comparing the four cases, it was found that case 4 appeared to be the best model, having the lowest MSE of 83.48, while the original data have the MSE value of 97.33. This means that the AHP technique can lower the MSE value, while the FCM model cannot lower the MSE in modelling scale of health in the ICU. In other words, it can be declared that the AHP technique can increase the accuracy of modelling prediction and should be used as a reference in hospitals to improve data accuracy.

REFERENCES

- [1] Bezdek, J. C. (1981). Pattern Recognition with Fuzzy Objective Function Algorithms. USA: Kluwer Academic Publishers.
- [2] Hathaway, R. J. & Bezdek, J. C. (1993). "Switching Regression Models and Fuzzy Clustering" in IEEE Transactions on Fuzzy Systems, 27 pp 195–204.
- [3] Saaty, T. L. (1977). A scaling method for priorities in hierarchical structures. Journal of Mathematical Psychology, 15(3), 234-281.
- [4] Saaty, T. L., Peniwati, K. & Shang, J. S. (2007). "The Analytic Hierarchy Process and Human Resource Allocation: Half the story" in Mathematical and Computer Modelling, 46 (7-8) pp 1041–1053.

- [5] Schniederjans, M. J. (2004). *Information technology investment : Decision-making methodology*. Singapore: World Scientific Publishing Company, Incorporated.
- [6] The Committee for National Audit on Adult Intensive Care Units (2002). *Protocol : National Audit on Adult Intensive Care Units*.
- [7] Colpan, A., Akinci, E., Erbay, A., Balaban, N. & Bodur, H. (2005). "Evaluation of Risk Factors for Mortality in ICUs: A Prospective Study from a Referral Hospital in Turkey" in *American Journal of Infection Control*, 33 pp 42-47.
- [8] Pilz, U. & Engelmann, L. (1998). "Integration of Medical Knowledge in an Expert System for Use in Intensive Care Medicine" in *Fuzzy and Neuro-Fuzzy Systems in Medicine*, 2 pp 290-315.
- [9] Rusiman, M. S., Mohd Daud, Z. & Mohamad, I. (2004). "The Comparison between Logit, Probit and Linear Probability Model toward Mortality Rate at ICU General Hospital" in *Jurnal Statistika Universitas Islam Bandung*, 4 pp 129-138.
- [10] Le Gall, J-R., Lemeshow, S., Saulnier, F (1993). "A new Simplified Acute Physiology Score (SAPS II) based on a European/North American multicenter study" in *The Journal of the American Medical Association*, 24 pp 2957-2963.
- [11] Dunn, J. C. (1973), "A Fuzzy Relative of the ISODATA Process and Its Use in Detecting Compact Well-Separated Clusters" in *Journal of Cybernetics*, 3 pp 32-57.
- [12] Abonyi, J. & Feil, B. (2007). *Cluster analysis for data mining and system identification*, USA: Springer.
- [13] Kung, C. C. & Su, J. Y. (2007). "Affine Takagi-Sugeno fuzzy modelling algorithm by fuzzy c-regression models clustering with a novel cluster validity criterion" in *IET Control Theory Application*, 1 pp 1255–1265.

Thermal and Solutal Mixed Marangoni Boundary Layers with Suction or Injection Effects

Noraini Ahmad*, Seripah Awang Kechil, Norma Mohd Basir

Faculty of Computer and Mathematical Sciences, Universiti Teknologi MARA
40450 UiTM Malaysia, Shah Alam, Selangor Darul Ehsan, Malaysia.

*Corresponding email: noraini.ahmad@rocketmail.com

Abstract

A steady two-dimensional Marangoni boundary-layer flow over a permeable flat surface is considered. The surface tension is assumed to vary linearly with temperature and solute concentration. The transformed similarity boundary layer equations are obtained and solved numerically by Runge-Kutta-Fehlberg with shooting technique. The Marangoni and external pressure gradient effects that generated in boundary layer flow are assessed. As the suction/ injection parameter increases from injection to suction, the velocity, temperature and concentration boundary layers thickness decrease but injection increases them. The thermosolutal surface tension ratio increases the velocity boundary thickness but decreases the temperature and concentration boundary layers.

Keywords: marangoni convection; surface tension, similarity solution; suction or injection effect

1. INTRODUCTION

Marangoni convection occurs when there is temperature or concentration differences on the surface of the fluid and the fluid will flow from region having low surface tension (high temperature region) to region having high surface tension (cold temperature region). In thermocapillary convection, the surface tension varies with temperature. However, small amounts of certain surfactant additives are also known to drastically change the surface tension. Surface-tension induced convection is important in study of nucleate and bubble growth dynamics because it causes undesirable effects in industrial processes [1,2,3].

Theoretical investigations on Marangoni flows include the works of by Christopher and Wang [3], Magyari and Chamkha [4,5], Zueco and Bég [6], Al-Mudhaf and Chamkha [7]. Christopher and Wang [2] examined the effect of Prandtl number to see the relative thickness of momentum and thermal boundary layers. The influence of temperature exponent using the power-law function of temperature in nucleate and vapour bubble growth was examined by Christopher and Wang [3]. Magyari and Chamkha [4,5] found the exact analytical solutions for the MHD thermosolutal Marangoni convection in the presence of heat and mass generation or consumption. Their analytical results showed that the thermosolutal surface tension ratio increases the wall velocity and mass flow rate. The effects of gravity, magnetic field and external pressure gradients on the Marangoni convection boundary layers have been considered by Zueco and Bég [6]. Al-Mudhaf and Chamkha [7], Hamid et al. [8] and Ahmad et al. [9] studied the effect of suction, injection on Marangoni boundary layer flow.

In this paper, we extend the work of Christopher and Wang [3] to include the effects of surface tension gradient due to insoluble surfactant on the development of momentum, thermal and concentration of Marangoni boundary layers flow.

2. PROBLEM FORMULATION

Consider the steady two-dimensional mixed Marangoni boundary layer flow with an external pressure gradient over a flat plate. The surface is assumed to be permeable in order to allow for possible suction or injection at the wall. The temperature variation is in the form of power law function and the boundary layer develops along the surface due to the coupled Marangoni convection. The governing equations are the balance laws of mass, momentum, energy and concentration given by,

$$\frac{\partial u}{\partial x} + \frac{\partial v}{\partial y} = 0, \quad (1)$$

$$u \frac{\partial u}{\partial x} + v \frac{\partial u}{\partial y} = \nu \frac{\partial^2 u}{\partial y^2} + u_e \frac{du_e}{dx}, \quad (2)$$

$$u \frac{\partial T}{\partial x} + v \frac{\partial T}{\partial y} = \alpha \frac{\partial^2 T}{\partial y^2}, \quad (3)$$

$$u \frac{\partial C}{\partial x} + v \frac{\partial C}{\partial y} = D \frac{\partial^2 C}{\partial y^2}, \quad (4)$$

where u and v are velocity components along the x and y axes, respectively, T is the fluid temperature, C is the solute concentration, D is the mass diffusivity, α is the thermal diffusivity, ν is the kinematic viscosity and $u_e(x)$ is the velocity of the external flow. The surface tension σ at the interface is assumed to vary linearly with temperature and surfactant concentration in the form,

$$\sigma = \sigma_0 - \gamma_T(T - T_\infty) - \gamma_C(C - C_\infty), \quad (5)$$

where σ_0 is the reference surface tension, $\gamma_T = \left. \frac{\partial \sigma}{\partial T} \right|_C$ and $\gamma_C = \left. \frac{\partial \sigma}{\partial C} \right|_T$.

The boundary conditions at the surface are

$$\mu \left. \frac{\partial u}{\partial y} \right|_{y=0} = - \left. \frac{d\sigma}{dT} \right|_C \left. \frac{\partial T}{\partial x} \right|_{y=0} - \left. \frac{d\sigma}{dC} \right|_T \left. \frac{\partial C}{\partial x} \right|_{y=0}, \quad (6)$$

$$v(x,0) = -v_0, \quad T(x,0) = T(0,0) + Ax^{k+1}, \quad (7)$$

$$C(x,0) = C(0,0) + A^* x^{k+1}. \quad (8)$$

and at the free stream, the boundary conditions are

$$u(x, \infty) = 0, \quad (9)$$

$$T(x, \infty) = T_\infty = T(0,0) \quad \text{or} \quad \left. \frac{\partial T}{\partial y} \right|_{y=\infty} = 0, \quad (10)$$

$$C(x, \infty) = C_\infty = C(0,0) \quad \text{or} \quad \left. \frac{\partial C}{\partial y} \right|_{y=\infty} = 0, \quad (11)$$

where A and A^* are the temperature and concentration gradient coefficient, respectively, and k is the constant exponent of the temperature and concentration, and v_0 is a constant which refers to suction or injection.

Following [6], we introduce the similarity transformations

$$\eta = C_1 x^d y, \quad f(\eta) = C_2 x^a \psi(x, y), \quad (12)$$

$$\theta(\eta) = \frac{[T(x, y) - T(0,0)]x^h}{A}, \quad (13)$$

$$\phi(\eta) = \frac{[C(x, y) - C(0,0)]x^h}{A^*}, \quad (14)$$

where η is the similarity variable, ψ is the stream function defined by $u = \partial \psi / \partial y$ and $v = -\partial \psi / \partial x$, $f(\eta)$ is the dimensionless stream function, θ is the dimensionless

temperature function and ϕ is the dimensionless concentration function. The exponents d , a and h in (12) and (14) are related to the temperature and concentration gradient exponent, k , given by the relation [6],

$$d = \frac{k-1}{3}, \quad a = \frac{-2-k}{3}, \quad h = -1-k. \tag{15}$$

By applying (12)-(14) on the governing equations (1)- (4) and boundary conditions (6) – (11), we obtained a coupled nonlinear system of ordinary differential equations,

$$f''' - (d - a)(f'^2 - 1) - aff'' = 0, \tag{16}$$

$$\theta'' - \text{Pr}(af\theta' - hf'\theta) = 0, \tag{17}$$

$$\phi'' - \text{Sc}(af\phi' - hf'\phi) = 0, \tag{18}$$

where Pr is the Prandtl number and Sc is the Schmidt number. The transformed boundary conditions are

$$f''(0) = (-1 - k)(1 + \varepsilon), \quad f(0) = f_w, \quad \theta(0) = 1, \quad \phi(0) = 1, \tag{19}$$

$$f'(\infty) = 0, \quad \theta(\infty) = 0 \quad \text{or} \quad \theta'(\infty) = 0, \quad \phi(\infty) = 0 \quad \text{or} \quad \phi'(\infty) = 0, \tag{20}$$

with $f_w > 0$ is the constant of suction parameter, $f_w < 0$ is the constant of injection parameter and ε is the thermosolutal surface tension ratio.

3. RESULTS AND DISCUSSION

The system of nonlinear ordinary differential equation (16) and -18) subject to boundary conditions (19) and (20) are solved numerically using Runge-Kutta-Fehlberg method with shooting technique. The three unknown conditions, $f'(0)$, $\theta'(0)$ and $\phi'(0)$ are determined.

Table 1: Comparison values of $f'(0)$, $-\theta'(0)$ and $-\phi'(0)$

	Al-Mudhaf and Chamkha (2005)	Present
$f'(0)$	1.587671	1.587401
$-\theta'(0)$	1.442203	1.442066
$-\phi'(0)$	1.220880	1.220711

Table 2: Effects of ε on $f'(0)$, $-\theta'(0)$, and $-\phi'(0)$

ε	$f'(0)$	$-\theta'(0)$	$-\phi'(0)$
0	1.7885555881	1.2608835684	1.0937432457
1	2.4660513411	1.4365160819	1.2404014544
3	3.6042256176	1.6923289378	1.4544116268
5	4.5838291117	1.8855580010	1.6163084822

Table 1 shows the numerical values of the wall velocity $f'(0)$, heat transfer coefficient $-\theta'(0)$ and mass transfer coefficient $-\phi'(0)$ when $Pr = 0.78$, $Sc = 0.6$, $f_w = 0$, temperature gradient exponent $k = 1$ and the pressure gradient is absent ($-dp/dx = u_e(x)du_e/dx = 0$). It can be observed that the numerical values of the Runge-Kutta Fehlberg with shooting technique are in good agreement with the results from the implicit finite-difference method of Al-Mudhaf and Chamkha [7].

Table 2 illustrates the influence of the thermosolutal surface tension ratio ε on $f'(0)$, $-\theta'(0)$, and $-\phi'(0)$. The increasing thermosolutal surface tension ratio ε increases $f'(0)$, $-\theta'(0)$, and $-\phi'(0)$. The effects of f_w and ε on the velocity, temperature and concentration profiles are presented graphically in Figures 1- 4.

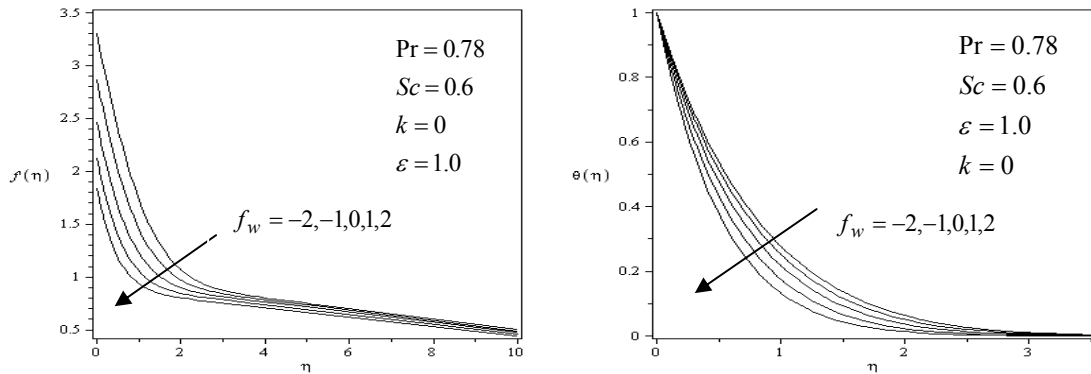


Figure 1: Effects of f_w on velocity and temperature profiles

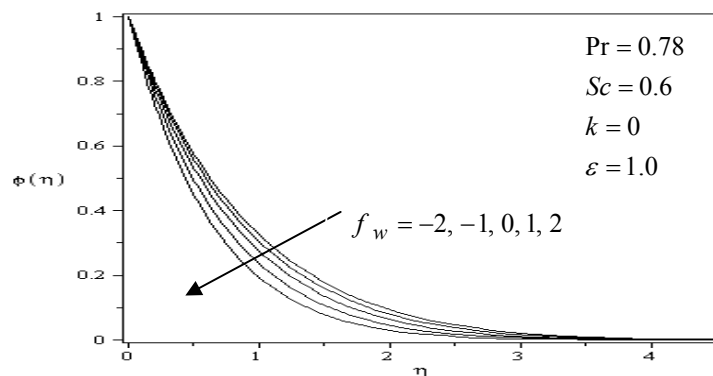


Figure 2: Effects of f_w on concentration profiles

Figure 1 presents the effects of suction or injection on velocity and temperature profiles and Figure 2 illustrates the effects of suction or injection on concentration profiles. Generally, suction decreases the velocity, temperature and concentration boundary layers thickness and injection shows the opposite effect. Figure 3 shows the influence of the thermosolutal surface tension ratio, ε on the velocity profiles. As ε increases, the Marangoni convection effect increases causing more induced flow. This induced flow starts at the surface and propagates in the boundary layer. Thus, the maximum velocity occurs at the wall. However, the increased velocity is caused by the increase in Marangoni convection effect followed by decreases in temperature and concentration as shown in Figure 4.

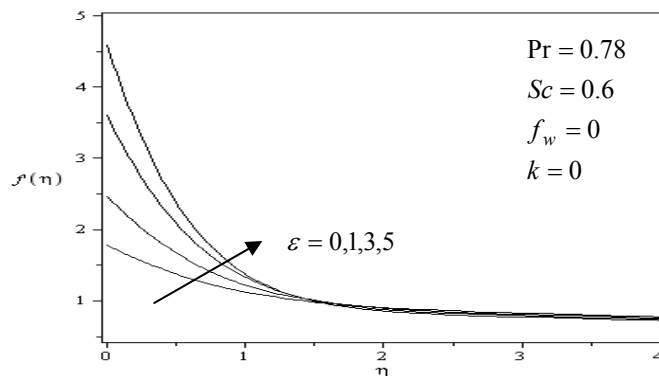


Figure 3: Effects of ε on velocity profiles.

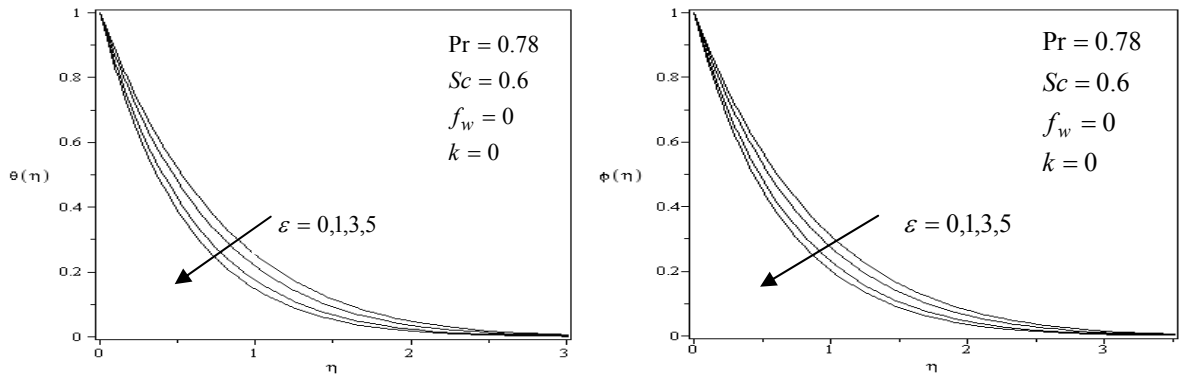


Figure 4: Effects of ε on temperature and concentration profiles

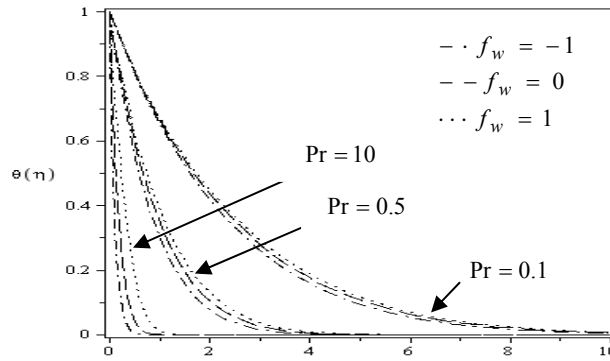


Figure 5: Effects of Pr on temperature profiles for various f_w when $Sc = 0.6$ and $k = \varepsilon = 0$.

In Figure 5, it can be seen that the thickness of the thermal boundary layer is influenced by the Prandtl number. Small values of Pr ($\ll 1$) correspond to liquid metals having high thermal conductivity and low viscosity but the value $Pr \gg 1$ corresponds to high viscosity oils. As the Prandtl number increases, the magnitude of the rate of heat transfer increases and the thermal boundary layers gets thinner for high Prandtl numbers. Suction reduces the rate of heat transfer.

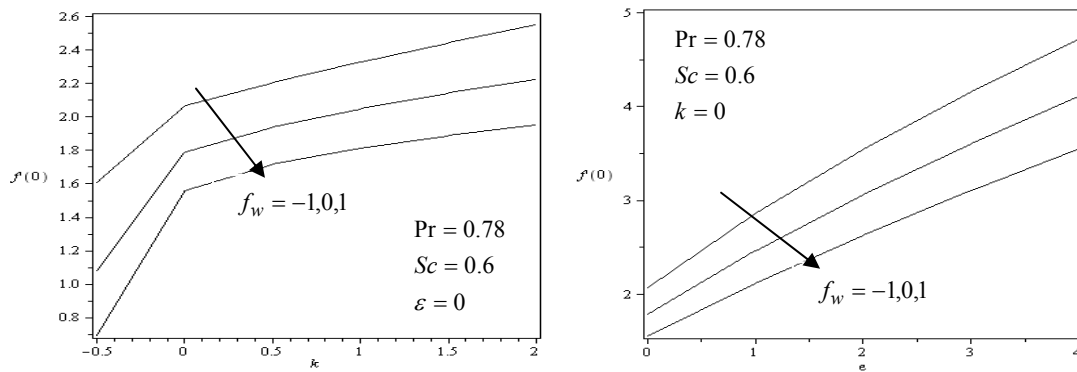


Figure 6: Effects of k and ε on surface velocity for various f_w

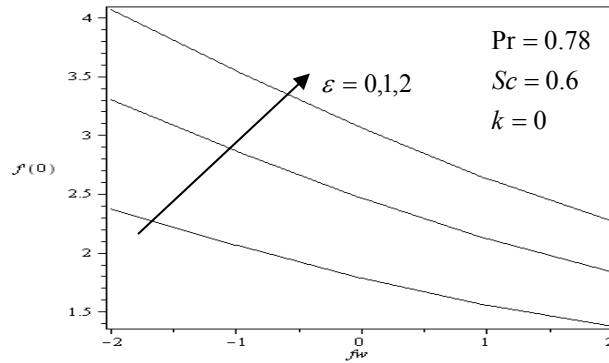


Figure 7: Effects of f_w on surface velocity for various ϵ

Figure 6 shows the effects of temperature exponent k and the thermosolutal surface tension ratio on the surface velocity for various f_w , respectively. The temperature exponent and the thermosolutal surface tension ratio increase the surface velocity thus reduce the velocity boundary layers but the increase from injection to suction reduces the surface velocity and thickens the velocity boundary layers. Figure 7 illustrates the effects of the thermosolutal surface tension ratio and suction or injection parameter on the surface velocity. Similar results can be observed that suction decreases the surface velocity but the wall velocity increases when thermosolutal surface tension ratio increases.

4. CONCLUSIONS

The steady Marangoni convection boundary layer flow in the presence of suction and injection effects was discussed and examined numerically. The basic governing equations in the form of partial differential equations were transformed to ordinary differential equations by similarity transformation. Numerical solutions of the similarity equations were obtained using Runge-Kutta with shooting technique. The effects of physical parameters on the velocity and concentration profiles were presented and evaluated. Suction decreases the velocity, temperature and concentration boundary layers thickness while injection increases them. The thermosolutal surface tension ratio increases the velocity boundary layer thickness but decreases the thickness of the temperature and concentration boundary layers. The temperature exponent, thermosolutal surface tension ratio and injection increase the surface velocity leading to the reduced velocity boundary layer thickness.

Acknowledgment

The authors would like to acknowledge the financial support received from the Ministry of Higher Education of Malaysia and Universiti Teknologi MARA under the Fundamental Research Grant Scheme (FRGS) 600-RMI/ST/FRGS 5/3/Fst (9/2011) and the Young Lecturer's Scheme Scholarship.

REFERENCES

- [1] Arafune, K. & Hirata, A. (1999). "Thermal and solutal Marangoni convection in In-Ga-Sb system in Journal of Crystal Growth, Vol. 197. pp. 811-817.
- [2] Christopher, D.M. & Wang, B. (2001a). "Prandtl number effects for Marangoni convection over a flat surface" in International Journal of Thermal Sciences, Vol. 40. pp. 564-570.
- [3] Christopher, D.M. & Wang, B. (2001b). "Similarity simulation for Marangoni convection around a vapor bubble during nucleation and growth" in International Journal of Heat and Mass Transfer, Vol. 44. pp. 799-810.
- [4] Magyari E. & Chamkha, A.J. (2007). "Exact analytical solutions for thermosolutal Marangoni convection in the presence of heat and mass generation or consumption" in *Heat and Mass Transfer*, Vol. 43. pp. 965-974.
- [5] Magyari, E. & Chamkha, A.J. (2008). "Exact analytical results for the thermosolutal MHD Marangoni boundary layer" in *International Journal of Thermal Sciences*, Vol. 47. pp. 848-857.
- [6] Zueco, J. & Bég, O.A. (2011). "Network numerical simulation of hydromagnetic Marangoni mixed convection boundary layers" in *Chemical Engineering Communications*, Vol. 198. pp. 552-571.
- [7] Al-Mudhaf, A. & Chamkha, A.J. (2005). "Similarity solutions for MHD thermosolutal Marangoni convection over a flat surface in the presence of heat generation or absorption effects" in *Heat and Mass Transfer*, Vol. 42. pp. 112-121.
- [8] Hamid, R., Arifin, N., Nazar, R., & Ali, F. (2011). "Radiation effects on Marangoni convection over a flat surface with suction and injection" in *Malaysian Journal of Mathematical Sciences*, Vol. 5. No. 1 pp.13-25.

- [9] Ahmad, N., Awang Kechil, S. & Basir, N.M. (2011). "Thermosolutal MHD Mixed Marangoni Boundary layer in the presence of suction or injection" in World Academy of Science, Engineering and Technology, Vol. 58. pp 459-464.